GE 136A: Winter 2025 Field Guide

Eastern San Diego Peninsular Range, Anza Borrego Desert and the Salton Sea

A view of the Anza Borrego and Ocotillo Wells desert highlighting one of the last remaining native California Fan Palms in the area.

Instructor: Joe Kirschvink
TAs: Nick Anderson
Cover Photo: Nick Anderson

Table of Contents

1 Trip Schedule **4**

2 Routes **4**

2.1 Day 1: February 14, 2025 4

2.2 Day 2: February 15, 2024 5

2.3 Day 3: February 16, 2024 6

3 Talks **7**

3.4 Day 1 7

(1) Clay Minerals: Lake Elsinore and Beyond 7

(2) The Petrogenesis of the Peninsular Ranges Batholith 9

(3) LCT Pegmatites: A Mineral Bonanza 11

(4) Exploring Exoplanets and Nonsingular Stars 13

(5) Palomar Observatory and Asteroids 15

(6) Uranian Satellites Discovered at Palomar Observatory 17

(7) Palomar and the Expansion of the Universe 19

(8) Kumeyaay Culture, History and Material Artifacts of San Diego County 21

(9) Light Pollution at Palomar and Beyond 23

(10) Dark Night Skies as a Window into Science and Culture 25

3.5 Day 2 27

(11) Mars at the Salton Sea 27

(12) Slab City: How Geology and Climate Shape Art and Culture 29

(13) Plate Tectonics of Salton Basin and the Gulf of California 31

(14) The Once Great Lake: Remnants of Lake Cahuilla and the formation of the Salton Sea 33

(15) Fossils in the Salton Trough 35

(16) Resources of California's largest lake 37

(17) The Resources of the Salton Sea: A Catalyst for a Green Energy Transition? 39

(18) Smelling the Salton Sea: Sulfur Dynamics in a Polluted Saline Lake 41

(19) The Salton Sea: Hazards and Resources 43

(20) Efforts towards restoration of the Salton Sea 45

(21) Obsidian and Volcanism in the Salton Sea (Salton Buttes) 47

(22) Post-Eruption Ecology 49

(23) Fungivores in the Algodones Dunes 51

3.6 Day 3 53

(24) Colorado River Hydrology 53

(25) Geodes: More than Just a Pretty Face(ies) 55

(26) Shallow Creeping Faults of the Imperial Valley 57

(27) El Niño–Southern Oscillation & Santa Ana Winds 59

(28) Rattlesnakes 61

(29) Biological Soil Crust (Biocrusts) 63

Day	Approximate Time (PDT)	Activity	Talks	Duration	Bathroom	Gas	Drive Time
Day 1 - 2/14	7:00	Meet at Arms Circle/ Caltech		1:00	X		
	8:00	Leave Arms Circle					1:20
	9:20	Lake Elsinore - Elm Grove Beach - 500 Lakeshore Dr/ Lake Elsinore/ CA 92530	Thalhammer	0:30	X		0:45
	10:35	Pala Mining District - 37020 Magee Rd/ Pala/ CA 92059	Sanchez	0:30			0:45
	11:50	Palomar Observatory and Lunch	Langley/ Sowell/ Stenmark/ Oke	2:00	X		0:55
	14:45	Julian Pie Company	Heiny	0:45	X	X	0:50
	16:20	Pictographs Trail Head	Hannahs	2:00			0:45
	19:05	Agua Caliente Camp	Seeger/ Williams	1:00	X		0:40
Day 2 - 2/15	8:30	Leave Agua Caliente			X		1:00
	9:30	Anza Borrego Visitor Center		0:30	X	X	0:30
	10:30	Calcite Slot Mine		1:00			0:50
	12:20	Painted Canyon		0:30			0:30
	13:20	Durmid / Salt Creek Beach Campground - 33.440918/ -115.830120 and Lunch	Kalucha/ Menezes/ Mullahoo/ Stone/ Bednarick/ Bennett	1:30	X		0:15
	15:05	Bombay Beach		0:15	X		0:25
	15:45	Slab City / Salvation Mountain	Alcabes	0:30	X		0:25
	16:40	Obsidian Butte	Chriem/ Artymowicz/ Chastain/ Keebler	0:30			0:35
	17:45	Algodones Dunes / Glamis Flats	Schmeer/ Horak	0:40			0:50
	19:15	Walter's Camp	Hunady	1:50	X		
Day 3 - 2/16	7:30	Leave Walters Camp	McCann		X		1:15
	8:45	Hauser Geode Beds	Westercamp/ Vescu	1:00			0:55
	10:40	Opal Hill Mine / Wiley's Well		0:30	X		1:45
	12:55	Cholla Cactus Garden	Aguilar/ Shivji	0:30	X		0:35
	14:00	Bagly Stone / Wall St Mill / Barker Dam		0:30	X		0:30
	15:00	Joshua Tree Visitor Center	Li	0:30	X		2:30
	18:00	Arrive at Arms Circle					

1. Trip Schedule

2. Routes

2.1 Day 1: February 14, 2025

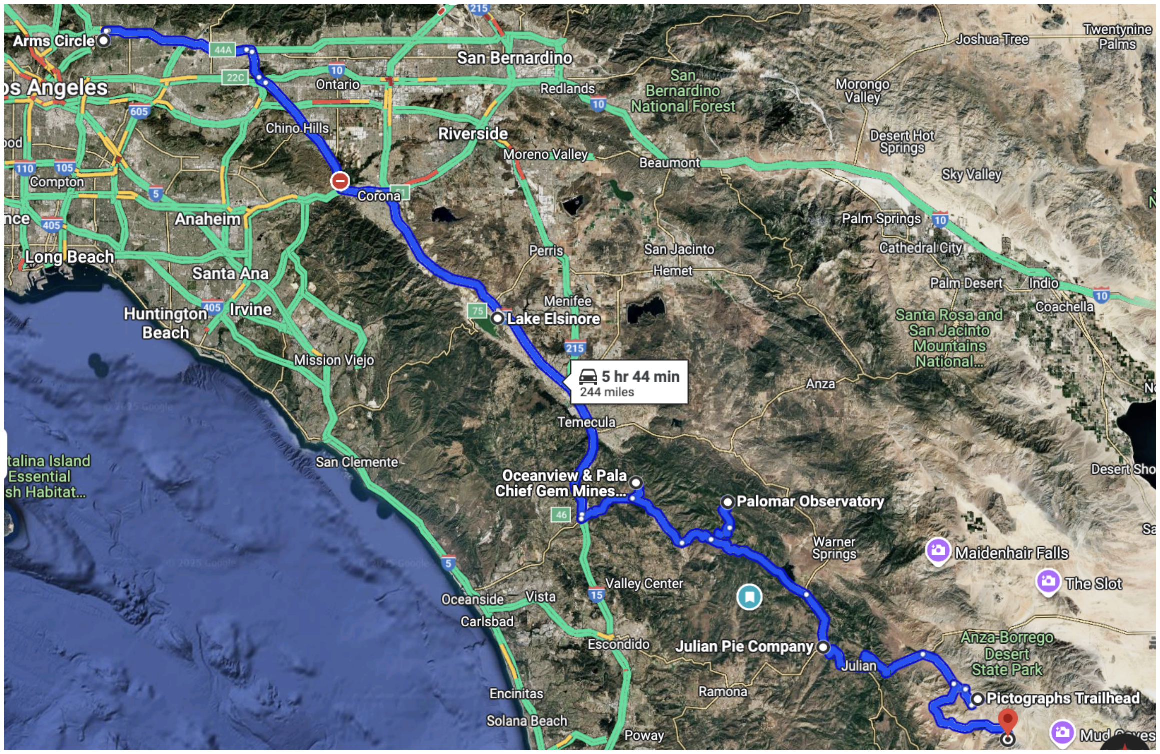
Arms Circle
Los Angeles
San Bernardino
Ontario
Redlands
San Bernardino National Forest
Joshua Tree
Twentynine Palms
Morongo Valley
Chino Hills
Riverside
Moreno Valley
Beaumont
Desert Hot Springs
Sky Valley
Compton
Corona
Anaheim
Palm Springs
Cathedral City
Long Beach
Perris
San Jacinto
Hemet
Santa Ana
Palm Desert
Indio
Coachella
Huntington Beach
Irvine
Menifee
Lake Elsinore
Santa Rosa and San Jacinto Mountains National...
Mission Viejo
5 hr 44 min
244 miles
Anza
Temecula
Catalina Island Essential Fish Habitat...
San Clemente
Oceanview & Pala Chief Gem Mines...
Palomar Observatory
Desert Shores
Warner Springs
Maidenhair Falls
The Slot
Oceanside
Vista
Carlsbad
Valley Center
Escondido
Julian Pie Company
Julian
Anza-Borrego Desert State Park
Ramona
Pictographs Trailhead
Encinitas
Solana Beach
Poway
Mud Caves

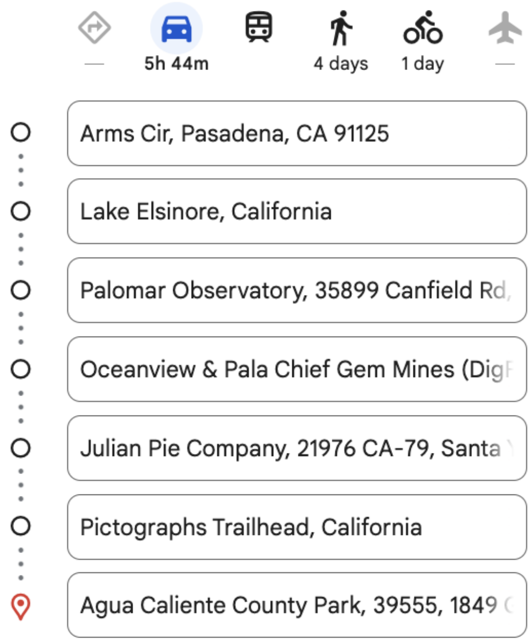
—
5h 44m
4 days
1 day
—

Arms Cir, Pasadena, CA 91125

Lake Elsinore, California

Palomar Observatory, 35899 Canfield Rd,

Oceanview & Pala Chief Gem Mines (Dig

Julian Pie Company, 21976 CA-79, Santa

Pictographs Trailhead, California

Agua Caliente County Park, 39555, 1849

2.2 Day 2: February 15, 2024

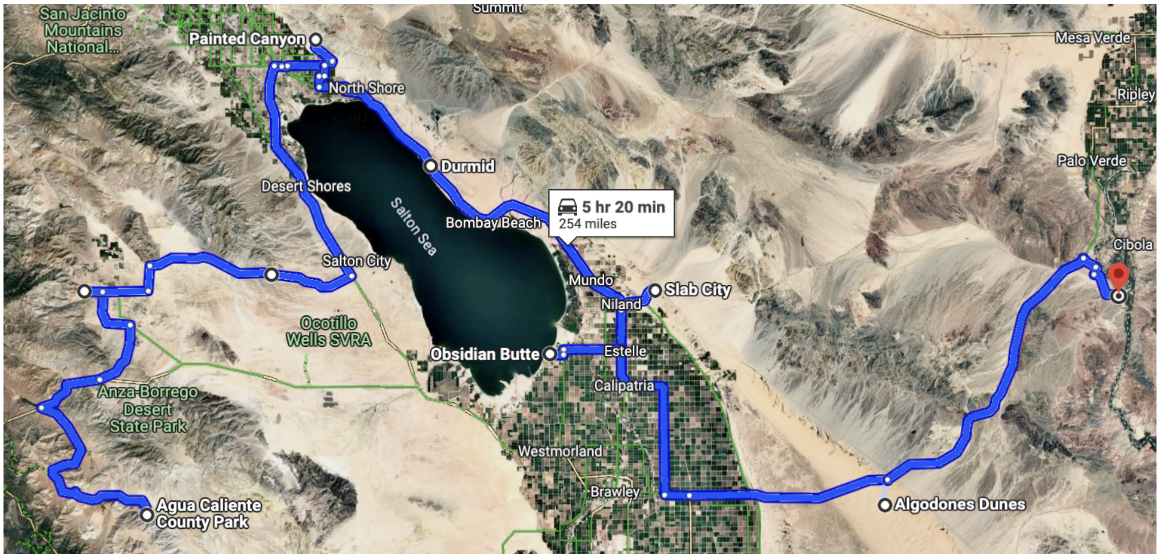
San Jacinto Mountains National...
Summit
Painted Canyon
North Shore
Durmid
Desert Shores
Salton Sea
Bombay Beach
5 hr 20 min
254 miles
Salton City
Mundo
Slab City
Niland
Ocotillo Wells SVRA
Obsidian Butte
Estelle
Calipatria
Anza-Borrego Desert State Park
Westmorland
Brawley
Agua Caliente County Park
Algodones Dunes
Mesa Verde
Ripley
Palo Verde
Cibola

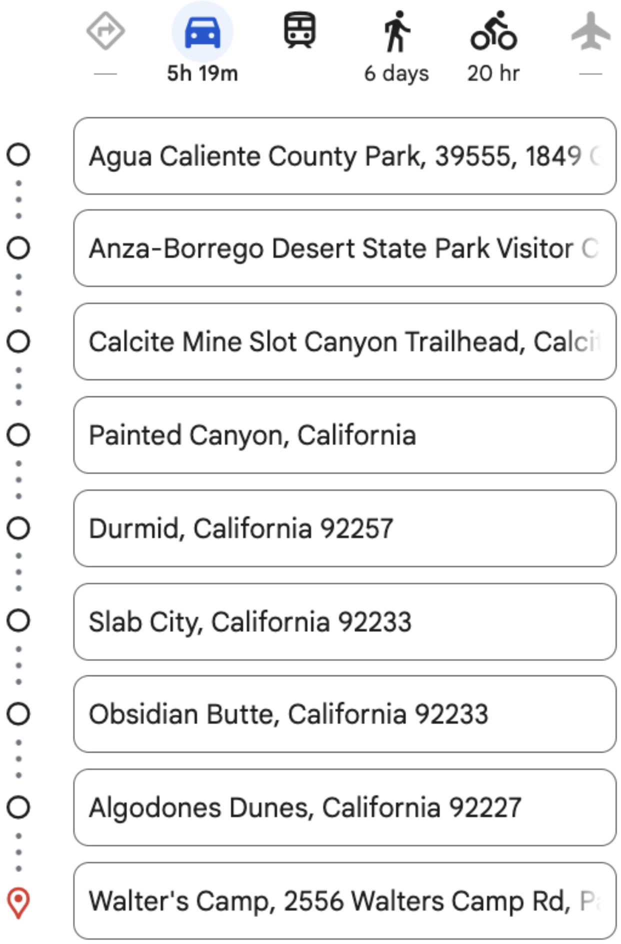
—
5h 19m
6 days
20 hr
—

Agua Caliente County Park, 39555, 1849

Anza-Borrego Desert State Park Visitor C

Calcite Mine Slot Canyon Trailhead, Calci

Painted Canyon, California

Durmid, California 92257

Slab City, California 92233

Obsidian Butte, California 92233

Algodones Dunes, California 92227

Walter's Camp, 2556 Walters Camp Rd, P

2.3 Day 3: February 16, 2024

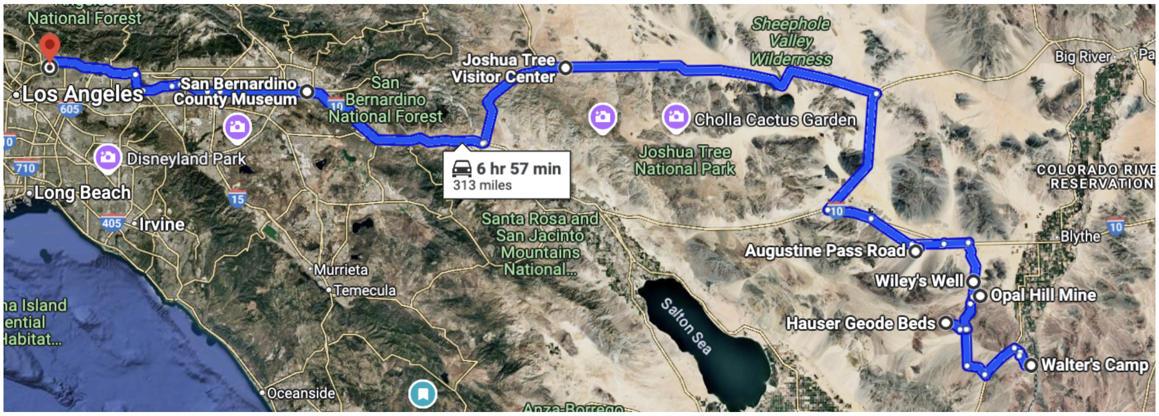
National Forest
Los Angeles
San Bernardino County Museum
San Bernardino National Forest
Joshua Tree Visitor Center
Sheephole Valley Wilderness
Big River
Cholla Cactus Garden
Joshua Tree National Park
COLORADO RIVE RESERVATION
Disneyland Park
Long Beach
Irvine
6 hr 57 min
313 miles
Santa Rosa and San Jacinto Mountains National...
Murrieta
Temecula
Salton Sea
Augustine Pass Road
Blythe
Wiley's Well
Opal Hill Mine
Hauser Geode Beds
Walter's Camp
Oceanside
Anza-Borrego

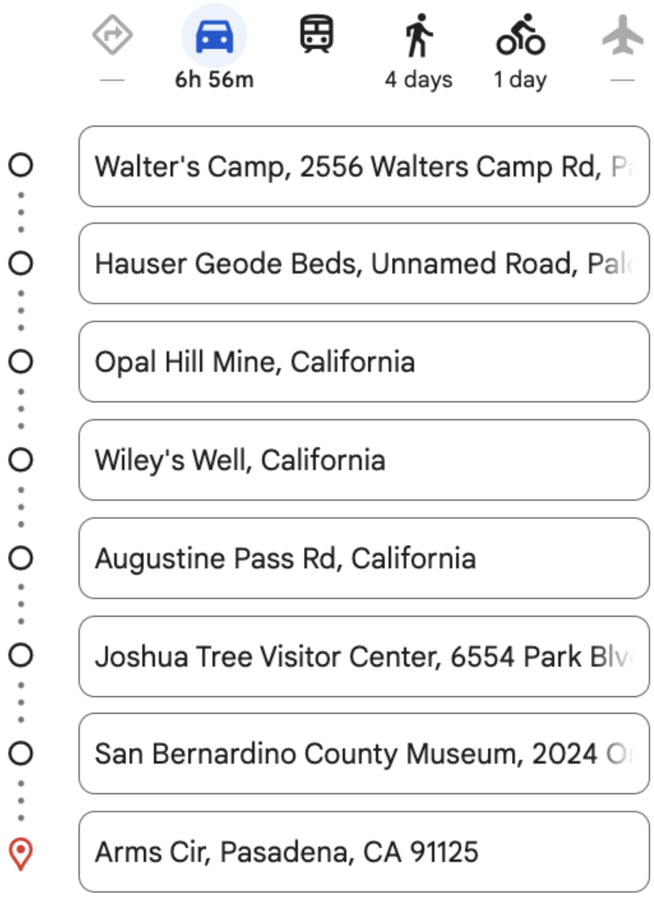
—
6h 56m
4 days
1 day
—

Walter's Camp, 2556 Walters Camp Rd, P

Hauser Geode Beds, Unnamed Road, Pal

Opal Hill Mine, California

Wiley's Well, California

Augustine Pass Rd, California

Joshua Tree Visitor Center, 6554 Park Blv

San Bernardino County Museum, 2024 O

Arms Cir, Pasadena, CA 91125

Clay Minerals:
Lake Elsinore and Beyond

Korbi Thalhammer

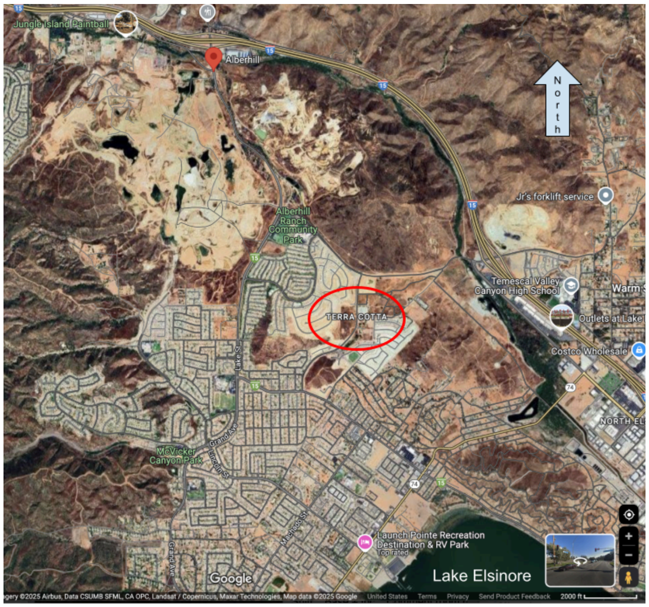
Jungle Island Paintball
Alberhill
North
Jr's forklift service
Alberhill Ranch Community Park
Temescal Valley Canyon High School
Warm
TERRA COTTA
Outlets at Lake
Costco Wholesale
NORTH EL
McVicker Canyon Park
Launch Pointe Recreation Destination & RV Park
Lake Elsinore
Google

At Lake Elsinore, white settlers have mined clay since the late 19th century at the area now known as Terra Cotta. Initially, the site also produced coal, which was used for processing about $20M worth of gold obtained at the Alberhill area and for heating nearby homes. The Alberhill region is also rich in clay and asbestos. Until WWII, when Lake Elsinore region clay production contributed to the war effort, clay was used to produce tile, brick, and pottery, including decorative figurines and vases. Today, Pacific Clay oversees clay production at Alberhill for brickmaking, although there are plans to develop the area for homes, presumably after a significant reclamation effort.

Argillaceous rocks contain significant proportions of clay. Two common examples are clay-rich limestone (marl) and greywacke (clay-rich sandstone).

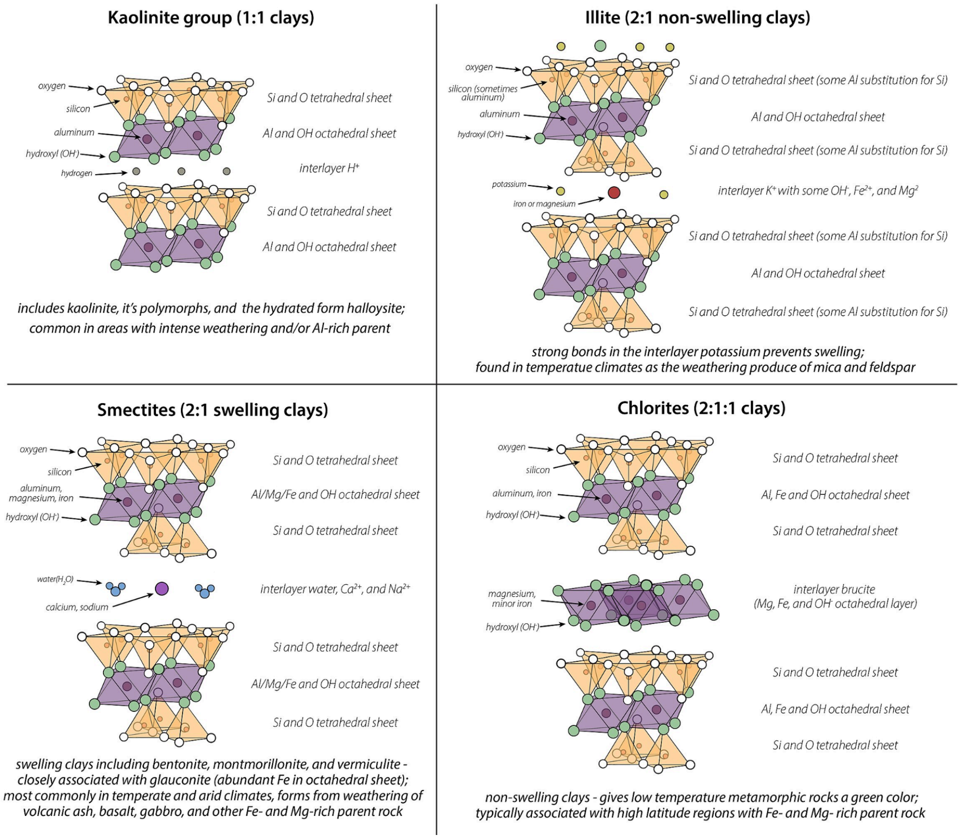

Kaolinite group (1:1 clays)

oxygen
silicon
aluminum
hydroxyl (OH)
hydrogen
Si and O tetrahedral sheet
Al and OH octahedral sheet
interlayer H+
Si and O tetrahedral sheet
Al and OH octahedral sheet

includes kaolinite, it's polymorphs, and the hydrated form halloysite; common in areas with intense weathering and/or Al-rich parent

Illite (2:1 non-swelling clays)

oxygen
silicon (sometimes aluminum)
aluminum
hydroxyl (OH)
potassium
iron or magnesium
Si and O tetrahedral sheet (some Al substitution for Si)
Al and OH octahedral sheet
Si and O tetrahedral sheet (some Al substitution for Si)
interlayer K+ with some OH-, Fe2+, and Mg2
Si and O tetrahedral sheet (some Al substitution for Si)
Al and OH octahedral sheet
Si and O tetrahedral sheet (some Al substitution for Si)

strong bonds in the interlayer potassium prevents swelling; found in temperatue climates as the weathering produce of mica and feldspar

Smectites (2:1 swelling clays)

oxygen
silicon
aluminum, magnesium, iron
hydroxyl (OH)
water(H2O)
calcium, sodium
Si and O tetrahedral sheet
Al/Mg/Fe and OH octahedral sheet
Si and O tetrahedral sheet
interlayer water, Ca2+, and Na2+
Si and O tetrahedral sheet
Al/Mg/Fe and OH octahedral sheet
Si and O tetrahedral sheet

swelling clays including bentonite, montmorillonite, and vermiculite - closely associated with glauconite (abundant Fe in octahedral sheet); most commonly in temperate and arid climates, forms from weathering of volcanic ash, basalt, gabbro, and other Fe- and Mg-rich parent rock

Chlorites (2:1:1 clays)

oxygen
silicon
aluminum, iron
hydroxyl (OH)
magnesium, minor iron
hydroxyl (OH)
Si and O tetrahedral sheet
Al, Fe and OH octahedral sheet
Si and O tetrahedral sheet
interlayer brucite (Mg, Fe, and OH- octahedral layer)
Si and O tetrahedral sheet
Al, Fe and OH octahedral sheet
Si and O tetrahedral sheet

non-swelling clays - gives low temperature metamorphic rocks a green color; typically associated with high latitude regions with Fe- and Mg- rich parent rock

The firing process drives off interstitial (~100ºC) and later structural water (~650ºC). Upon higher heating, sintering and remineralization occur, transforming the clay mineral's delicate silicate and alumina sheets into quartz (SiO_2), feldspar ($xAl(Al,Si)_3O_8$, with x Ca, K, or Na), and the needle-shaped aluminosilicate mullite ($3Al_2O_32SiO_2$ or $2Al_2O_3$ SiO_2).

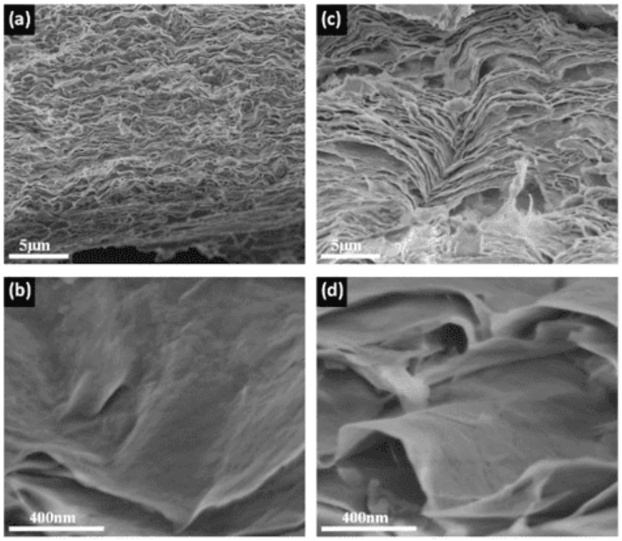

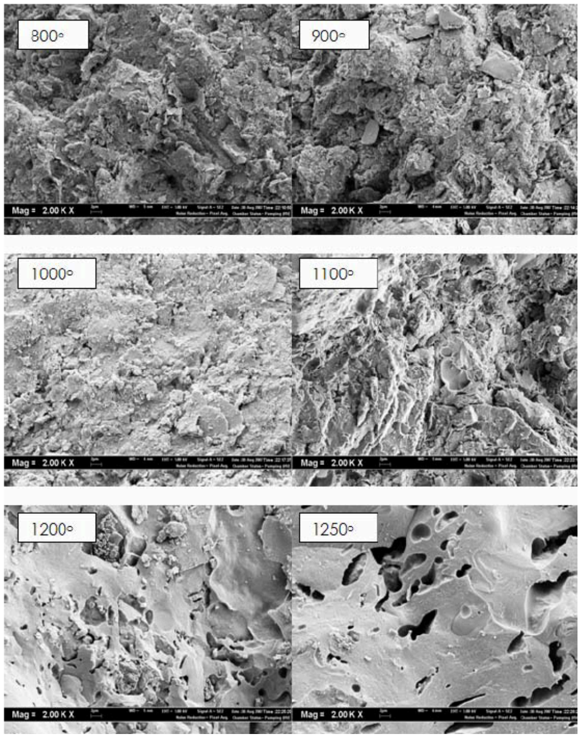

Clays catalyze diverse chemistries as a result of their incredible surface areas (often tens to hundreds of square meters per gram) and the large numbers of unsatisfied, reactive O-R bonds at those surfaces. Notable examples include regioselective RNA polymerization (mimicing the 5' to 3' bonding observed in modern organisms) and pollutant adsorption and degradation.

In smectite clays, iron can substitute for aluminum in the octahedral sheet and can change redox states, donating and accepting electrons to/from microbes and heavy metals.

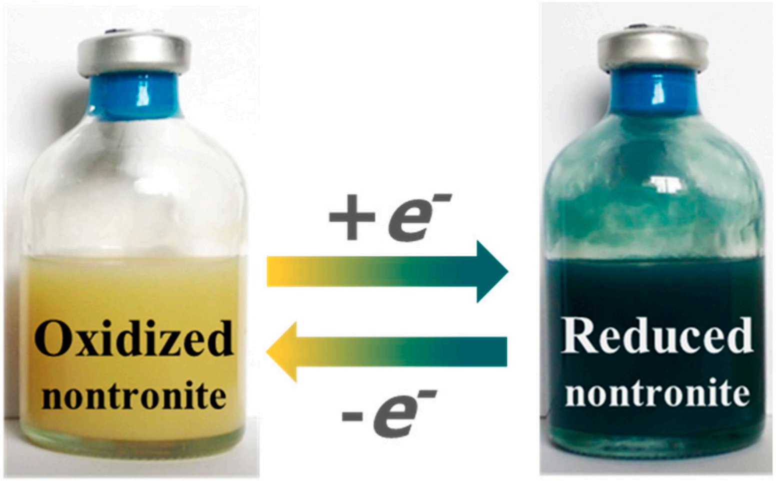

References:

1. **One-Step, Regioselective Synthesis of up to 50-mers of RNA Oligomers by Montmorillonite Catalysis.** Wenhua Huang and James P. Ferris. *Journal of the American Chemical Society.* 2006 *128* (27), 8914-8919. DOI: 10.1021/ja061782k
2. **The structure of montmorillonite gels revealed by sequential cryo-XHR-SEM imaging.** Mouzon, Johanne et al. *Journal of colloid and interface science* 465 (2016): 58-66. https://doi.org/10.1016/j.jcis.2015.11.031
3. **City of Lake Elsinore General Plan Update 2011.**
4. https://en.wikipedia.org/wiki/Clay_mineral
5. **Effect of the change of firing temperature on microstructure and physical properties of clay bricks from Beruas (Malaysia).** Johari, Izwan & Said, S. & Abu, Badorul & Bakar, B.H. & Ahmad, Zainal. (2010). Science of Sintering. 42. 10.2298/SOS1002245J.

The Petrogenesis of the Peninsular Ranges Batholith

Elizabeth Heiny

The Peninsular Ranges Batholith (PRB) is the largest segment of a Mesozoic continental arc that was generated by subduction of the Farallon oceanic plate beneath North America. The PRB was generated by a single sequence of magmatic activity that occurred between 140 and 80 Ma, but it was initially subdivided into two batholiths, the Eastern PRB (EPRB) and Western PRB (WPRB), based on changes in the distribution of rock ages. In the EPRB, U-Pb zircon ages range between 140-105 My and do not vary with geographic distribution ("static arc") while in WPRB, zircon ages range from 105 to 80 My and systematically decrease from east to west ("migrating arc") (Silver and Chappell 1988). Further analysis of the two batholiths also showed that they are chemically and isotopically distinct, and these differences presumably reflect differences in the paths of the magmas through the overlying crust. People still disagree over the details of the different paths (e.g., Bell and Kirkpatrick 2021; Kimbrough, Grove, and Morton 2015; Lee et al. 2007; Silver and Chappell 1988), so this is just a summary of some of the main observations and the most widely accepted conclusions.

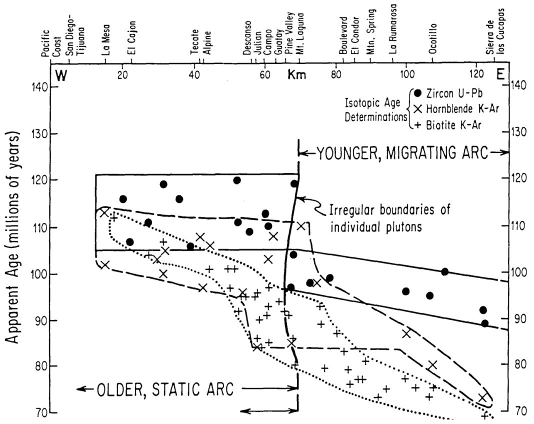

Figure 1 (from Silver and Chappell, 1988)

In both the EPRB and WPRB, plutons show differentiation trends that extend from gabbroic endmembers with nearly flat REE patterns, low initial $^{87}Sr/^{86}Sr$ ratios, and bulk chemical compositions that suggest that they were in equilibrium with mantle peridotite. As such, the most primitive magmas associated with both batholiths probably derived from a common, partially contaminated depleted mantle source (Kimbrough, Grove, and Morton 2015). However, the compositional differences between more evolved rocks in the WPRB and the EPRB indicate that differentiation paths followed by the primary magmas differed significantly between the two batholiths.

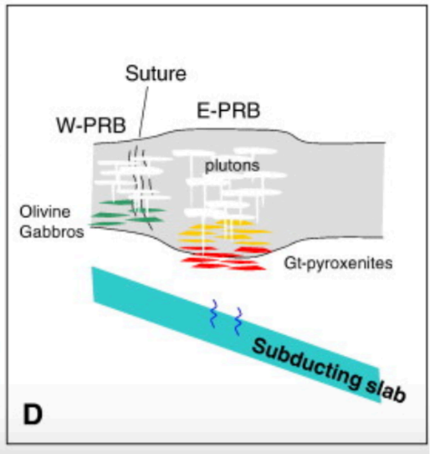

Figure 2 (from Lee et al., 2007)

In the WPRB, the beginning of the differentiation trend is defined by a decrease in MgO and increase in SiO_2 that is characteristic of olivine fractionation. Given the stability region of olivine, this implies that early differentiation in the WPRB occurred at relatively low pressure (<1 GPa). The presence of negative Eu anomalies (which are indicative of plagioclase fractionation) and uniformly low Gd/Yb ratios (which suggest that garnet was not involved) in the sequence further imply that that differentiation in the WPRB occurred exclusively at relatively low pressures (Lee et al. 2007; Silver and Chappell 1988).

In the EPRB, the beginning of the differentiation trend does not suggest olivine fractionation. Instead, the variations in MgO and SiO_2 imply the removal of a component with lower MgO and/or higher SiO_2 than olivine. Several authors have suggested that this most likely indicates pyroxene fractionation, which would be expected under both hydrous conditions and higher pressures. The high Gd/Yb and Sr/Y ratios of the EPRB plutons also suggest the presence of garnet sometime in their genesis (Lee et al. 2007; Silver and Chappell 1988). This further supports the hypothesis that differentiation began significantly deeper in the EPRB than in the WPRB. At the same time, negative Eu anomalies – although smaller than those in the WPRB – suggest plagioclase fractionation at some point during the differentiation path. Taken together, these observations imply that although differentiation likely began deeper in the EPRB, it continued to shallow levels similar to those of the WPRB (Silver and Chappell 1988).

Among all rock types in the WPRB (from gabbro to monzogranite), initial $^{87}Sr/^{86}Sr$ ratios are relatively low, $^{143}Nd/^{144}Nd$ ratios are relatively high, and $\delta^{18}O$ values are relatively low. These observations could imply that (i) the either the entire differentiation trend resulted from closed-system fractionation of magmas derived from slightly enriched mantle or (ii) the pre-existing crust assimilated by the magmas during differentiation was similar in age (e.g., the accreted Alisotos island arc terrane), such that the elapsed time between formation of the island arc, accretion, and subsequent continental arc magmatism was too short to permit significant isotopic evolution (Lee et al. 2007; Silver and Chappell 1988). The isotopic characteristics of the EPRB are quite different from those of the WPRB: initial $^{87}Sr/^{86}Sr$ ratios are higher and more variable, $^{143}Nd/^{144}Nd$ ratios are lower, and $\delta^{18}O$ values are higher than in WPRB. To first order, this implies significant assimilation and/or remelting of older crust/sediments during the formation of the EPRB, so most studies have concluded that the EPRB was emplaced through the Paleozoic continental margin of North America (Bell and Kirkpatrick 2021; Lee et al. 2007; Silver and Chappell 1988).

Bell, Elizabeth A., and Heather M. Kirkpatrick. 2021. "Effects of Crustal Assimilation and Magma Mixing on Zircon Trace Element Relationships across the Peninsular Ranges Batholith." *Chemical Geology* 586: 120616. doi:10.1016/j.chemgeo.2021.120616.

Kimbrough, David L., Marty Grove, and Douglas M. Morton. "Timing and Significance of Gabbro Emplacement within Two Distinct Plutonic Domains of the Peninsular Ranges Batholith, Southern and Baja California | GSA Bulletin | GeoScienceWorld." https://pubs.geoscienceworld.org/gsa/gsabulletin/article/127/1-2/19/126074/Timing-and-significance-of-gabbro-emplacement (February 5, 2025).

Lee, Cin-Ty Aeolus, Douglas M. Morton, Ronald W. Kistler, and Alexander K. Baird. 2007. "Petrology and Tectonics of Phanerozoic Continent Formation: From Island Arcs to Accretion and Continental Arc Magmatism." *Earth and Planetary Science Letters* 263(3): 370–87. doi:10.1016/j.epsl.2007.09.025.

Silver, L. T., and B. W. Chappell. 1988. "The Peninsular Ranges Batholith: An Insight into the Evolution of the Cordilleran Batholiths of Southwestern North America." *Earth and Environmental Science Transactions of The Royal Society of Edinburgh* 79(2–3): 105–21. doi:10.1017/S0263593300014152.

LCT Pegmatites: A Mineral Bonanza

Paolo Sanchez | Ge 136b | Winter 2025

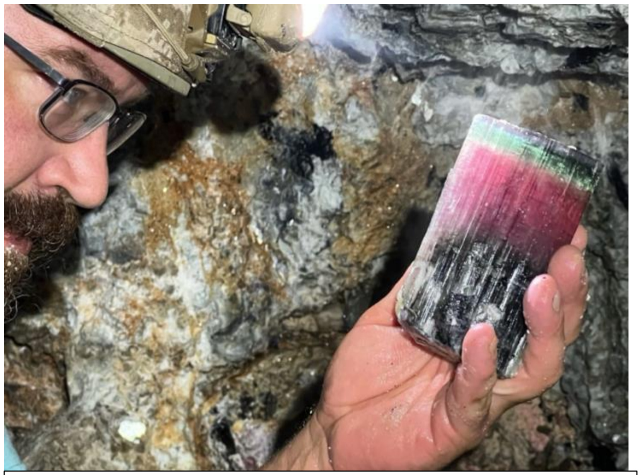

Figure 1: Kiel S., one of the miners of the Tourmaline King Mine in Pala, holding a museum quality elbaite tourmaline crystal freshly dug from a crystal pocket.

In a strict sense, pegmatites are defined as rigid, irregular or dike intrusive igneous bodies with a definitive mineralogical composition and, more famously, with distinctly large (cm to even tens of meters!) crystals [1]. Although pegmatites can exist from more mafic compositions, those that are particularly important to science are granitic pegmatites. Granitic pegmatites are host to the world's most valuable deposits of lithium, beryllium, critical metals, industrial minerals as well as gemstones and mineral specimens (Fig. 1).

What are LCT pegmatites? Granitic pegmatites are classified based on their mineralogy, and more recently, their trace element composition [2]. One important example is the lithium-cesium-tantalum (LCT) class of pegmatites, named after their enriched concentrations of these specific elements. All LCT pegmatites practically host quartz, muscovite, K-feldspars, tourmaline and garnet. Most examples also contain lepidolite (a Li-rich mica), spodumene (a Li-Al pyroxene) beryl, monazite, apatite, zeolites and a variety of rare phosphate and oxide minerals.

How do pegmatites form, and why such huge crystals? Similar to how granites are formed through the process of fractional crystallization and differentiation, granitic pegmatites begin forming when the last residual bit of melt is concentrated. As a cooling granitic body crystallizes, more elements that are easily incorporated into crystal structures (termed *compatible* elements) are extracted. The remaining melt is further concentrated in elements that have ionic charges or radii too difficult to fit neatly within a crystal lattice (termed *incompatible* elements, e.g. Li, Nb, U, Be, K). The result is a pegmatitic fluid that is very viscous and super enriched in incompatibles. One important inference is that pegmatitic fluids lack the necessary nucleation centers for crystals to properly form so that the fluid is supercooled and can exist ~150º-200ºC below granite's solidus [4]. This supercooling also explains why, despite a high viscosity, pegmatitic fluids can travel kilometers from their source pluton [4,6].

Contrary to how granites and other intrusive rocks get their large crystals from slow, gradual cooling, crystals in granitic pegmatites can grow extremely fast, up to a meter per day [6]! This is due to the process of nucleation centers finally forming when thermodynamic conditions make it ideal for crystals to form. One analogy to this phenomenon is taking a water bottle out of a freezer that still has liquid water. When a disturbance is applied, e.g. hitting the bottle on a hard surface, nucleation centers form and in seconds the water turns to ice. Such a low amount of nucleation sites also explains why crystals can be meters in size. As pegmatites represent the last drops of melt to crystallize, the last drops of a pegmatite to crystallize are supersaturated with water and other fluids and gases forming miarolitic cavities. These are the so-called "pocket minerals" that from beautiful gems (Fig. 1), large euhedral crystals, and rare mineral species.

Where can LCT pegmatites be found? LCT pegmatites are generally associated with peraluminous S-Type granites, granites that are derived from the melting of aluminum-rich sedimentary or metamorphic rocks. These pegmatites are largely found throughout ancient convergent margins, generally where subduction of oceanic lithosphere results in the partial melting of seafloor sediments (i.e., metapelites) that can have concentrations of lithium in the tens to hundreds of ppm [1]. This creates a granitic melt that can be further differentiated to make pegmatites. There are current studies which also suggest that LCT pegmatites are formed less from processes of differentiation and more from the anatexis of pre-existing country rock, where the intrusion of a hot magma results in the partial melting of country rocks that are already rich in the necessary elements to create LCT pegmatites [4]. Other well-known examples of LCT pegmatites are the pegmatites of Minas Gerias, Brazil, the Tanco pegmatite in Canada and the Koktokay pegmatite in China, [1].

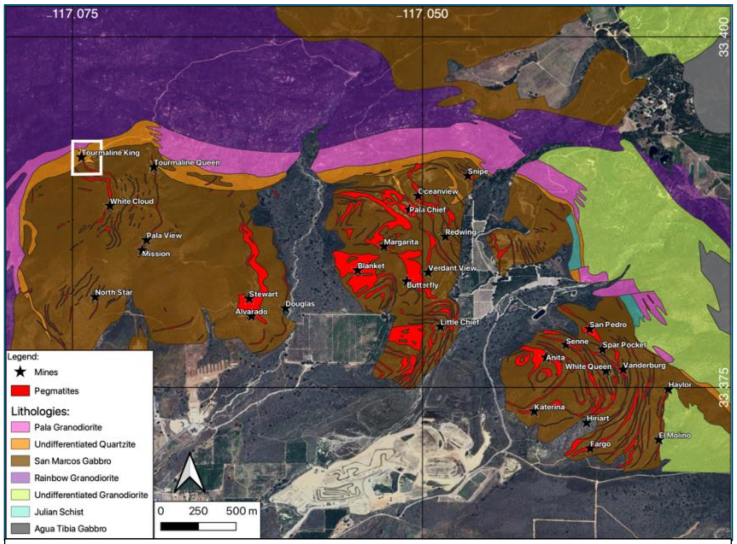
-117.075
-117.050
33.400
33.375
Tourmaline King
Tourmaline Queen
White Cloud
Pala View
Mission
North Star
Stewart
Alvarado
Douglas
Snipe
Oceanview
Pala Chief
Redwing
Margarita
Blanket
Verdant View
Butterfly
Little Chief
San Pedro
Senne
Spar Pocket
Anita
White Queen
Vanderburg
Haylor
Katerina
Hiriart
Fargo
El Molino
Legend:
★ Mines
🟥 Pegmatites
Lithologies:
Pala Granodiorite
Undifferentiated Quartzite
San Marcos Gabbro
Rainbow Granodiorite
Undifferentiated Granodiorite
Julian Schist
Agua Tibia Gabbro
0 250 500 m

Figure 2: Geologic map of the Pala Mining district, with pegmatite dikes in red. The white box indicates the Tourmaline King Mine, where active gem mining and geologic fieldwork is currently being done.

What makes Pala so special? The Pala Mining District of northern San Diego County is one of the world's richest LCT-pegmatite districts for gemstones and mineral specimens (Fig. 2). Gems, specifically elbaite (tourmaline), aquamarine, morganite, kunzite and crystal-clear quartz has been historically mined here since the 1800s [3]. Originally, many of the mines supplied rubellite, a red-pink variety of elbaite, to Qing Dynasty China where it was highly prized (_). For a moment in the 1930s-40s, lithium rich minerals were mined in the Stewart Mine to produce lithium grease. In the 1970s, a booming market of mineral collectors resulted in today's mines being some of North America's most famous localities for museum-quality tourmaline, spodumene and other pegmatite minerals.

However, identification of the magmatic source has remained elusive. They, like many other pegmatite districts in Southern California, are hosted not in granite, but instead in mafic gabbro [3,5]. In 1951, Jahns (a former Caltech professor known for pegmatology) and Wright [3] conducted the first in-depth geological study of the Pala pegmatites yet concluded that even though more felsic granodiorites do exist surrounding the pegmatites, isotopic and geochemical signatures between the pegmatites and the granodiorites do not correlate [5]. Today, the author of this report is conducting a detailed geochronologic and geochemical study to test if the pegmatites may be derived from the anatexis of surrounding metamorphic country rocks.

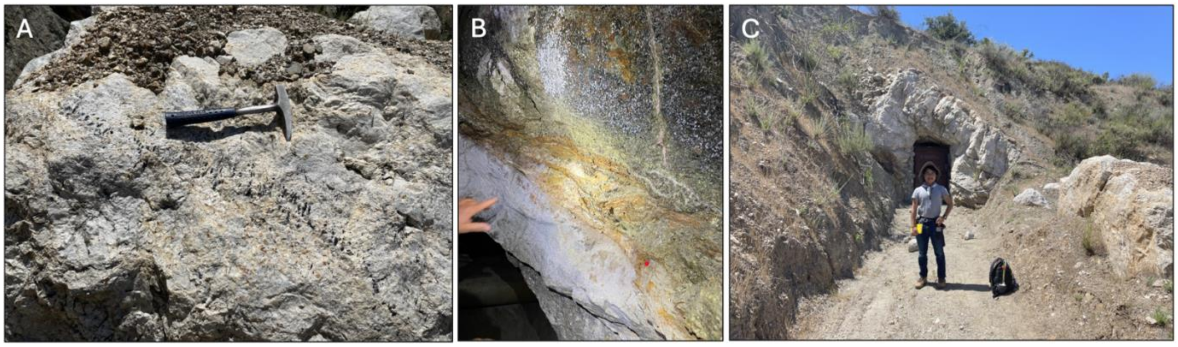

Figure 3: Field photos taken at the Tourmaline King Mine in northwestern Pala. A) Typical pegmatite with schorl (black tourmaline) in the Pala district. B) An altered contact between the pegmatite dike (bottom) with the host gabbro (top). C) The author in front of a currently mined, westerly-dipping pegmatite dike in background.

References: [1] Bradley, D.C., et al., 2017. 48p. [2] Cerny, P., Erict, T.S., *Can. Min.* [3] Jahns, R.H., Wright, L.A., 1951. 72p.[4] London, D.L. 2018. *Ore Geo. Rev.* [5] Morton, D.M., et al. 2018. *Lithos*. [6] Weber, K.L. et al. 1999. *Can. Min.*

Exploring Exoplanets and Nonsingular Stars

Marisa Langley

Acknowledgements: This report was inspired by David Ciardi's talk at the Palomar Science Meeting 2023.

Background: P3K, PHARO, and PARVI

Typically, atmospheric turbulence significantly distorts the vision of Earth-based telescopes. Adaptive optics (AO) is a technique which adaptively corrects for these effects, allowing telescopes to reach high angular resolutions. Palomar's adaptive optics system PALM-3000 (P3K) was implemented in 2009, and became the first adaptive optics system to be able to work in the range of visible light. P3K can deliver diffraction-limited images in both the near-infrared and visible range, and the system has undergone continual improvement over the years while making vast numbers of high-quality observations. In the figure below, we can see a comparison between a Spitzer Space Telescope image in 2005 and an image taken at Palomar in 2007 using the Hale Telescope.

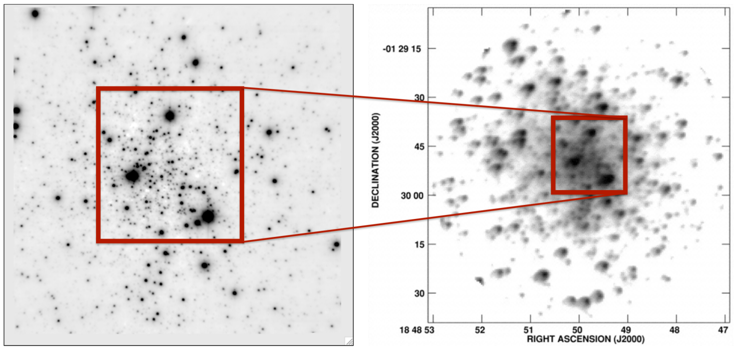

Figure 1: A figure from [11]. The fuzzy image on the right was taken by Spitzer from space, and the high-resolution image was taken at Palomar using the Hale Telescope.

One of P3K's goals was to study exoplanets, and it has used many other instruments to aid its study. Notably, it works in conjunction with the Palomar High Angular Resolution Observer (PHARO), an infrared imager, and the Palomar Radial Velocity Instrument (PARVI), a spectrograph for measuring the radial velocity of exoplanets. The Project 1640 instruments mounted on P3K perform low-resolution spectroscopy in order to help determine the compositions, temperatures, and surface gravities of exoplanets. Shown in the figure is an image from P3K of four planets in the HR 8799 system.

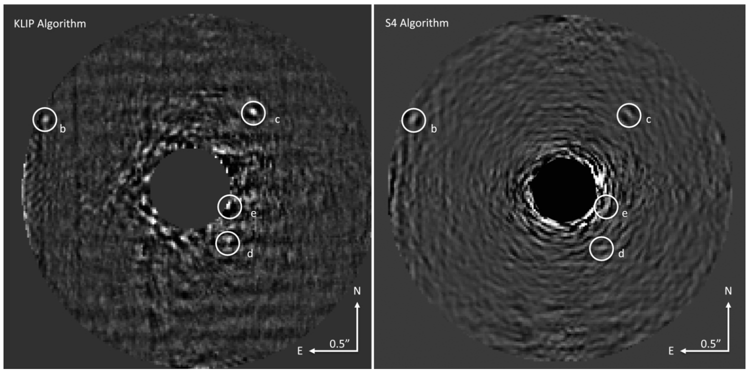

Figure 2: A figure from [9]. Four planets in HR 8799 are circled in the images. The two images are actually the same, they just show the usage of two different methods of speckle suppression.

(For this section, see [5], [10], [4], [1], [3], and [9].)

Exoplanets in Binary Systems

It is difficult to determine whether planets exist in binary star systems, and it has long been thought that the presence of more than one star could be detrimental to the formation and continued existence of planets [7]. A paper from 2016 used data from Keck Observatory to clarify the relationship between binary stars and planets, finding that wide binaries, in which the second star is far from the central star, are similar to single star systems and can easily host planets, while close binary systems, in which the two stars are close together, rarely host planets [7].

Another group, which did employ observations from P3K and PHARO, found that none of the 308 star systems they studied hosted planets and two stars within 50 AU of each other, and only one had planets and two stars within 100 AU of each other [6]. This study also suggested that the number of planets (0.1-10 M_J) in binary star systems was actually higher than in single-star systems. To the right is a figure from the paper showing the distributions for different types of systems.

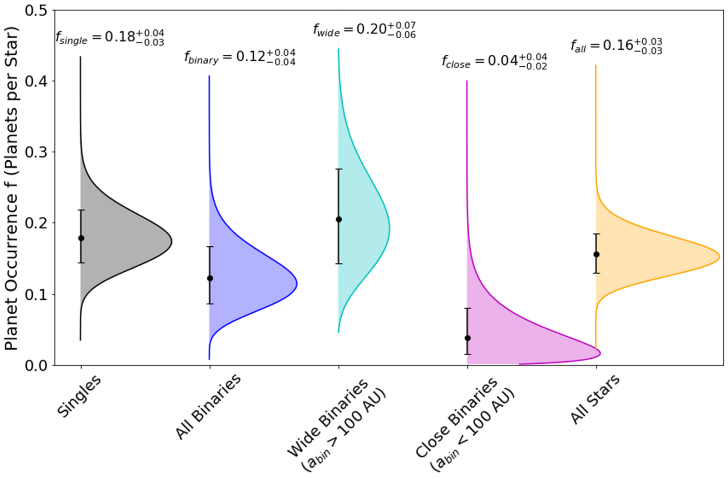

Kepler, K2, and TESS have identified large numbers of exoplanet and possible exoplanets in recent years, and Palomar has helped us learn more about them. One interesting usage of ground-based telescopes such as Hale has been in the identification of multiple stars in known planetary systems [8]. A group which studied planetary systems found by TESS using data from Gemini Observatory and WIYN Observatory found that the mean distance between the stars in binary systems hosting planets is 100 AU, which is much larger than the general mean distance between stars in binary systems, which is estimated to be 50 AU [8].

The discovery of stellar companions in planetary systems is useful. When calculating the radius of an exoplanet, we obtain different results depending on how many stars we assume the system has [2]. In particular, if you assume that a star system contains only one star when it actually contains multiple stars, you may significantly underestimate the radius of the planet [2], so Palomar's discoveries of stellar companions have helped us calculate the radii of the exoplanets.

References

[1] Antonin H. Bouchez et al. "Status of the PALM-3000 high-order adaptive optics system". In: *Astronomical Telescopes + Instrumentation*. 2009. URL: `https://api.semanticscholar.org/CorpusID:39540612`.

[2] David R. Ciardi et al. "UNDERSTANDING THE EFFECTS OF STELLAR MULTIPLICITY ON THE DERIVED PLANET RADII FROM TRANSIT SURVEYS: IMPLICATIONS FOR KEPLER, K2, AND TESS". In: *The Astrophysical Journal* 805.1 (May 2015), p. 16. DOI: `10.1088/0004-637X/805/1/16`. URL: `https://dx.doi.org/10.1088/0004-637X/805/1/16`.

[3] Richard G. Dekany et al. "First exoplanet and disk results with the PALM-3000 adaptive optics system". In: 2013. URL: `https://api.semanticscholar.org/CorpusID:215857366`.

[4] Richard G. Dekany et al. "PALM-3000: visible light AO on the 5.1-meter Telescope". In: *SPIE Astronomical Telescopes + Instrumentation*. 2006. URL: `https://api.semanticscholar.org/CorpusID:10653048`.

[5] Thomas L. Hayward et al. "PHARO: A Near-Infrared Camera for the Palomar Adaptive Optics System". In: *Publications of the Astronomical Society of the Pacific* 113 (2001), pp. 105–118. URL: `https://api.semanticscholar.org/CorpusID:55824223`.

[6] Lea A. Hirsch et al. "Understanding the Impacts of Stellar Companions on Planet Formation and Evolution: A Survey of Stellar and Planetary Companions within 25 pc". In: *The Astronomical Journal* 161.3 (Feb. 2021), p. 134. DOI: `10.3847/1538-3881/abd639`. URL: `https://dx.doi.org/10.3847/1538-3881/abd639`.

[7] Adam L. Kraus et al. "THE IMPACT OF STELLAR MULTIPLICITY ON PLANETARY SYSTEMS. I. THE RUINOUS INFLUENCE OF CLOSE BINARY COMPANIONS". In: *The Astronomical Journal* 152.1 (June 2016), p. 8. DOI: `10.3847/0004-6256/152/1/8`. URL: `https://dx.doi.org/10.3847/0004-6256/152/1/8`.

[8] Kathryn V. Lester et al. "Speckle Observations of TESS Exoplanet Host Stars. II. Stellar Companions at 1–1000 au and Implications for Small Planet Detection". In: *The Astronomical Journal* 162.2 (July 2021), p. 75. DOI: `10.3847/1538-3881/ac0d06`. URL: `https://dx.doi.org/10.3847/1538-3881/ac0d06`.

[9] B. R. Oppenheimer et al. "RECONNAISSANCE OF THE HR 8799 EXOSOLAR SYSTEM. I. NEAR-INFRARED SPECTROSCOPY". In: *The Astrophysical Journal* 768.1 (Apr. 2013), p. 24. DOI: `10.1088/0004-637X/768/1/24`. URL: `https://dx.doi.org/10.1088/0004-637X/768/1/24`.

[10] *Palm 3000*. URL: `https://ao.jpl.nasa.gov/palm3000.html`.

[11] *Palomar Adaptive Optics System*. URL: `https://ao.jpl.nasa.gov/palao.html`.

Palomar Observatory and Asteroids

Michael Sowell

The Telescopes

While the 200-inch Hale Telescope may be the most impressive telescope at Palomar Observatory, the first telescope to become operational at Palomar was actually the 18-inch Telescope, which saw first light on September 5, 1936 [1]. The 18-inch was a Schmidt telescope that took wide photographs, with frames spanning 8.75 degrees (imagine 17 full moons stretching across the photo) [1] [2]. In order to take these pictures, astronomers had to cut a circle out of film with a “cookie cutter,” then place this within a film holder, and finally position the film holder at the back of the telescope [1] [3]. The 18-inch was never updated to charge-coupled divide (CCD) detectors and was decommissioned after 1995. It is now on display purely for historical reasons, but one could imagine being an astronomer in the 20th century, scribbling numbers into a logbook at night and developing film by day [1].

While the 18-inch would one day become known for its use for surveying asteroids, the first asteroid survey at Palomar was actually its bigger brother: the 48-inch Samuel Oschin Telescope, which saw first light on September 29, 1948. The 48-inch Oschin was actually the second telescope to become operational at Palomar, as the 200-inch Hale saw first light on January 26, 1949. Like the 18-inch, the 48-inch Oschin is a Schmidt telescope, designed to take clear wide pictures of the sky. Unlike the 18-inch, the 48-inch Oschin is larger (duh) and still operational [1]. It was upgraded to CCD detectors in the year 2000 (I highly doubt the film detectors would have exploded during Y2K, however) [1].

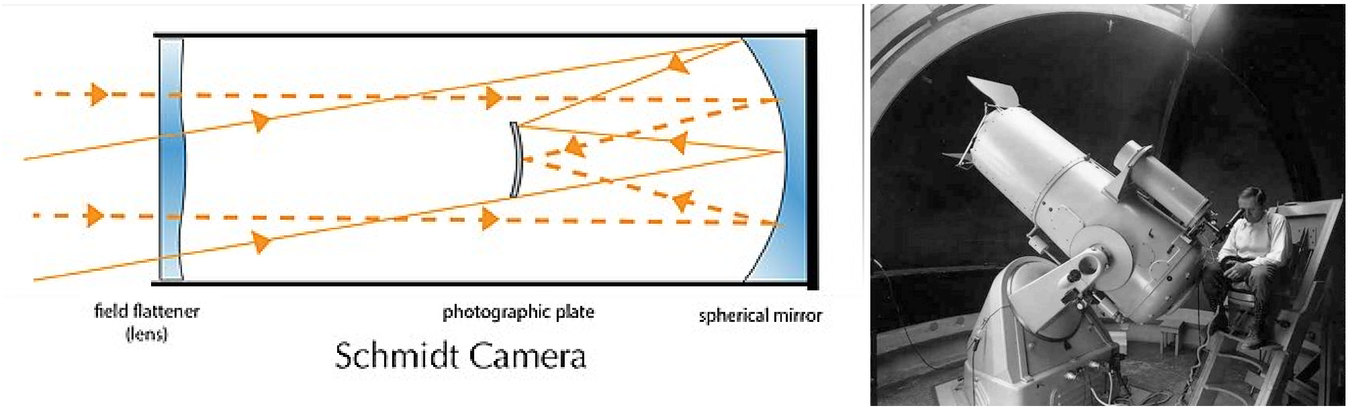

Left is a diagram of a Schmidt camera from Wikipedia. Right is a picture of Caltech’s Fritz Zwicky at the 18-inch from around 1936 [1].

Asteroid Surveys

The early history of both the 18-inch and the 48-inch telescopes revolved around characterizing and surveying supernovae and galaxies. In 1960, the 48-inch Oschin was used in collaboration with Leiden Observatory in the Palomar-Leiden Survey, which found over 2000 asteroids in just 11 nights of surveying. The 70s brought about 3 Palomar-Leiden Trojan Surveys, which found 500 asteroids in 1971, 1200 asteroids in 1973, and 1400 asteroids in 1977 [1].

Starting in 1973, the 18-inch telescope began to be used for asteroid surveys as well. The Palomar Planet-Crossing Asteroid Survey (PCAS) targeted specifically Earth-crossing asteroids and was manned by the prolific Eleanor Helin and the GPS Division's Eugene Shoemaker [1]. PCAS would make observations in 4- or 5-night "runs" each lunar cycle. On nights with "good seeing" (when atmospheric aberrations don't blur the stars much), they could photograph up to 35 areas of the sky. Each area (or field) was photographed in film, which would be developed immediately upon capture. Before the start of the next observing night, Helin and Shoemaker would study each frame with a microscope. Fast-moving objects would be tracked during the following runs, the goal of which were to obtain accurate ephemerides to characterize the orbits of each asteroid [2].

In 1982, Eugene Shoemaker left the PCAS project to work on the PACS project with his wife Carolyn Shoemaker [1]. The Palomar Asteroid and Comet Survey (PACS) was a "mom and pop" endeavor, funded only for film, housing, travel, and food, and was thus sustained by volunteer work from its collaborators and students from Northern Arizona State University and Lowell Observatory at Flagstaff. It discovered "44 near-Earth objects, 67 Mars crossers, 47 Jupiter Trojans, and many other asteroids of peculiar motion," as well as 33 comets. One of these comets was discovered on a particularly inauspicious night in 1993, with film that had been ruined by poor storage. Follow-up observations of Shoemaker-Levy 9 found that the comet had been torn into 21 little pieces by Jupiter's gravity, forming a "string of pearls" with an orbit decaying into Jupiter. A scientific wonder, SL9 crashed into Jupiter in 1994. It sparked an interest in asteroid safety, and the dust from its impact allowed astronomers to track Jupiter's winds [3]. I would recommend reading Carolyn Shoemaker's paper, as it provides a very personal perspective on the project [3].

The Shoemakers' PACS project ended in December of 1994, and Helin's PCAS project ended in June of 1995. The 18-inch was decommissioned in the mid-90s, but the 48-inch Oschin began a new asteroid survey with JPL's Near-Earth Asteroid Tracking (NEAT) program. This program ran from 2001-2007 and discovered 300 near-Earth asteroids and 13 comets. A survey of the new age, it was completely automated and computerized: an amazing feat considering the fact that just a decade earlier, the PACS program had been cutting film into circles with a cookie cutter [1]. I hope by now you appreciate the rich history of asteroid surveys on Palomar Mountain. It's quite amazing to me how the 18-inch was the first and only telescope at Palomar for 13 years, yet made such great contributions to science.

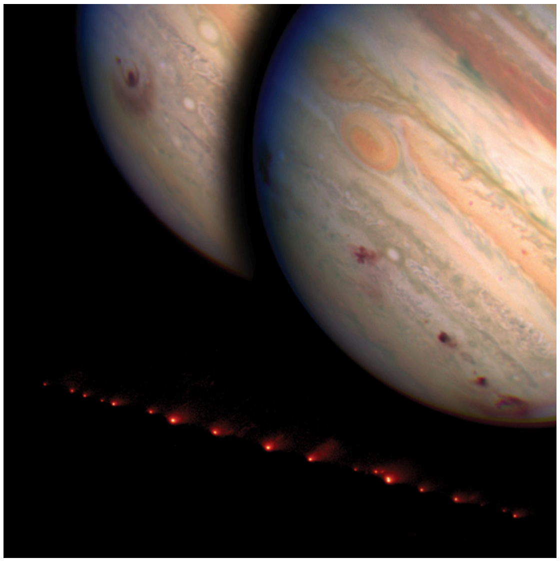

On the left is Gene and Carolyn Shoemaker posing in front of the 18-inch [1]. On the right is a Hubble picture of Comet Shoemaker-Levy 9, which has been described as a "bead of pearls" [1].

[1] "Welcome to Palomar Observatory." https://sites.astro.caltech.edu/palomar/homepage.html [2] Helin and G. Shoemaker (1979). https://doi.org/10.1016/0019-1035(79)90021-6 [3] C. Shoemaker (1995). https://adsabs.harvard.edu/full/1996JRASC..90...18S

Uranian Satellites Discovered at Palomar Observatory

Elin Stenmark

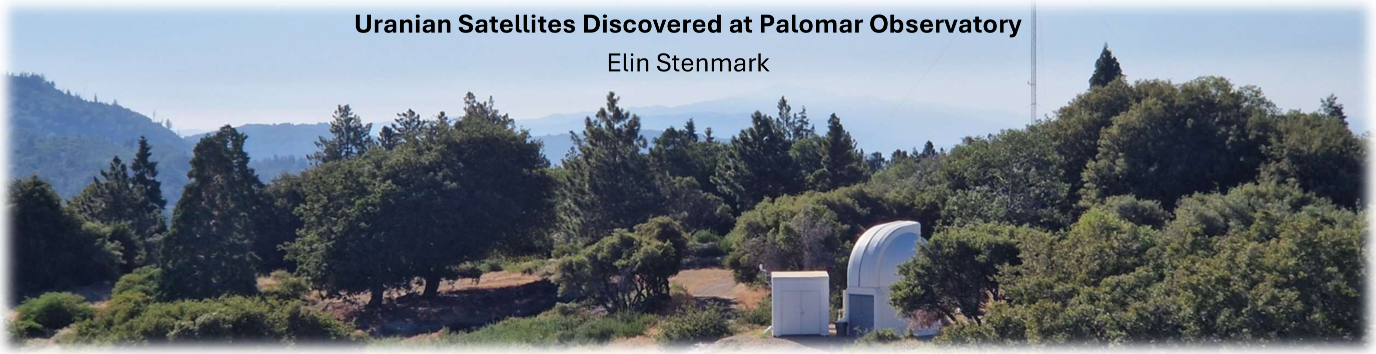

In 1997, Gladman et. al. [1] discovered two Uranian moons using the 200-inch Hale telescope on Palomar Mountain. Named Sycorax and Caliban, after the mother-son duo in Shakespeare's play *The Tempest* [2], they continued the tradition of naming Uranian moons after characters from the works of Shakespeare and Alexander Pope.

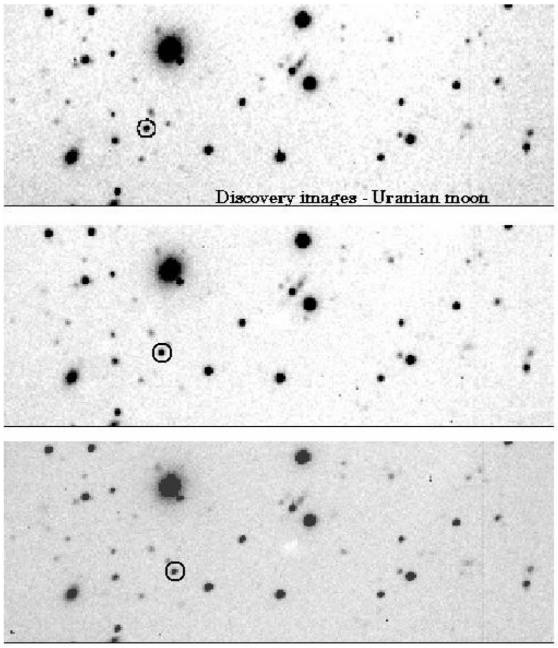

Fig 1: The September 7, 1997 discovery images of Sycorax (circled) [1]. Each panel is photographed in ca. one-hour intervals.

The moons were the first in the Uranian system to be labeled "irregular", characterized by their eccentric, retrograde orbits, evidence that they may have been captured later in the Solar System's lifetime instead of coevolving with Uranus since their formation. Other lines of evidence for this include rotation frequencies and thermal emission modelling [5] that seem to match that of Trans-Neptunian Objects (TNOs) better than other gas giant satellites [6].

On the Magnitude of Species. In astronomy, magnitude is measured on an inverse logarithmic scale, with the apparent magnitude "m" denoting the brightness of an object as seen from an observer's POV. The zero point of the magnitude scale was arbitrarily chosen to match the apparent magnitude of Vega, a 25-lightyear distant, bright star in the constellation Lyra. Astronomers use the bottom left relation to convert between apparent magnitude m and radiative flux f of two celestial bodies.

$$\mathrm{m}_1 - \mathrm{m}_2 = -2.5\log_{10}\frac{\mathrm{f}_1}{\mathrm{f}_2}$$

As a caveat, different bodies radiate or reflect light in different amounts across the electromagnetic spectrum. To account for this, a bolometric magnitude can be employed, wherein the brightness contribution is integrated across all wavelengths.

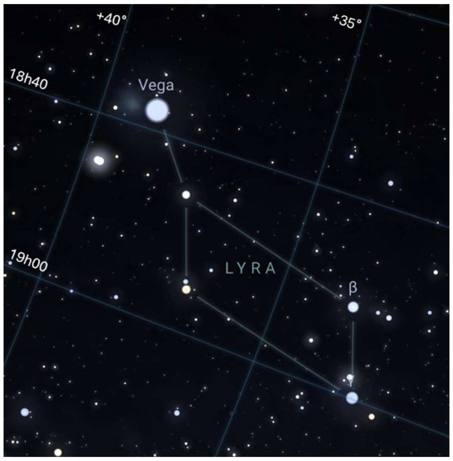

Fig 2: The constellation Lyra, feat. the star Vega, used as calibration for the apparent magnitude scale. Image credit: Stellarium Web.

The brightest object in the sky is of course the Sun, at m=-26.7, with Uranus at m=+5.5, above the typical Naked Eye Limiting Magnitude (NELM) of +6 [4]. Unfortunately, you will not be able to spot Caliban or Sycorax, as they require an exposure time on the order of an hour to be seen even by the 200-inch telescope.

Banner image taken by ES from the 200-inch dome balcony.

Table 1: Characterization of Caliban, Sycorax and S/2023 U1 at the time of their respective discoveries.

Moon	Temporary designation	Discovery Number	Apparent magnitude	Diameter [km]	Orbital period [d]	Semi-major axis [R_U/AU]	Eccentricity
Caliban	S/1997 U 1	16	21.9	30	654	305/0.0521	0.2
Sycorax	S/1997 U 2	17	20.4	60	495	253/0.0432	0.4
TBD	S/2023 U 1	28	26.6	7	679	312/0.0533	0.187

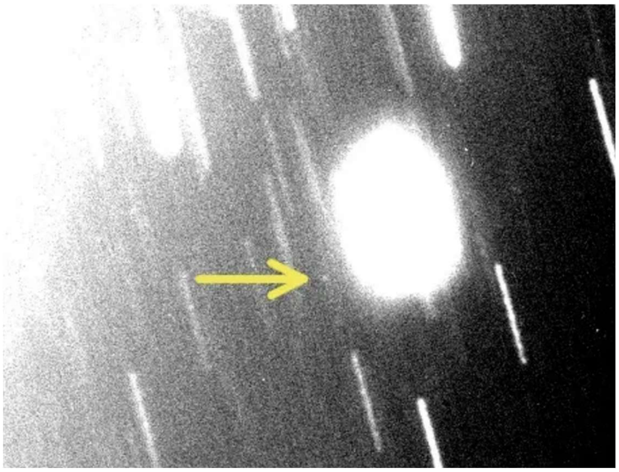

Fig 3: The discovery image of S/2023 U 1 captured by the 6.5m Magellan telescope at Las Campanas Observatory in Chile [3].

Since Gladman et. al.'s publication, 11 new moons have been discovered, the latest of which is S/2023 U 1 [3], which has yet to be named – perhaps you can come up with a fitting suggestion following the Shakespearean naming convention?

See table 1 for a summary of the characteristics of Caliban, Sycorax, and S/2023 U 1. Note, in particular, the increased precision with which we have detected recent satellites, both in terms of the higher resolution, reflected in the smaller diameter and much fainter magnitude, as well as more precise eccentricity measurement. In fact, using the equation on the previous page, we find that S/2023 U 1 is about 250x fainter than Caliban and Sycorax!

According to Sheppard et. al., all Uranian satellites greater than 8 km and/or with magnitude <26.5 should now be discovered, given that the moons have albedos >0.1, i.e. reflect 10+% of the incident sunlight [3].

[1] Gladman, Brett J., et al. 'Discovery of Two Distant Irregular Moons of Uranus'. *Nature*, vol. 392, no. 6679, Apr. 1998, pp. 897–899, https://doi.org/10.1038/31890.

[2] Shakespeare, William, 1564-1616. *The Tempest.* Cambridge: Harvard University Press, 1958.

[3] Sheppard, Scott S., et al. 'New Moons of Uranus and Neptune from Ultradeep Pencil-Beam Surveys'. *The Astronomical Journal*, vol. 168, no. 6, Dec. 2024, p. 258, https://doi.org/10.3847/1538-3881/ad7fed. arXiv.

[4] Texas Parks & Wildlife. (2023). *Astronomy Definitions*. https://tpwd.texas.gov/state-parks/park-information/links/astronomy-definitions. Accessed 2/7/2025

[5] Farkas-Takács, A., et al. "Properties of the irregular satellite system around Uranus inferred from K2, Herschel, and Spitzer observations." *The Astronomical Journal* 154.3 (2017): 119.

[6] Lellouch, E., et al. "“TNOs are Cool”: A survey of the trans-Neptunian region-IX. Thermal properties of Kuiper belt objects and Centaurs from combined Herschel and Spitzer observations." *Astronomy & Astrophysics* 557 (2013): A60.

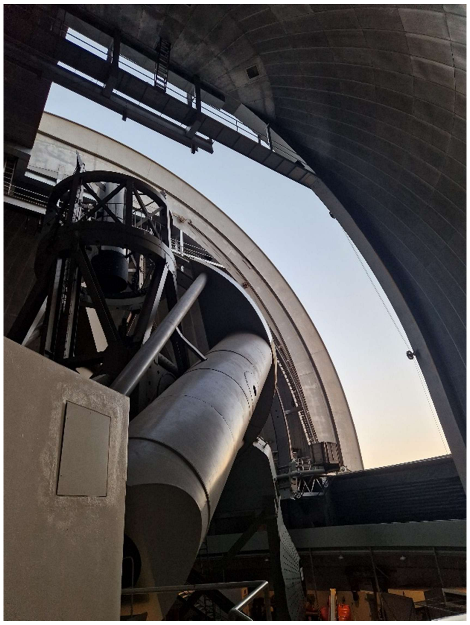

Fig 4: The Palomar 200-inch Hale telescope. Image taken by ES from inside the opened protective dome.

Palomar and the expansion of the universe

Tejas Oke

1 The Doppler effect and Hubble

Have you ever noticed how an ambulance siren sounds higher-pitched as it approaches and lower-pitched as it moves away? That's the **Doppler Effect** in action! Here's what's happening: When the ambulance moves toward you, the sound waves in front of it get compressed. This means the sound waves reach your ears more frequently, making the pitch higher. When the ambulance moves away from you, the sound waves get stretched out, making the pitch lower. This happens with any moving sound source—cars, trains, even a person shouting while running toward or away from you.

The same effect happens with light, but instead of hearing a pitch change, we see a color change. If an object is moving toward us, its light waves get compressed, shifting the color toward the blue end of the spectrum (higher frequency than the actual)—this is called blueshift. If an object is moving away, its light waves stretch out, shifting the color toward the red end of the spectrum—this is called redshift. This is particularly useful in measuring the relative displacement of astronomical objects as we have their reference wavelengths (based on for example their composition and temperature) and observed wavelengths (see [1] for more details on this). American astronomer Vesto Slipher at Lowell Observatory made the first measurements of redshifts in spiral nebulae (now known as galaxies). By 1917, he found that most of these nebulae were moving away from us at enormous speeds—much greater than typical stellar motions. However, at the time, it was still debated whether these nebulae were part of the Milky Way or separate galaxies. Using the 100-inch Hooker Telescope at Mount Wilson (Yes, the one visible from Caltech!), Edwin Hubble measured distances to galaxies using Cepheid variable stars (see [2] for more details) as cosmic distance markers. When he compared galaxy distances with Slipher's redshift data, he found a striking pattern: the farther a galaxy was, the more redshifted its light was.

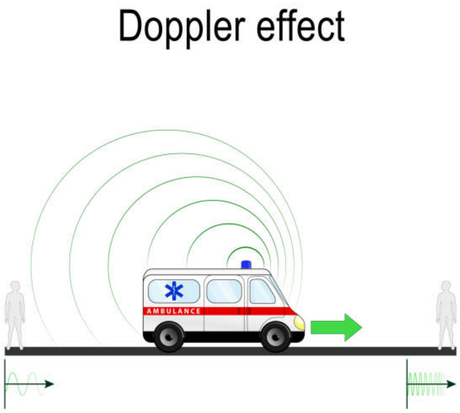

Figure 1: Doppler effect with sound

2 The Hubble's law

Hubble discovered a relation between the distance and the redshift that the velocity that an astronomical object is moving away is directly proportional to the distance of the object. This can be written mathematically as existance of a constant H_0 such that v (which is the velocity with which the star is moving away) and d (the distance of the star from the Earth) satisfy,

$$v = H_0 d.$$

Hubble's estimate for the constant H_0 was 500 km/s/Mpc. What does that mean? Mpc also called as the Megaparsec is a unit of distance (1 Mpc = 10^6 Parsec = 3.26×10^6 lightyears). And the number 500 km/s/Mpc means that an object at a distance of 1 Mpc is moving away from us at a enormous velocity of 500 km/s!

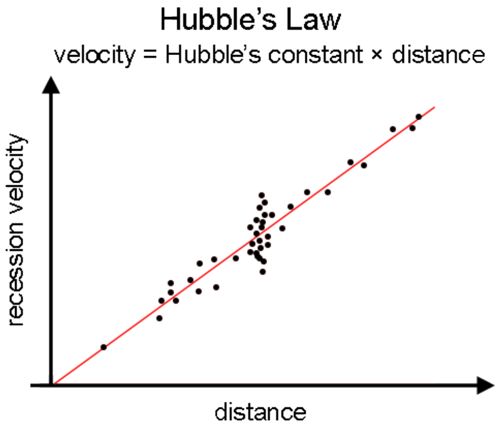

Figure 2: Linearity of distance and velocity: Hubble's law

3 Palomar and refinements to H_0

The Hubble's measurement of the constant of expansion of universe was a revolution and while his measurement of the constant was within a fair range of the modern value in terms of order of magnitude, it was very far from accurate. The main obstacle for the accurate observations was lack of very powerful telescopes with high light collection (large aperture) to reliably observe redshift in far away galaxies. This was to a large extent addressed after the construction of the 200-inch Hale telescope at the Palomar observatory. The Hale telescope was named after astronomer and telescope builder George Ellery Hale.

One of the key figures in refining the Hubble constant was Allan Sandage (PhD student at Caltech at that time!), who was a student of Hubble, used the Hale Telescope extensively in the 1950s and 1960s. Sandage systematically re-evaluated galaxy distances and redshifts, correcting errors in Hubble's original measurements. His work helped bring down the estimate of from Hubble's initial 500 km/s/Mpc to a much lower estimate of 55-75 km/s/mpc, which is ver close to the modern estimated value using space based telescopes.

4 Fun Fact

While most galaxies in the universe are redshifted due to cosmic expansion, the Andromeda Galaxy is an exception—it is actually blueshifted. This means Andromeda is moving toward the Milky Way rather than away from it. Currently, it is approaching at a speed of approximately 110 km/s, and astronomers predict that in about 4.5 billion years, the Milky Way and Andromeda will collide and eventually merge into a single galaxy.

Figure 3: Hale telescope at Palomar observatory

References

[1] Jason P. Aufdenberg. "Stellar Spectroscopy". In: *Encyclopedia of Physical Science and Technology (Third Edition)*. Ed. by Robert A. Meyers. Third Edition. New York: Academic Press, 2003, pp. 15–44. ISBN: 978-0-12-227410-7. DOI: `https://doi.org/10.1016/B0-12-227410-5/00735-3`. URL: `https://www.sciencedirect.com/science/article/pii/B0122274105007353`.

[2] Wikipedia contributors. *Cepheid variable — Wikipedia, The Free Encyclopedia*. `https://en.wikipedia.org/w/index.php?title=Cepheid_variable&oldid=1274156872`. [Online; accessed 7-February-2025]. 2025.

Kumeyaay Culture, History and Material Artifacts of San Diego County

Material evidence of the civilization from San Pasqual through Baja stretches back to 1000-1200 years ago. Those archaic eras are grouped by changes in technology of basket weaving, pottery and eventually linguistics. The early speakers of the Yumayan language established pottery-using agricultural communities along the Colorado River and trade routes with the surrounding peoples beginning in 700AD. By 1000 AD cultural traditions centered on the coast and valley and the desert emerged, these were the Kumeyaay peoples, who inhabit the lands stretching from the coast near oceanside to Baja California in this late modern period and persist there to this present day.[8]

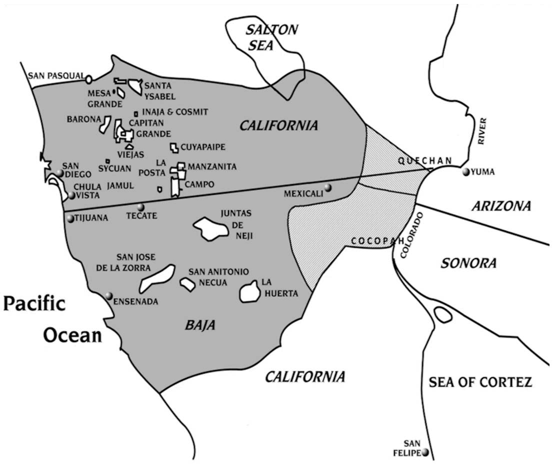

The Kumeyaay Nation, sourced from [11]

The Kumeyaay (Kū-mē-yai) were seasonally nomadic, traveling between summer and winter villages to maintain access to game, seasonal plants and other resources. Much of the tangible archeological remains of the peoples of this areas are lost as the nomadic nature of their society did not lend itself to permanent scturcute, in fact summer villages were burned upon leaving for the winder villages [4], and much of their original lands and settlement have been targeted by foreign settlement beginning with the Spanish colonizers. Therefore much of the exact meaning and contexts of the remaining village complexes, petroglyphs and evidence of materials quarried from the Cumyacca mountains must be speculated on using the oral histories of the modern Kumeyaay people and modern ethnography practices. This article will give a very general overview of the nature of the Kumeyaay culture and material features of culture remaining in the landscape of southern California with a focus on those in Anza-Borrego park.

The Kumeyaay people were made up of patriarchal family groups called Sh'mulq who each maintained specific seasonal villages and lands. Many Sh'mulq congregated seasonally in specific areas for resources, festivals, trade, as well as occasions for exchange of people through marriage and family ties. Men were expected to marry outside of their family joining the woman's Sh'mulq, therefore the leaders (Kwaipai) of a Sh'mulq were often from an outside family,[3] titles could be inherited but they could often be appointed or chosen as part of the congregation of these many bands.[3] The villages of consisted of many dwellings made of woven structure matched with grasses, these could dug out into the ground and sometimes incorporated natural rock features as part of the building structure. Foundations of these houses and the cremated remains of the dead what markes historical kumeyaay villages.[4,9]

The oak and pine groves of Torrey state part, would have been such a place to gather for access to water and the traditional food sources, namely acorns of the coastal live oak, but food sources also included pinyon nuts, choke cherries, manzanita berries, tepary and mesquite beans, yucca, and mescal, as well as game and fish from the area. These places of habitation are often marked with metate, round indentations in the stone for the purpose of riding acorn meal, or smaller marks, known as cuple, for the purpose of cracking acorns.[4]

There is evidence of extensive trade networks with the neighboring tribes, as well as conflicts. Kumeyaay village sites in the Cuyamaca Mountains, Mason valley and Anza-Borrego park include notable collections of shell beads which was a common material of exchange and potentially currency for the Chumash natives of the Santa Barbra area.[5] The Kumeyaay also have evidence of trading quarried Obsidian from the obsidian butte and extensive evidence of quarrying of the soapstone features of the Cuyamaca mountains.[10] Soapstone in particular is used for a number of specialized tools such and arrow shaft straighteners and blowing straws, warming stones and the soapstone powder is also used in coming of age rituals for both men and women. A cross hatch pattern on soap stones is noted as a common feature of artifacts created for these important cultural traditions.[10] The small cuple which are sometimes used to crack acorns are also speculated to have strong cultural significance. Many historical and modern accounts attribute certain stones to have aspects of power to certain stones thus grinding material, such as pigments of herbs, ground in specific cuple could be a type of ritual to access these attributes. Some cuple patterns have been identified to be representative of constellations, and associated with game trails.[6] Outcrops of the mineral phonolite, a fine grained type of syenite with the composition of Nephelin is featured in several historical accounts as "ringing stones" to be struck by great warrior of the Kumeyaay to ask for approval from deities on military endeavors (often against the Quechan) or hunts as these rocks produce a rising sound when struck.[1]

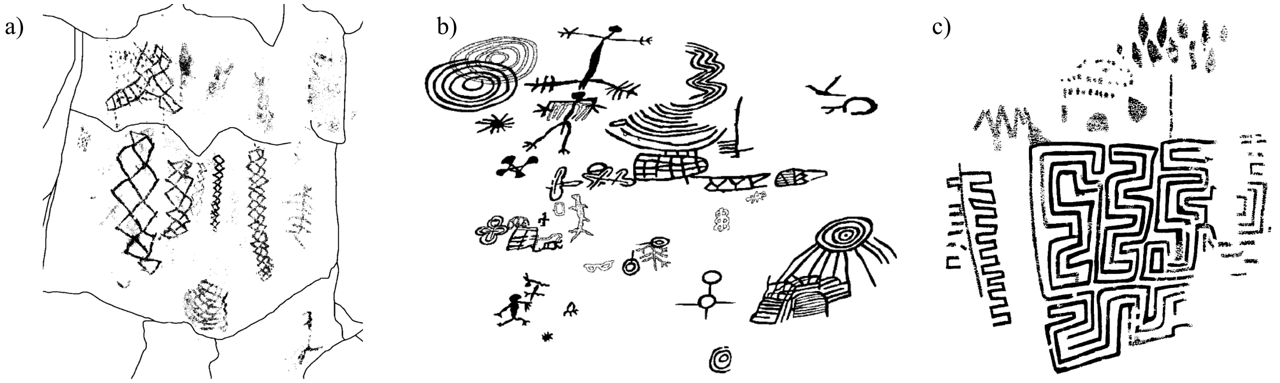

a) San Luis Rey style from San Margarita River, Camp Pendelton, San Diego county b) La Rumorosa style in Las Pilitas, Baja California c) Rancho Bernardo style from Deidra's Pintadas, San Diego County, all images sourced from [7]

Petroglphys appear near many Kumeyaay villages which are attributed to be contemporary with the habitation. However, as stated before, the Kumeyaay were not the first civilization in the territory they occupied, Some petroglyphs of souther California and Baja are prehistoric, and the styles are not localized enough to attribute a specific style to a specific group, it was likely multiple styles were created by a variety of groups over many centuries.[7, 9] Dating Petroglyphs is specific to their creation. Some are scratched into the "desert varnish," a layer of manganese oxide which builds up on exposed rock in desert regions, the weathering build up of vanish can be a method of dating these petroglyphs by comparing the build up of surrounding varnish. For petroglyphs painted with iron oxides, the relative ratio of the more mobile cations (Ca and K) versus the larger les mobile ions (Ti, Zr) can be compared. This ionic Ratio can establish the relative age of features which then can be compared to isotope studies to create an absolute dating range.[12] It is unclear that a chronology has been established for San Diego county petroglyphs yet (I could not find one) but for the petroglyphs of the San Bernadino mountains, most were dated around 1000 years ago. The petroglyphs of Kumeyaay lands are mostly in the San Luis Rey, La Rumorosa and Rancho Bernardo styles. The exact origin and purpose of the petroglyphs is debated, the petroglyphs are found along game routes, and may be associated with astronomy the Kumeyaay's seasonal migration but also may have all be created by other peoples passing through Kumeyaay lands following game, or predate Kumeyaay culture. It is known in Kumeyaay tradition that both the spring and winter solstice's are recognized, Therefore their people had knowledge of the astronomical cycles that indicated these times of year, however no specific connection of astronomy to their petroglyphs has been consistently established.[8]

Beginning in the 1752 the creation of the Spanish missions began to impinge on the traditional nomadic patterns of The Kumeyaay as the missions (notably San Diego) was placed on the site of a kumeyaay village with a military fort to maintain it. The missions depended on forced labor from the natives they displaced and were set on christianizing the people of the area, while some were converted, it is noted that a number of roof and floor tiles in the missions at San Diego and san Luis Rey, which would have been constructed by natives, bear symbols similar to those seen in petroglyphs of the region, including the characteristic crosshatching associated with Kumeyaay soapstone artifacts[2]. Despite the threat of the Missions, they were also a source for trade and exchange, some Sh'mulqs stayed in the orbit of the Missions for access to European goods of glass beads, and linen. The Spanish also introduced many new species of flora and fauna to the lands hoping for the spread of their familiar agricultural species, including many grazing and foraging animals which began to degrade the ecosystem and water quality.[2, 4]

In 1775 after the years of forced labor and rampant sexual assault within in the missions and fort, the Kumeyaay attacked the fort of San Diego, burning the mission to the ground, killing the Bishop, and driving the Spanish settlers to the coast. The missions were subsequently secularized but the the Spanish settlers remained a presence of the area and continued to attempt to extract resources and labor from the Kumeyaay. The Kumeyaay's land was further divided with the Mexican revolution in 1821 as the part of the land became part of the new Mexican republic. A series of violent outbreaks occurred between the Mexican settlers as they attempted to wrest control of the their newly government granted lands from the inhabitants. This culminated in a siege of San Diego, which, while unsuccessful at taking the city, cut off all Mexican land routes past the Colorado river, in part due to similar resistance from the Quechan in the east.

The Kumeyaay's remained largely neutral in the Mexican-American War. The final treaty of the Mexican-American solidified the split of Kumeyaay lands between the border of the two countries. Many bands of the northern Kumeyaay in American territory joined efforts with the Quechan in the Yuma wars where the natives of the south west fought to protect their people from the growing violence from American settlers moving west in search of gold and land, this preceded the organized effort of the American and California government to fully eliminate these peoples in what is known as the California Genocide. During the war a set of Kumeyaay leaders traveled the National US government to seek legal protections from the settlers and the state funded militias. This became part of the 18 treaties of California, which eventually became part of the modern reservation system. [4] The treaties offered little protection and the serial killings of natives by white militia groups continued until the 1890's. The Kumeyaay suffered fewer losses than other peoples as the pursuit of gold containing lands was largely north of their territory and many Kumeyaay persisted in rural villages in the mountains continuing their historical way of life, evidence of habitation in the Cuyamaca mountain villages lasts as late 1870.[5, 9] It is estimated two thirds of the Kumeyaay people were killed in the genocide.

To this day the Kumeyaay people are divided by the US-Mexican Border, efforts to secure safe passage between the US reservations and those in Baja Mexico has been a regular source of conflict with the US government. The Kumeyaay community college still teaches their language and History to this day and the tribal government operates out of San Diego county.

Sources:

[1] Carrico, R. L. (2011). 'Awi Kuseyaay: The Ringing Rock of San Bernardo. *Journal of California and Great Basin Anthropology*, *31*(1), 98–101. http://www.jstor.org/stable/23215390

[2] Carrico, R. (01 2018). *Kumeyaay Inscriptive Art at Three Spanish Colonial Period Sites in San Diego: Cultural Continuity, Syncretic Behavior, or Resistive Art?* 81–92.

[3] Gamble, L. H., & Zepeda, I. C. (2002). Social Differentiation and Exchange among the Kumeyaay Indians during the Historic Period in California. *Historical Archaeology*, *36*(2), 71–91. http://www.jstor.org/stable/25616993

[4]Gamble, L. H., and Wilken-Robertson, M. (2008). *Kumeyaay Cultural Landscapes of Baja California's Tijuana River Watershed. Journal of California and Great Basin Anthropology*, 28(2), 127–152. http://www.jstor.org/stable/27825888

[5] Gamble, L. H., King, C. D. (2011). Beads and Ornaments from San Diego: Evidence for Exchange Networks in Southern California and the American Southwest. *Journal of California and Great Basin Anthropology*, *31*(2), 155–178. http://www.jstor.org/stable/23215649

[6] Hector, S. M. (2009). Cupule Petroglyphs as Elements of the Cultural Landscape. *Journal of California and Great Basin Anthropology*, *29*(1), 68–76. http://www.jstor.org/stable/27825903

[7] Hedges, K. (2002). Rock Art Styles in Southern California. *American Indian Rock Art*, *28*, 25–40.

[8] Hudson, T., Lee, G., & Hedges, K. (1979). Solstice Observers and Observatories in Native California. *Journal of California and Great Basin Anthropology*, *1*(1), 38–63. http://www.jstor.org/stable/27824945

[9]Laylander, D. (2005). Ancestors, Ghosts, and Enemies in Prehistoric Baja California. *Journal of California and Great Basin Anthropology*, *25*(2), 169–186. http://www.jstor.org/stable/27825802

[10] Parkman, E. B. (1983). Soapstone for the Cosmos: Archaeological Discoveries in the Cuyamaca Mountains. *Journal of California and Great Basin Anthropology*, *5*(1/2), 140–155. http://www.jstor.org/stable/27825140

[11] Rodriguez, Stan. (2022, June 7). *Kumeyaay History and Culture* [Triton Talks]. 2022 UC San Diego, San Diego, Ca, United States. https://www.uctv.tv/shows/Triton-Talks-The-Kumeyaay-Nation-in-San-Diego-38071

[12] Whitley, D. S., & Dorn, R. I. (1987). Rock Art Chronology in Eastern California. *World Archaeology*, *19*(2), 150–164. http://www.jstor.org/stable/124548

Light Pollution at Palomar and Beyond

Becky Williams   Ge136B   2025

Light pollution is the increase in brightness of the night sky due to artificial lights, which is particularly problematic near urban areas, but is increasingly affecting rural areas, too. We often think of light pollution as a problem for astronomers, but light pollution also has negative effects on both human and ecosystem health.

The Problem

The increase in light pollution over the past century has made ground-based astronomy observing much more difficult. Figure 1 shows measurements of the light pollution levels at the major ground-based observatories in the world, with the black and red lines showing the 1% and 10% levels above background brightness, respectively [3]. In this list, Palomar is the 3rd brightest, showing that the increasing population growth (and subsequent increasing light pollution) in Southern California has made Palomar one of the telescopes most affected by light pollution.

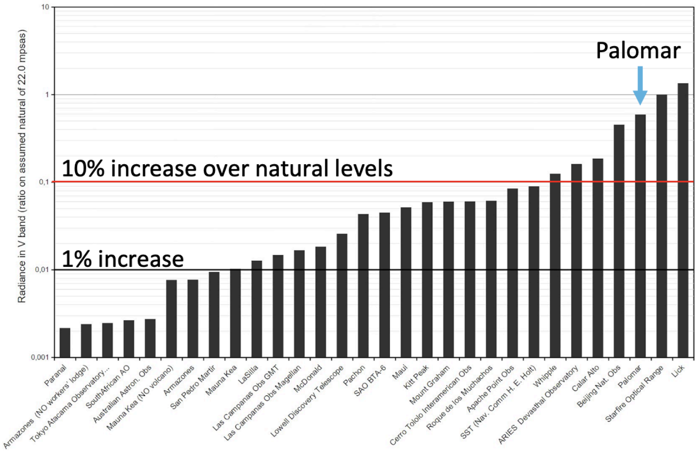

Figure 1: Light pollution at all major observatories [3].

It is not just astronomers who need to be concerned about light pollution. Life evolved for several billion years with the Moon as the brightest object in the night sky, until humans suddenly introduced artificial lights that can be several thousand times brighter than the Full Moon. These artificial lights disrupt animal circadian rhythms, which in humans has been linked to a whole host of health problems, including depression, insomnia, cardiovascular disease, and cancer [2]. In ecosystems, many impacts have been observed [2]; sea turtle hatchlings can become disoriented by lights and fail to make it to the sea. Birds that migrate at night can be confused by lights and collide with buildings; an estimated 98 million to 1 billion birds are killed in North America every year from such collisions. Frogs reduce mating calls, and bat feeding behavior changes, when artificial light is present.

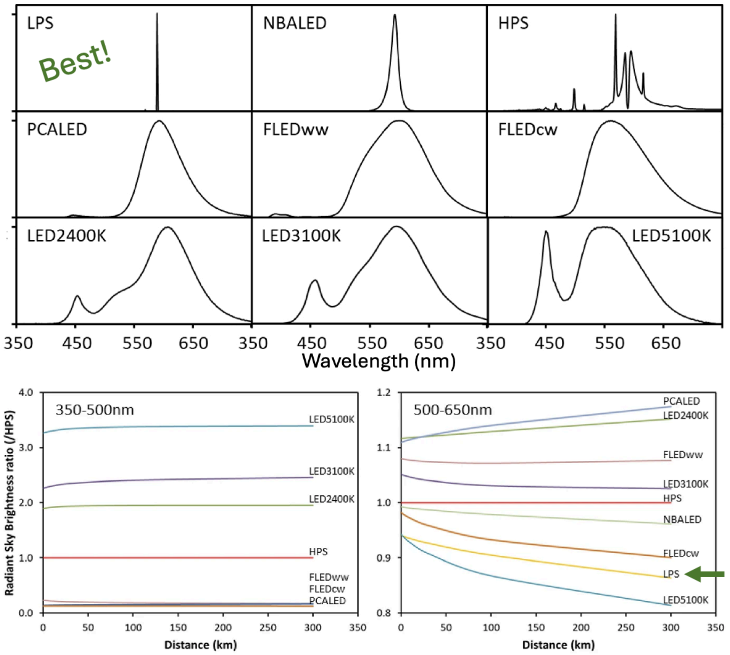

Figure 2: Spectra of different types of lights, and overall brightness of these lights with distance [4].

The Solution

Unlike other forms of pollution, light pollution is completely and instantly reversible - if we turned off every light in the world right now, we would immediately eliminate the problem. In practice, of course, this is a monumental and infeasible endeavour. Nevertheless, there are several measures that can be implemented to reduce and limit the effects of light pollution. Shielded light fixtures, such that the light is directed downwards, prevents light from escaping into the sky. Additionally, choice of lightbulb is important, as different light bulbs give off vastly different emission spectra (Figure 2) [4]. Low-pressure sodium (LPS) lights are the best option, as they only emit light at a single wavelength (instead of a broad emission spectrum).

One success story of minimizing light pollution is the city of Flagstaff, Arizona, the first city to adopt outdoor lighting codes to preserve the night sky for nearby observatories. There, light pollution mitigation measures (including improved shielding and switching to low-pressure sodium lighting) have been so successful that sky brightness has *decreased* by 10% from the late 1980s to 2015 [4]. Figure 3 shows the sky brightness looking toward Flagstaff, Arizona, compared to the city of Cheyenne, Wyoming. Both cities have similar population sizes, but it is clear that Flagstaff produces much less light pollution than Cheyenne.

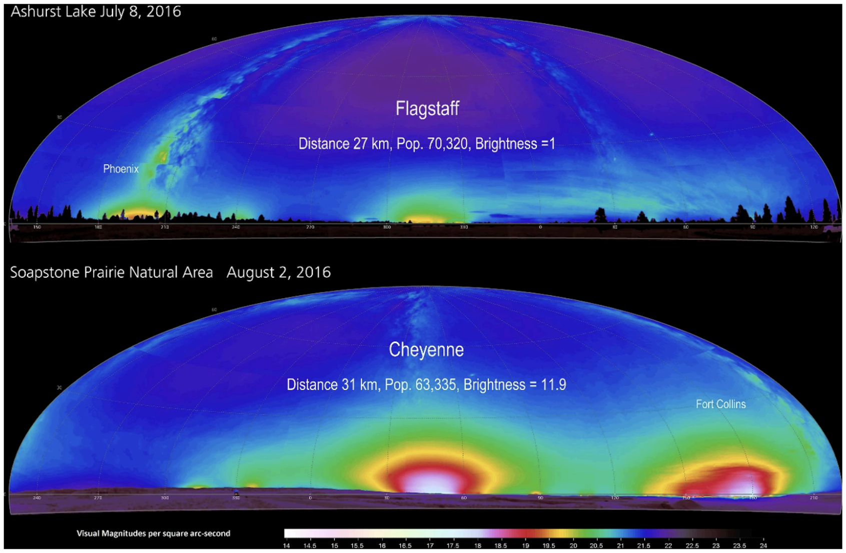

Figure 3: Comparison of light pollution between Flagstaff, AZ and Cheyenne, WY [4].

Light Pollution at Palomar

Light pollution first became an issue at Palomar in the 1960s, when emission from street lights started showing up in spectra taken with the telescope [1]. In 1981, a program was started in Riverside County to try to mitigate the effects of light pollution. Following the start of the program, several ordinances were put into place in surrounding counties and cities, including requirements that new street lights installed be low-pressure sodium, certain lights must have shielding, and decorative outdoor lighting must be turned off by 11pm. Even so, light pollution is such a prevalent problem in Southern California that Palomar continues to be one of the most affected observatories [3], as can be seen in Figure 4.

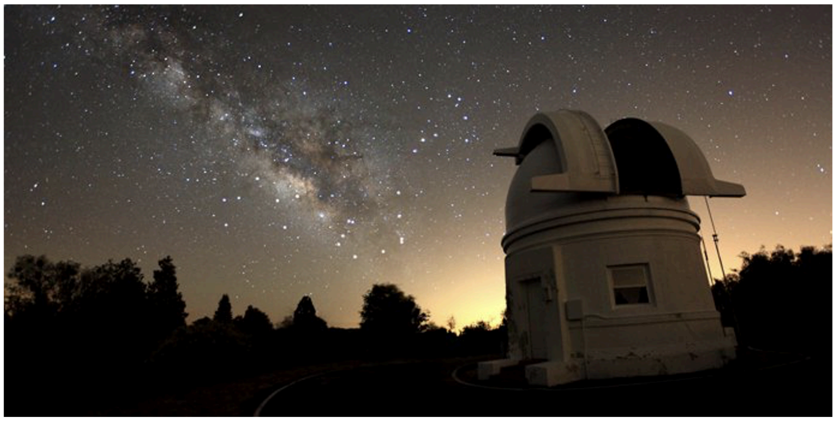

Figure 4: The night sky at Palomar, with light pollution evident on the horizon [5].

> "Happiness can be found, even in the darkest of times, if one only remembers to turn ~~on~~ off the light."
> - Albus Dumbledore

Sources:

1. Brucato (1991). https://doi.org/10.1017/S0252921100003614
2. Chepesiuk (2009). https://doi.org/10.1289/ehp.117-a20
3. Falchi et al. (2022). https://doi.org/10.1093/mnras/stac2929
4. Green et al. (2022). https://doi.org/10.1007/s00159-021-00138-3
5. https://palomarskies.blogspot.com/2011/05/milky-way-over-palomar.html

Dark Night Skies as a Window into Science and Culture

Tina Seeger

How to see the dark night sky: get out of the city!!

If you step outside at night in Pasadena, you are likely to see a few bright stars—and lately, several planets—in addition moon and countless airplanes heading over to LAX. This night sky is a far cry from what it looked like 100 years ago, as light pollution (ambient light scattered upwards and artificially brightening the sky) has steadily increased. We need a dark night sky to be able to see the wonders of the cosmos, including the constellations that have been part of human culture for thousands of years, all across the globe. We also need dark skies to be able to see the Mily Way, our own galaxy stretching across the sky in a milky white ribbon of diffuse starlight, which is tragically now invisible to **80% of Americans** (Falchi et al., 2016). 80%!!!!!! You should find this very worrisome and depressing!!!

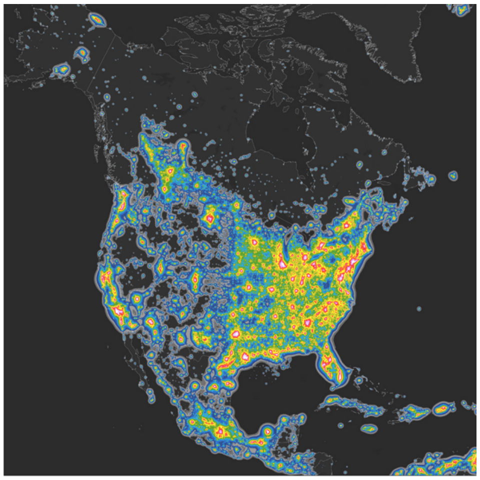

Figure 1. Map of North American artificial night sky brightness (Falchi et al., 2016)

Constellations: Technically, the international Astronomical Union has divided the night sky up into 88 regions called "constellations," and all deep space objects found within these regions are named according to the constellation name (IAU Constellation Report). However, most people are more familiar with the informal names given to patterns that have been identified in the stars by cultures around the world. See next page for a tool to help you find your own constellations!

Tongva Culture and Astronomy: The Tongva people, stewards of the lands and waters of the Los Angeles Basin since time immemorial, have several stories significant to their culture that are based around stars and constellations we see in the sky. Oftentimes, star stories are sacred to indigenous people, and taking them out of context by telling them as a white person is inappropriate, so I won't attempt here but encourage you to listen to recordings (search "The Seven Sisters: A Tongva Creation Story). Tongva culture is intimately interwoven into astronomy at Palomar Observatory, thanks to a discovery by our very own Mike Brown! In June 2002, while observing at Palomar, he discovered a ringed dwarf planet in the Kuiper Belt. The IAU has strict naming conventions, and non-resonant Kuiper belt objects must be named after creation deities. Therefore, this object, with the blessing of Tongva tribal historian Marc Acuña, was named Quaoar, after the creation force of the universe in Tongva mythology. Quaoar first sings and dances to create a new deity, Weywot (Sky Father), which was the name given to the small moon orbiting Quaoar (also discovered by Mike Brown in 2007).

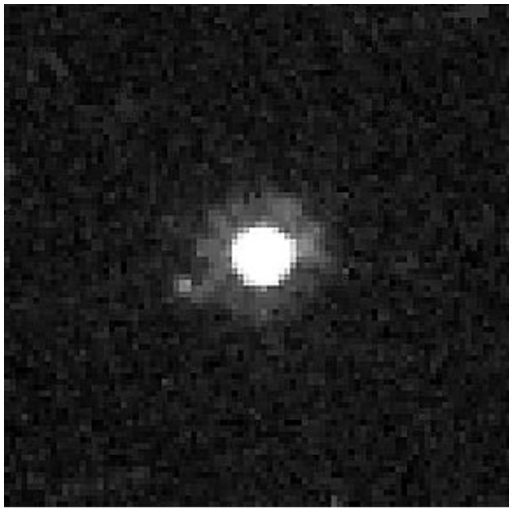

Figure 2. Hubble Space Telescope image of Quaoar and its moon Weywot (HST/Brown, 2006)

References

Falchi, F., Cinzano, P., Duriscoe, D., Kyba, C. C., Elvidge, C. D., Baugh, K., ... & Furgoni, R. (2016). The new world atlas of artificial night sky brightness. *Science advances*, *2*(6), e1600377.

International Astronomical Union Report on Constellations: https://www.iau.org/public/themes/constellations/

Brown, Michael E. (7 December 2010). "Chapter Five: An Icy Nail". *How I Killed Pluto and Why It Had It Coming*. Spiegel & Grau. pp. 63–85.

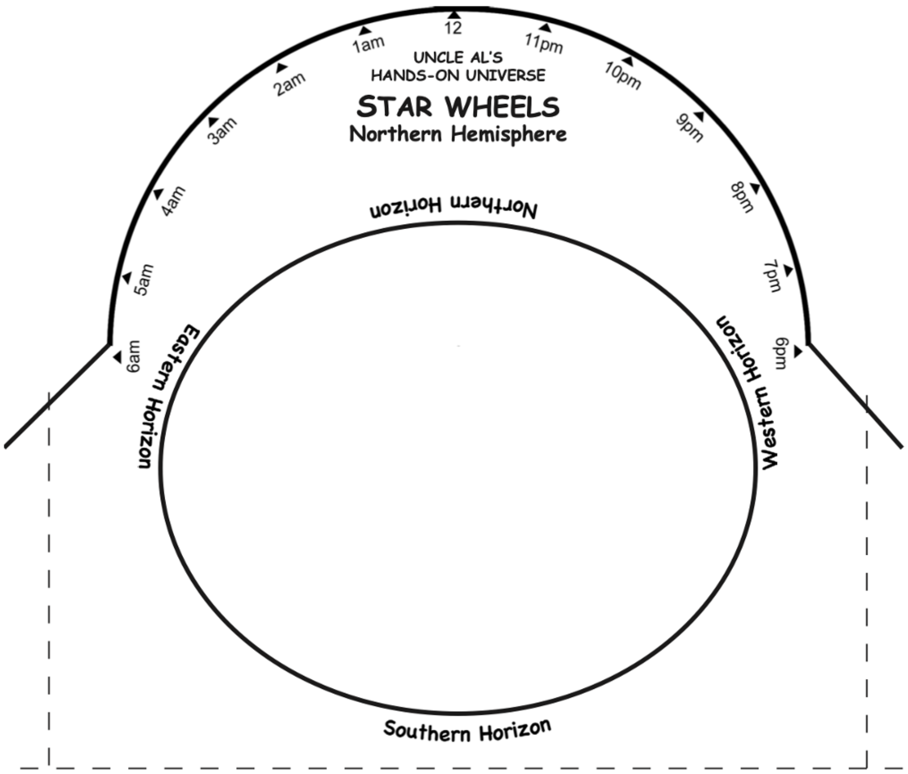
UNCLE AL'S
HANDS-ON UNIVERSE
STAR WHEELS
Northern Hemisphere
6am
5am
4am
3am
2am
1am
12
11pm
10pm
9pm
8pm
7pm
6pm
Northern Horizon
Eastern Horizon
Western Horizon
Southern Horizon

Version: May 2009

Instructions for Using Uncle Al's Star Wheels

1. Align your date and time, and then look up at the sky
2. Locate the constellation you want to find on the map.
3. Turn your map so the horizon it is closest to is at the bottom.
4. The star positions in the sky should match those on the wheel.

© 2006, 2009 by the Regents of the University of California

Uncle Al's Star Wheels are based on LHS Sky Challengers created by Budd Wentz and
available through LHS Museum Store
510-642-1016 http://www.lhs.berkeley.edu/pass/ast110&111&121.html
Download Uncle'Al's Sky Wheels from http://lhs.berkeley.edu/hou/img/uncleal

Version: May 2009

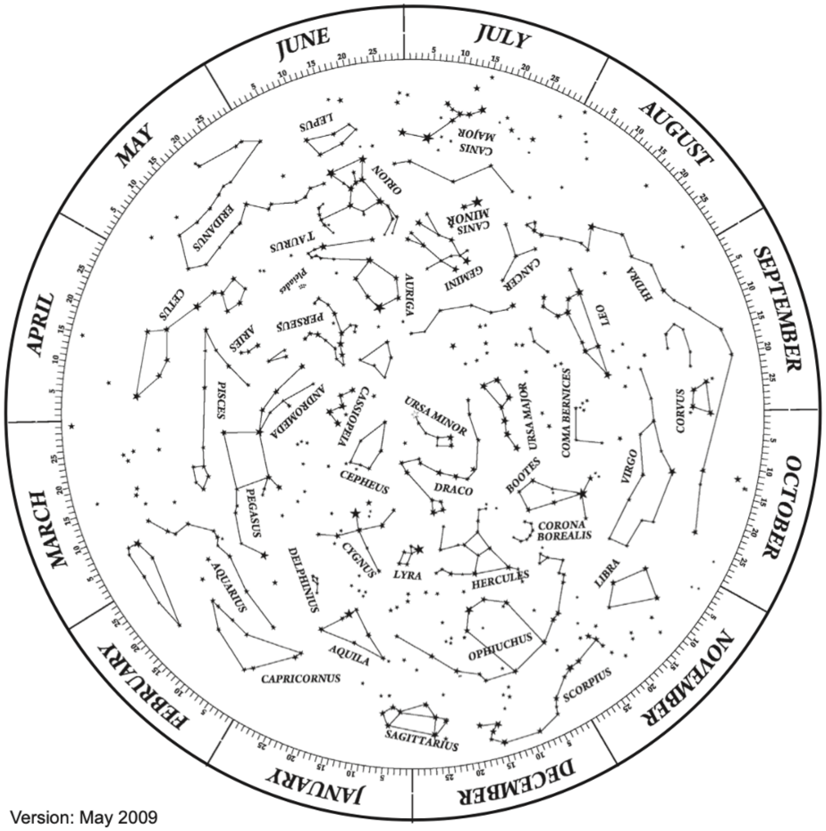
JUNE
JULY
AUGUST
SEPTEMBER
OCTOBER
NOVEMBER
DECEMBER
JANUARY
FEBRUARY
MARCH
APRIL
MAY
LEPUS
CANIS MAJOR
ERIDANUS
ORION
CANIS MINOR
TAURUS
Pleiades
GEMINI
CANCER
CETUS
PERSEUS
AURIGA
HYDRA
ARIES
LEO
PISCES
ANDROMEDA
CASSIOPEIA
URSA MINOR
URSA MAJOR
COMA BERNICES
CORVUS
CEPHEUS
DRACO
BOOTES
VIRGO
PEGASUS
CORONA BOREALIS
CYGNUS
LYRA
HERCULES
LIBRA
DELPHINUS
AQUARIUS
AQUILA
OPHIUCHUS
CAPRICORNUS
SCORPIUS
SAGITTARIUS

Version: May 2009

INSTRUCTIONS FOR ASSEMBLING UNCLE AL'S STAR WHEELS

Step 1: Print out all pages either on heavy cardstock or paste them onto a file folder or any other sturdy piece of cardboard.

Step 2: Cut along the black outer circle of the Star Wheel and along the solid lines on the Star Wheel Holder. Remove the interior oval shape on the Star Wheel Holder.

Step 3: On the Star Wheel Holder, fold the cardboard along the dashed lines.

Step 4: Tape or staple along the edges of the Star Wheel Holder forming a pocket.

Step 5: Place the Star Wheel in the Star Wheel Holder.

© 2006, 2009 by the Regents of the University of California

Uncle Al's HOU Star Wheels are based on LHS Sky Challengers created by Budd Wentz and
available through the LHS Discovery Corner Store 510-642-1016

Mars at the Salton Sea

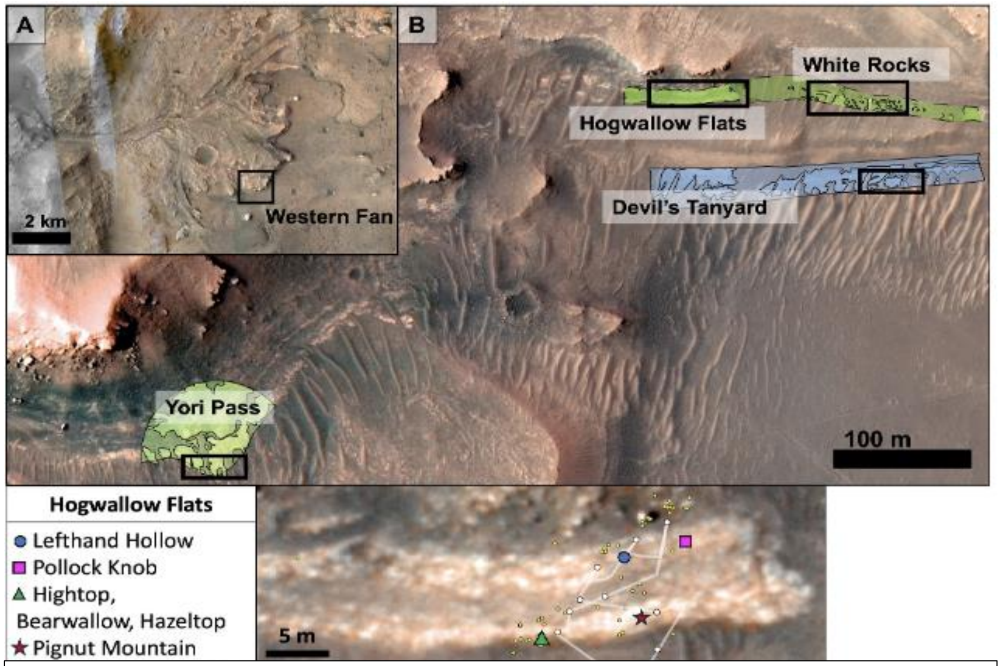

Figure 1. Hogwallow Flats member in Jezero Crater, Mars. Adapted from [6].

Perseverance Rover has been exploring Jezero Crater, Mars since 2021 [1]. Jezero Crater is a ~45 km wide crater with a sedimentary fan deposit at the northwestern edge of the crater, originating from the Naretva Vallis inlet [1]. In exploring the fan system, the rover identified a sulfate rich lacustrine unit known as the Hogwallow Flats member, which consists of light-toned platy fractured rocks with rare planar lamination [2]. The lithology consists of silt sized sediment derived from basalt with variable admixtures of authigenic iron oxide, sulfate, and phyllosilicate phases [3,4]. This unit hosts a variety of sulfate phases such as Fe,Mg sulfates in the rock matrix (up to 30 wt%), gypsum and anhydrite crystals, and jarosite patches [3], which has led to different hypotheses of sulfate formation in terms of diagenetic timing and in-situ alteration vs transported phases [3,4]. Two cores from the Hogwallow Flats member that will be returned to Earth by the Mars Sample return mission [5].

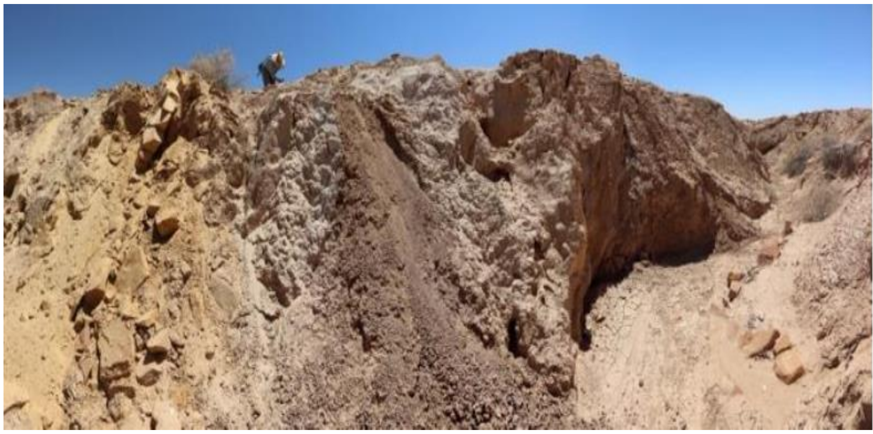

Figure 2. View of sedimentary layers at Salton Sea in the sample region. The yellowish sandstone layer near the left side of the image was sampled. Adapted from [7].

In 2023 an external expert science group, the “Rock Sample Team”, sampled various terrestrial analog sites based on the different lithologies found in Jezero Crater in order to test all the science analyses for Mars Sample return [7]. The terrestrial analog site for the Hogwallow Flats member was the yellow strata of the outcrop in the Salton Sea (33.440918, -115.830120, Figure 2).

Stratigraphy of the outcrop

Sedimentary rocks within the Salton trough range in age from the late Pliocene to Holocene. The sediments near the axis of the trough are deltaic sand, silt, and clay deposited by the Colorado River. This outcrop is part of the Pleistocene, brackish lacustrine deposit from Lake Cahuilla named the Borrego formation, a 1,475-m-thick section which has been divided into six informal units [8]. Evaporite layers are interbedded with clay and silt for 2000 m along strike, indicating repeat desiccation of the basin during deposition. It lies directly on top of the coarser, fluvial Shavers Well formation [8]. The Borrego formation exposed here has been folded into the Durmid anticline due to the structural effects of the San Andreas fault in the late Pleistocene and has been uplifting since then. The layers may thus appear almost vertical or highly slanted. In your exploration of this formation, look for the minerals listed in the condensed stratigraphic column below and see if you can identify any units or unit contacts.

Unit	Stratigraphic Height (m)	Description
6	1405-1495	Upper 18 meters of unit is very fine yellowish - brown quartz sandstone. The lower 69 meters is tan, clayey siltstones.
5	765-1405	This unit consists entirely of brown claystones having a few silty interbeds except for two marker horizons. The upper marker horizon is 150 centimeters of white volcanic ash. The lower is a 27 meters interval of massively bedded orangeish - tan, medium-grained quartz sandstones interbedded with claystones.
4	535-765	Interbedded brown claystone (75 %) and laminated **reddish-tan weathering laminated siltstones.** A few **gypsum** layers less than 30 centimeters thick are scattered throughout the unit. Some thin beds of gypsum-cemented quartz sandstone are present near the top of the unit.
3	225-535	The upper half of the unit is interbedded fine- grained quartz sandstone (50 %) and **yellow and grey clays** (50%). The lower half of the unit is massive tan sandstone, which weathers to a blocky surface. The sandstone is medium to fine grained and consists of quartz with a little biotite + feldspar.
2	60-225	Interbedded chocolate brown claystone and tan laminated siltstones consisting of quartz and biotite. Occasional **gypsum beds** 15-30 centimeters thick. A single bed of granite pebble conglomerate is present near the top of the unit.
1	0-60	Interbedded chocolate brown claystones 85% and tan sandstones 15% , consisting of well-sorted medium-sized quartz grains

[1] Farley, K. A., Williford, K. H., Stack, K. M., et al. *Space Science Reviews,* **216** (2020).
[2] Stack, K. M., Ives, L. R., Gupta, S. et al. *Journal of Geophysical Research: Planets,* **129,** 2 (2024).
[3] Broz, A. P., Horgan, B. H., Kalucha, H., et al. *Journal of Geophysical Research: Planets,* **129,** 11 (2024).
[4] Benison, K. C., Gill, K. K., Sharma, S. et al. *Journal of Geophysical Research: Planets,* **129,** 2 (2024).
[5] McCubbin, F. M., Farley, K. A., Harrington, A. D. et al. *Proceedings of the National Academy of Sciences*, **122**, 2 (2025).
[6] Kalucha, H., Broz, A.P. et al. *Journal of Geophysical Research: Planets*, **129**, 8 (2024).
[7] Thiessen, F., Orgel, C., Beaty, D. W. et al. *LPI contributions*, 3040, 1208 (2024).
[8] Babcock, E. A. *Geological Society of America Bulletin*, **85,** 3 (1974).

Slab City: How Geology & Climate Shape Art & Culture

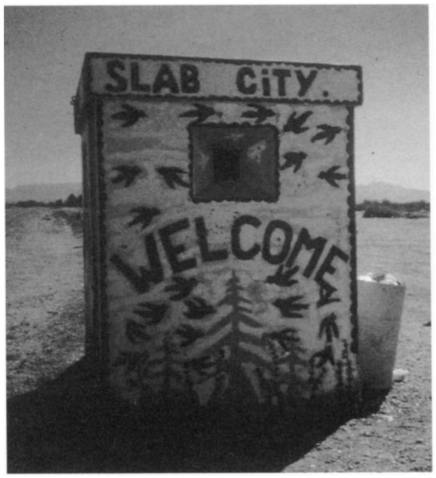

Figure 1. The entrance to Slab City.

What is Slab City?

On October 15, 1942, in the middle of World War II, a Marine Corps training base was opened called Camp Dunlap. The base essentially led to the creation of a small city: there were buildings, a swimming pool, and a grid with street signs. By 1961, the defense needs were over, and the land was given back to the state of California. They removed all of the buildings, but there were no orders about the concrete slabs that the buildings were built on, so those were left behind (Camp Dunlap).

People have been squatting in Slab City, or "The Last Free Place," since the 1950s. Charlie Hailey, an architect who wrote a book about Slab City, noted that the presence of concrete on sand is like an "invitation for settlement". Since the 1950s, the built environment has grown as individuals have created new structures, sometimes in line with the grid structure and sometimes built over it (Nalewicki 2018).

Population

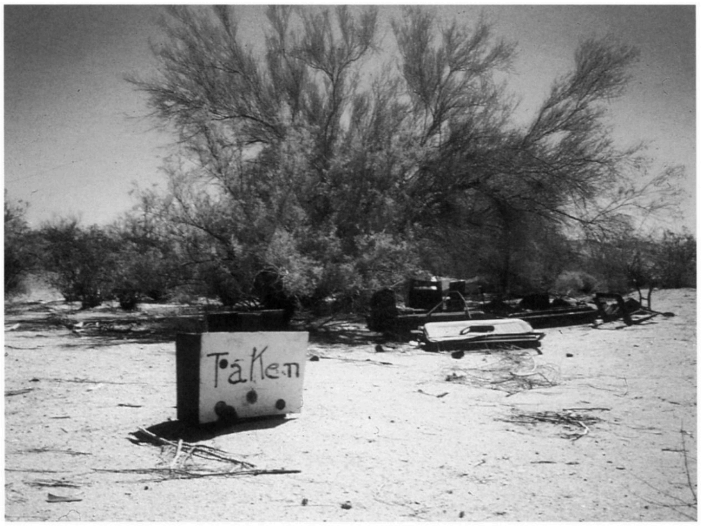

Figure 8. Claimed property

The population of Slab City has varied throughout time, but is largely separated into two groups: the "Slabbers," who are permanent residents that live in the city year round, including during the extremely hot (120 degree) summers, and "Snowbirders," folks who come to the city during the winter months from colder places, usually with RVs. The population appears to have grown substantially over the past couple of decades, with only about a dozen full timers back in 2003, increasing to about a hundred in 2014, and approximately 800 now (Van de Walle 2014, PBS SoCal 2024). The population swells significantly in the winter months, with an additional 5,000 snowbirders living there temporarily. Notably, the city expands and shrinks with economic trends. Du Bry & Rissolo (2001) note that settlement in Slab City can be thought of as an "adaptive strategy for some to deal with poverty" (Du Bry & Rissolo 2001) and that there was a significant increase in the population during economic turmoil in the late eighties (Van de Walle 2014), although many in Slab City are drawn there rather than driven by their own circumstances.

The range of people and class status in Slab City can vary greatly. There are artists, retirees, eccentrics, drug users, criminals, and folks deemed "homeless" by the Imperial County census (but not necessarily by themselves). Indeed, Slab City is known as a place to go if you don't want to be found, which has resulted in popularity for those looking for a way to escape different situations, or looking for a certain freedom that cannot be found in traditional cities (PBS SoCal 2024).

Governance

Slab city is largely self governed. There is no electricity, running water, or sewage system. In many ways, it may be considered something of an anarchy, not necessarily by design but rather by necessity. The Imperial County police will visit the city in the case of crimes, murders, or if they are looking for someone, but usually Slab City residents aim to prevent police involvement. Border agents will regularly conduct raids to try to catch any people who may have crossed over the border from nearby Mexico. Fires do break out, and although Slab City does have a resident titled "Aquaman" with a fire extinguisher, the fire department can also arrive. Drugs are also prevalent as many folks arriving in Slab City might be using, although there are a number of accounts of people who moved to Slab City and have since been able to become clean and run programs to help others.

The land Slab City is built on is officially owned by the State of California, and although there are not necessarily accounts of the state trying to kick people out of the land, there is a growing potential and worry that the state may desire to sell the land to an energy corporation, which could lead to the displacement of the people living there.

Art, National Acclaim, and Tourism

Perhaps what makes Slab City most famous is its connections to the American art scene. Leonard Knight was a resident of Slab City since the 1980s, and his work has reached national acclaim. His piece "Salvation Mountain" is a hillside made of clay, sand, straw, and other found materials, upon which he would continually paint. Recently I was in Baltimore at the American Visionary Museum and was able to see another one of his works, a hot air balloon ten stories high with the words "God is Love" painted on it, made from the imperfect materials from Ravens Industries, the biggest balloon-maker the time. Notably, Knight has been criticized by local populations for the adverse environmental effects of his paint runoff, which has brought toxins into the nearby environment.

DON'T BE YOURSELF
BE LIKE TV
BLAH
YOU'RE TOO THIN
BUY MORE TVs
SPEND YOUR WAY
FREE THOUGHT
THIS MACHINE KILLS BRAIN CELLS
OUR VALUES ARE YOUR VALUE
MEN FEEL NOTHING
TO SALVATION
REMOTE CONTROL
IS THIS YOUR ONLY WINDOW TO THE WORLD
DELUSIONS OF PROPA-GRANDEUR
WASTED TIME MACHINE
LOOK WHAT THEY'VE DONE TO ME
MENTAL MASTER BATION
TV FOR PRESIDENT
DEMOCRATS ARE EVIL
SIDE EFFECTS MAY INCLUDE
OVERT POLITICAL
WHILE SUPPLIES LAST
I WAS YOUTUBE

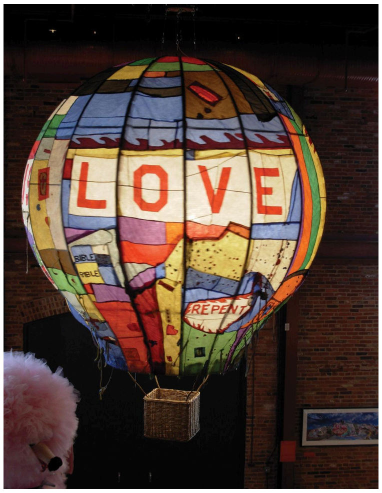
LOVE
REPENT

Another notable artist is Charles Russell or "East Jesus," whose work was also featured in the museum. "East Jesus" also is an area near Slab City. He made art cars, and Burning Man vehicles, as well as curated an art garden. He passed away in 2011, after which the Chasterus Foundation was founded in his name that now features art residencies with a focus on consumerism and that creates performance spaces, art education, and curating sustainable practices in Slab City (PBS Socal).

Some other notable artists are Flip Cassidy and Kenny Irwin. Most of the art created in Slab City comes from found materials and "gleaning" – the process of collecting junk for art. One place to do this is Slab Mart, both Slab City's dump as well as discarded things that artists or others may desire. Notably, the lack of trash collection & the climate can lead to issues with the dump that the community may try to fix, but with the lack of infrastructure can fall short. Additionally, Slab City has been featured in movies like Into the Wild.

The high prevalence of renowned art brings a large amount of tourism to Slab City. Tourists, labeled "Normies" by the Slabbers, can sometimes number up to 2,000 visitors on a winter weekend to visit East Jesus. Tourism has led to economic opportunities for those in the area. For example, Dot is an art shop owner (the House of Dots) who is an artist, and after living nomadically for a while, she realized she could make a living selling her art in Slab City and creating a tourist attraction.

Du Bry, Travis, and Dominique Rissolo. "Slab City: Squatters' Paradise?" *Journal of the Southwest* 43, no. 4 (2001): 701–15.

"Historic California Posts: Camp Dunlap." Accessed February 7, 2025. https://www.militarymuseum.org/CpDunlap.html.

"Leonard Knight's Salvation Mountain at Slab City | San Diego Reader." Accessed February 7, 2025. https://www.sandiegoreader.com/news/2005/nov/03/salvation-mountain/.

Magazine, Smithsonian, and Jennifer Nalewicki. "Inside Slab City, a Squatters' Paradise in Southern California." Smithsonian Magazine. Accessed February 5, 2025. https://www.smithsonianmag.com/travel/inside-slab-city-squatters-paradise-southern-california-180970218/.

PBS SoCal. "Bombay Beach Biennale: Co-Creating a Cultural Revival at the Salton Sea," September 20, 2024. https://www.pbssocal.org/shows/artbound/bombay-beach-biennale-co-creating-a-cultural-revival-at-the-salton-sea.

PBS SoCal. "Slab City: Creative Homesteading in a Desert of Extremes," October 25, 2024. https://www.pbssocal.org/shows/artbound/slab-city-creative-homesteading-in-a-desert-of-extremes.

Van de Walle, Mark. "At Home at the Other End of the Rainbow: Goin Off the Grid (and Into the Desert) to Live the American Dream." *The Virginia Quarterly Review* 90, no. 1 (2014): 72–89.

Plate Tectonics of Salton Basin and the Gulf of California

Mira Menezes

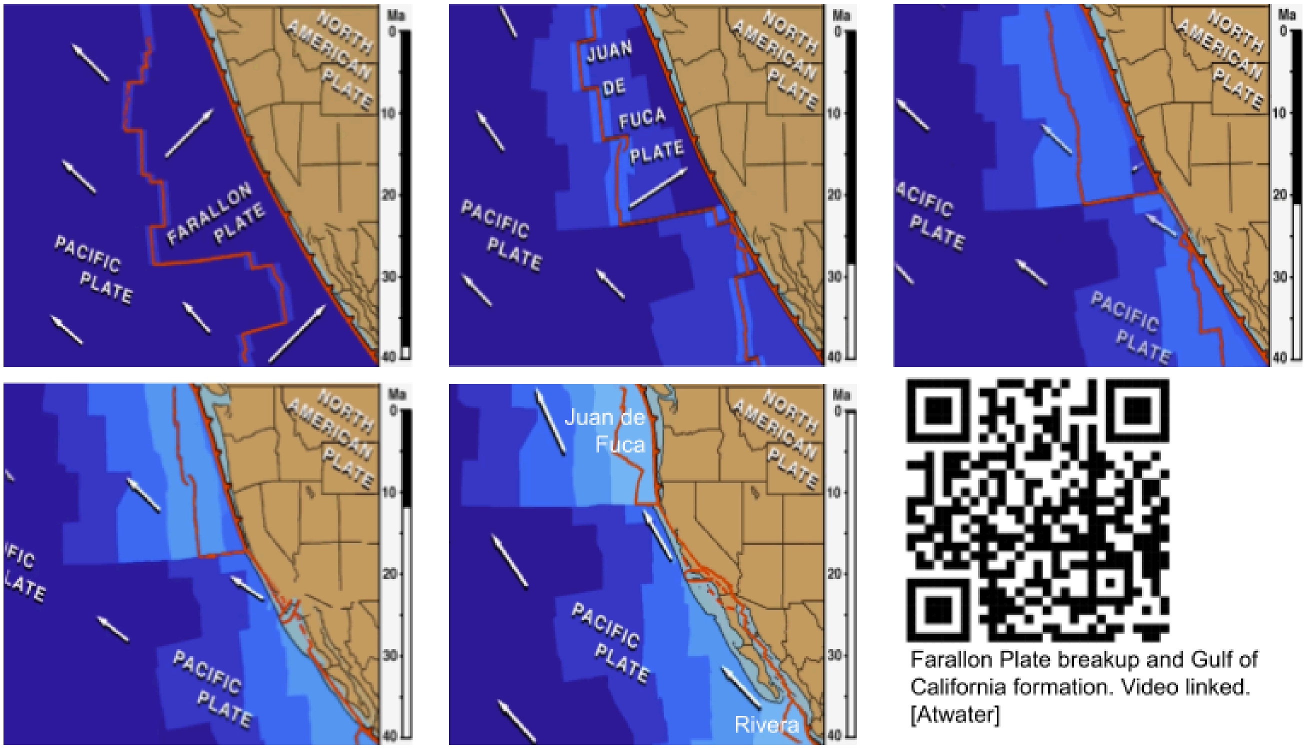
NORTH AMERICAN PLATE
FARALLON PLATE
PACIFIC PLATE
JUAN DE FUCA PLATE
Juan de Fuca
Rivera
Ma
0
10
20
30
40

Farallon Plate breakup and Gulf of California formation. Video linked. [Atwater]

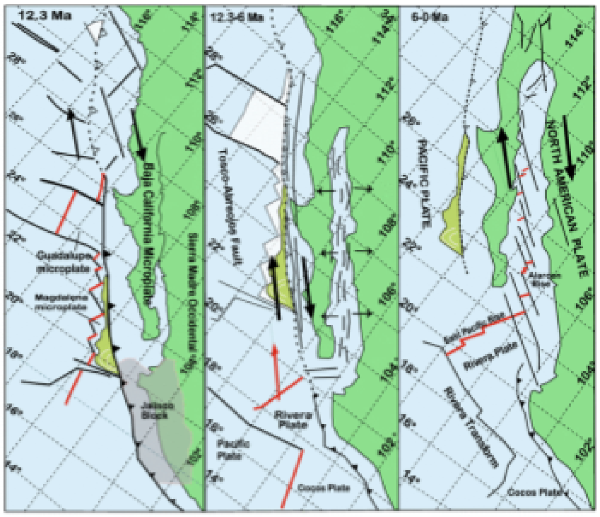
12.3 Ma
12.3-6 Ma
6-0 Ma
Baja California Microplate
Sierra Madre Occidental
Tosco-Abreojos Fault
Guadalupe microplate
Magdalena microplate
Jalisco Block
Rivera Plate
Pacific Plate
Cocos Plate
PACIFIC PLATE
NORTH AMERICAN PLATE
Alarcon Rise
East Pacific Rise
Rivera Transform

Gulf of California formation [Ortega]

The (late) Farallon plate has been subducting under the North American (NA) plate since 160Ma, diverging from the pacific plate in the west. The Farallon plate moved northeast relative to the NA plate, subducting and driving the creation of the Rocky Mountains, Colorado plateau, Sierra Nevadas, and more. Around 30Ma, the mid-ocean spreading ridge between the Farallon and Pacific plates began to subduct in some places, and the Farallon plate broke up into many pieces (including Juan de Fuca, Rivera, Cocos, Nazca, and more!).

Today, some parts of the NA plate are now exposed to the northwest motion of the pacific plate. North of LA, this transverse motion drives the San Andreas fault. In the Gulf of California, the fault is mostly transverse, but has small diverging rifts. The Salton Trough is the northmost part of this rifting zone, where it meets the San Andreas Fault. The Gulf of California has displaced Baja California around 450km northwest. Before this rift developed, the tip of Baja California was near where Jalisco is today. Today, the fault moves around 46mm/yr.

Fast Rift Formation

Divergent motion between Baja California and Mexico (near the edge of a continent) began around 12.5Ma, and rifted after only 6-10Myr of extension due to:

1. Baja California and the western Sierra Madres have strong north-south batholiths.
2. The area between the batholiths was weak due to the recent subduction-caused volcanic arc.
3. The plates diverge rapidly at around 46mm/yr.
4. The divergence is extremely oblique, most of the fault is transverse, with tensile stress concentrated in small areas.
5. The continental crust was thin, compression bypassed this area and created mountains inland.
6. The divergent Pa-Fa boundary subducted below the Gulf of California, and became the new boundary.

Baja - B.C. Hypothesis

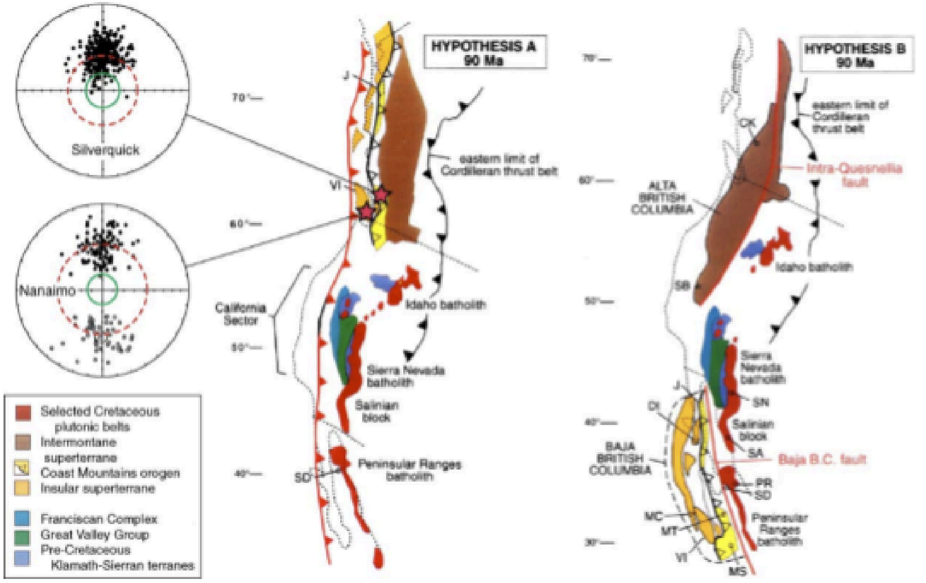
Silverquick
Nanaimo
HYPOTHESIS A
90 Ma
70°
60°
50°
40°
J
VI
eastern limit of Cordilleran thrust belt
Idaho batholith
California Sector
Sierra Nevada batholith
Salinian block
Peninsular Ranges batholith
SD
Selected Cretaceous plutonic belts
Intermontane superterrane
Coast Mountains orogen
Insular superterrane
Franciscan Complex
Great Valley Group
Pre-Cretaceous Klamath-Sierran terranes
HYPOTHESIS B
90 Ma
70°
60°
50°
40°
30°
CK
eastern limit of Cordilleran thrust belt
Intra-Quesnellia fault
ALTA BRITISH COLUMBIA
Idaho batholith
SB
Sierra Nevada batholith
J
DI
SN
Salinian block
SA
BAJA BRITISH COLUMBIA
Baja B.C. fault
PR
SD
MC
MT
VI
MS
Peninsular Ranges batholith

Comparing no movement (left, terranes near current positions) and Baja B.C. (right). Two locations close today have vastly different magnitizations. [Krijgsman]

What do Mexico and Canada have in common? According to some paleomagnetists, their rocks. The Baja B.C. theory proposes that the Insular and Intermontane terrane and Vancouver island originated near Baja California and traveled up to 3500km northward over 80Myr. Some paleomagnetic evidence supports this, showing that sedimentary deposits from the Jurassic and Cretaceous were deposited around 27°N. The contrast is particularly striking, as at the time magnetic north was located in Alaska, so British Columbia would have had near-vertical magnetic polarization. This surprising finding was repeatedly questioned in the 90s and early 2000s, with the theories that sediments were re-magnetized, tilted, or subsequently flattened. However, paleomag data has continued to support this theory, and it has become somewhat accepted that these terrane originated in Southern California or Baja California, and were displaced 1000-2000km northwards by forces from the Kula plate's northward motion.

Sources

A Atwater and Stock, 1998, Int. Geol. Rev., v. 40, p. 375: https://animations.geol.ucsb.edu/2_infopgs/IP4WNATect/bNEPacWNoAm.html

Umhoefer, 2011, Why did the Southern Gulf of California rupture so rapidly?—Oblique divergence across hot, weak lithosphere along a tectonically active margin https://rock.geosociety.org/net/gsatoday/archive/21/11/article/i1052-5173-21-11-4.htm

R. Ortega, L. Quintanar, E. Huesca-Pérez, 2016. Geometric Aspects of the Full Moment Tensors in the Gulf of California and the Mexican East Pacific Rise. https://www.researchgate.net/publication/287973444

P. Ward, J. Hurtado, J. Kirschvink, K. Verosub, 1997, Measurements of the Cretaceous Paleolatitude of Vancouver Island: Consistent with the Baja-British Columbia Hypothesis https://www.jstor.org/stable/pdf/2894137.pdf

R. Butler, G. Gehrels, K Kodama, 2001, A Moderate Translation Alternative to the Baja British Columbia Hypothesis https://rock.geosociety.org/net/gsatoday/archive/11/6/pdf/i1052-5173-11-6-4.pdf

P. Umhoefer, 2019, Update of the Moderate Baja British Columbia (AKA Mojave BC) Hypothesis for 1600km of Northward Translation from ~90 - 40Ma https://gsa.confex.com/gsa/2019CD/webprogram/Paper329812.html

The Once Great Lake: Remnants of Lake Cahuilla and the formation of the Salton Sea

by James Mullahoo

During the Holocene, floodwaters from the Colorado River flowed into a vast depression within what is now the Salton Trough region, including Coachella Valley and Imperial Valley. Once connecting to the Gulf of California, this region became blocked off from the gulf by a buildup of silt deposited from the Colorado River ~40,000 years ago, eventually forming an inland sea that dried up, leaving behind a depression below sea level emphasized over time by the mountain ranges on either side and active faulting. As these Colorado River flooded, it formed Lake Cahuilla, once one of the largest lakes in North America. At its largest was more than 5,400 km^2 (~160 km x 56 km) and almost 100 m deep[1]. The lake underwent repeated desiccation and flooding, with 7 events occurring in the last 2500 years, including the most recent estimate of the lake's presence as late as the 1730's[2]. Measurements of the ages of the lake and the extent come from a combination of sedimentology, carbon dating of stumps, archaeological evidence, and oral histories[2–4]. Estimates from desiccations rates and Colorado River inputs indicated that it took 13-20 years to completely refill during inundation periods, and another ~50 years to fully desiccate as the lake evaporated[4].

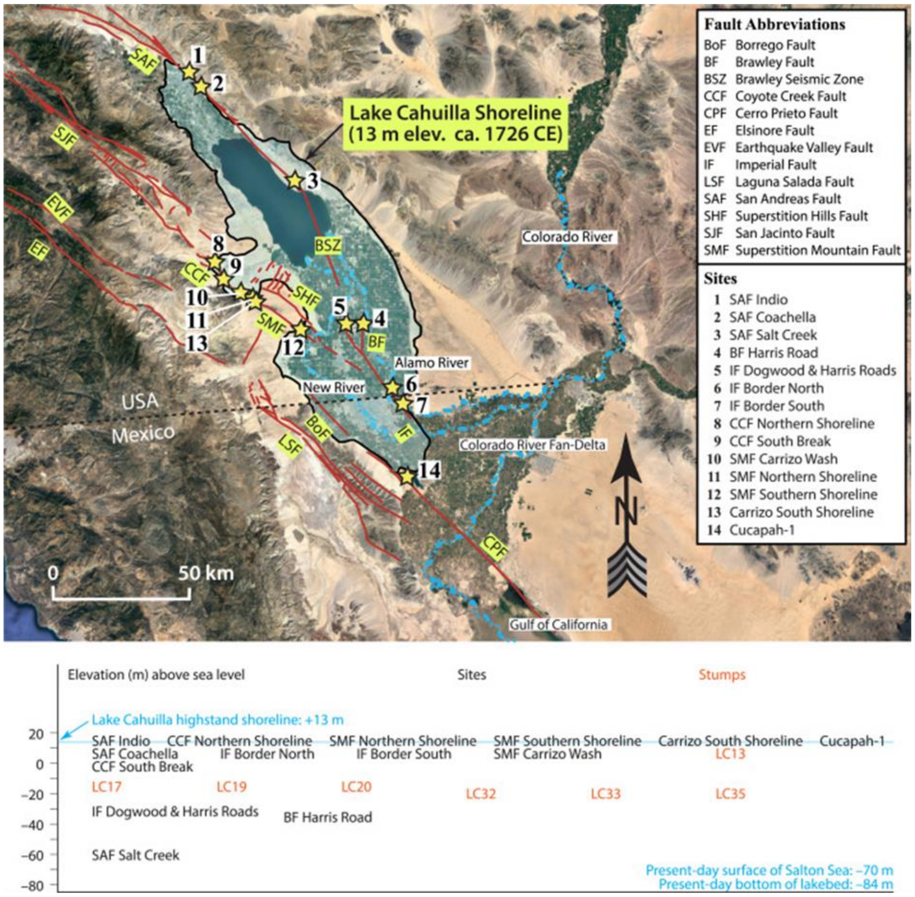
Lake Cahuilla Shoreline
(13 m elev. ca. 1726 CE)
SAF
SJF
EVF
EF
CCF
SHF
SMF
BSZ
BF
BoF
LSF
IF
CPF
1
2
3
4
5
6
7
8
9
10
11
12
13
14
Colorado River
Alamo River
New River
USA
Mexico
Colorado River Fan-Delta
Gulf of California
N
0
50 km
Fault Abbreviations
BoF Borrego Fault
BF Brawley Fault
BSZ Brawley Seismic Zone
CCF Coyote Creek Fault
CPF Cerro Prieto Fault
EF Elsinore Fault
EVF Earthquake Valley Fault
IF Imperial Fault
LSF Laguna Salada Fault
SAF San Andreas Fault
SHF Superstition Hills Fault
SJF San Jacinto Fault
SMF Superstition Mountain Fault
Sites
1 SAF Indio
2 SAF Coachella
3 SAF Salt Creek
4 BF Harris Road
5 IF Dogwood & Harris Roads
6 IF Border North
7 IF Border South
8 CCF Northern Shoreline
9 CCF South Break
10 SMF Carrizo Wash
11 SMF Northern Shoreline
12 SMF Southern Shoreline
13 Carrizo South Shoreline
14 Cucapah-1
Elevation (m) above sea level
Sites
Stumps
Lake Cahuilla highstand shoreline: +13 m
20
0
-20
-40
-60
-80
SAF Indio
SAF Coachella
CCF South Break
CCF Northern Shoreline
IF Border North
SMF Northern Shoreline
IF Border South
SMF Southern Shoreline
SMF Carrizo Wash
Carrizo South Shoreline
Cucapah-1
LC13
LC17
LC19
LC20
LC32
LC33
LC35
IF Dogwood & Harris Roads
BF Harris Road
SAF Salt Creek
Present-day surface of Salton Sea: -70 m
Present-day bottom of lakebed: -84 m

Figure 1: Adapted from Rockwell et al. 2022, figure 1. Shoreline of Lake Cahuilla superimposed over the Salton Sea. Blue lines are Colorado River channels, red lines are faults, and yellow stars indicate sampling locations in the study.

Native peoples including the Cahuilla after whom the lake is named would fish along the shoreline, leaving behind evidence of traps and other tools[5]. Their oral histories clearly indicated the natural cycles of flooding and drying, and the would take advantage of the return of these temporary lakes. When refilled by the Colorado River, new inputs of freshwater and fish would revitalize Lake Cahuilla, with as many as 64 different species of fish identified, including carps and minnows, and a range of freshwater invertebrates. Fossil evidence points to reasonably freshwater conditions while the lake was at its maximum extent, and as the lake receded it became brackish after dropping to ~60 m depth, and finally salt water by ~25 m depth. Lake Cahuilla is also a useful proxy for determining the age of rupturing events along the San Andreas fault that runs through the deposits.

After Lake Cahuilla had dried up in the 1700's, it remained so until 1905. Prior to this, the area began to be harnessed for its highly productive soil, and water from the Colorado River was being fed towards the Alamo River to increase irrigation to the region. Due to the high silt content of the Colorado River, the canals, dams and irrigation channels were constantly being blocked and had to be cleared out, and in 1905 flooding of the Colorado River overwhelmed the construction and excess water flooded into the Salton Trough, forming what is now the Salton Sea. The Salton Sea is now considered an endorheic sea as it has no outlets, with an extent of ~890 km^2 and a maximum depth of 15 m[6]. It is currently drying out, with only modest input of new water from irrigation outflow, though there are some efforts to attempt to conserve the Salton Sea by diverting the Colorado River to prevent loss of the habitats and communities that now surround it.

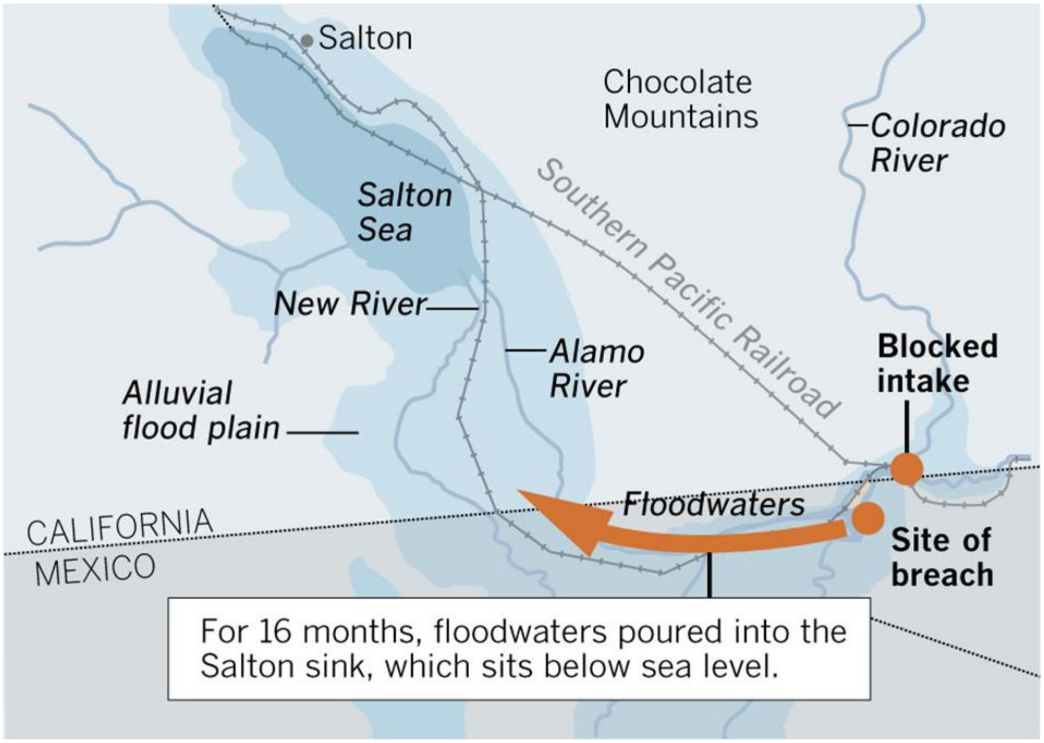
Salton
Chocolate Mountains
Colorado River
Salton Sea
Southern Pacific Railroad
New River
Alamo River
Alluvial flood plain
Blocked intake
Floodwaters
Site of breach
CALIFORNIA
MEXICO
For 16 months, floodwaters poured into the Salton sink, which sits below sea level.

Figure 2: Rañoa Raoul, "Drawdowns and Death of the Salton Sea", LA Times, Oct 21, 2014.[7]

References

1. Patten, M., McCaskie, G. & Unitt, P. *Birds of the Salton Sea: Status, Biogeography, and Ecology*. (University of California Press, 2003).
2. Rockwell, T. K., Meltzner, A. J., Haaker, E. C. & Madugo, D. The late Holocene history of Lake Cahuilla: Two thousand years of repeated fillings within the Salton Trough, Imperial Valley, California. *Quat. Sci. Rev.* 282, 107456 (2022).
3. Phukan, A., Braje, T. J., Rockwell, T. K. & Ullah, I. Shorelines in the Desert: Mapping Fish Trap Features along the Southwest Coast of Ancient Lake Cahuilla, California. *Adv. Archaeol. Pract.* 7, 325–336 (2019).
4. Rockwell, T. K., Meltzner, A. J. & Haaker, E. C. Dates of the Two Most Recent Surface Ruptures on the Southernmost San Andreas Fault Recalculated by Precise Dating of Lake Cahuilla Dry Periods. *Bull. Seismol. Soc. Am.* 108, 2634–2649 (2018).
5. Laylander, D. The Last Days of Lake Cahuilla: The Elmore Site. *Pac. Coast Archealogical Soc. Q.* 33, (1997).
6. Bradley, T. J., Ajami, H. & Porter, W. C. Ecological transitions at the Salton Sea: Past, present and future. *Calif. Agric.* 76, (2022).
7. 7. Rañoa, R. Drawdowns and death of the Salton Sea. *Los Angeles Times* https://www.latimes.com/local/california/la-me-g-drought-drawdowns-and-death-of-the-salton-sea-20141021-htmlstory.html (2014).

Fossils in the Salton Trough

Ge136 Winter 2025 Report, Miles Stone

bed of fossilized mussels and scallop shell taken from along Route 15 north of Adams Avenue [kpbs]

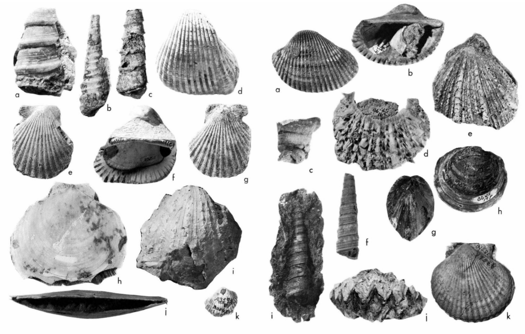
a
b
c
d
e
f
g
h
i
j
k
a
b
c
d
e
f
g
h
i
j
k

Tertiary Caribbean mollusks and the index fossil Anadara vanderhoofi and other Fossil mollusks represented in the Loreto area, Baja California Sur. Pliocene, Carmen and Marquer formations [Smith]

Fossilized brain coral (damaged by graffiti [Fry]

Mollusks - Oligocene, Miocene, Pliocene

Helpful for identifying paleoshorelines, as chronostratigraphic markers, and as members of phylogenetic lineages whose ranges have both temporal and paleogeographic significance

When associated with radiometrically dated volcanic rocks, they provide improved resolution for correlating upper Oligocene to Pliocene sediments in the Gulf of California and its northern extension, the Salton Trough of California (where lake Cahuilla was, and the Salton Sea is now) index species like pectens, turritellas, and spondylids are the most useful for correlation in the Gulf area. Evolutionary lineages within these groups can be calibrated with absolute ages and tectonostratigraphic events. (the chronostratigraphic ranges of some index species may vary with latitude, so correlations based on combined radiometric, megafaunal, and microfaunal data tend to be more accurate.)

Specifically, the presence of mollusks with Caribbean affinities in the Imperial Formation suggests that, at one time, the region had a direct marine connection to the proto-Gulf of California. This implies that the Salton Basin was once part of a larger shallow sea before the Baja California Peninsula began moving northwest due to tectonic activity. By the late middle Miocene (13 Ma), the Gulf of California extended to Isla Tiburon, Sonora, where it supported a distinctive molluscan fauna. Before the late Miocene (6 Ma), some of the same mollusks lived as far north as the Salton Trough."(Smith)

Fossilized marine mollusks, particularly species from Turritella, Anadara, and Aequipecten,can also indicate that periodic flooding events from the Gulf of California once extended into what is now the Salton Basin. Their presence helps geologists reconstruct the timing and extent of marine incursions into the region.

From the **late Oligocene to late Miocene [30-23.7 Ma]**, the Baja California peninsula was contiguous with mainland Mexico

In the **Early Miocene to Early Middle Miocene [23.7-15 Ma]** A series of penecontemporaneous marine basins developed along the west Mexican mainland between the Rio Ameca. Early Miocene seas that covered western Baja California were shallower and less extensive than those of the late Oligocene

During the **middle Miocene [16-14 Ma]** the sea invaded the area of the Cabo Trough, adjacent to the Mexican mainland.

In the central Gulf at Santa Rosalia the **late middle to late Miocene [14-12 Ma]** shoreline lay west of the head of Arroyo del Boleo and east of a divide between San Ignacio and the Gulf.

Gulf waters in the Santa Rosalia area deepened in the **late Miocene to middle Pliocene[12-2 Ma]**, and flat-lying yellow sandy sediments were deposited unconformably on hills and valleys on the Boleo Formation.

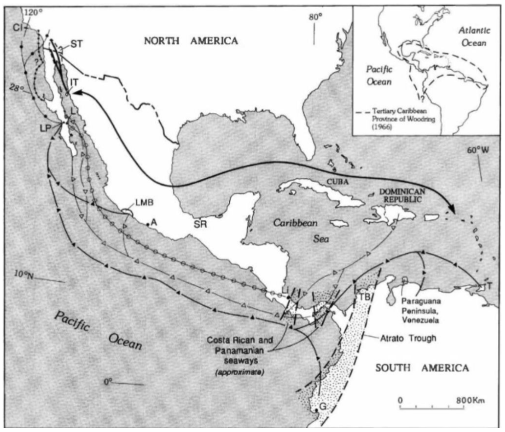
120°
80°
NORTH AMERICA
CI
ST
IT
28°
LP
LMB
A
SR
CUBA
DOMINICAN REPUBLIC
Caribbean Sea
10°N
Pacific Ocean
Costa Rican and Panamanian seaways (approximate)
0°
TB
Paraguana Peninsula, Venezuela
Atrato Trough
SOUTH AMERICA
G
T
0
800Km
60°W
Atlantic Ocean
Pacific Ocean
Tertiary Caribbean Province of Woodring (1966)

Faunal affinWes of west Mexican Tertiary marine molluscan species. Data from Smith, 1984, 1986, and unpublished information; Durham et al., 1981. Lines connect areas of similar molluscan faunas; dispersal paths are schematic [Smith]

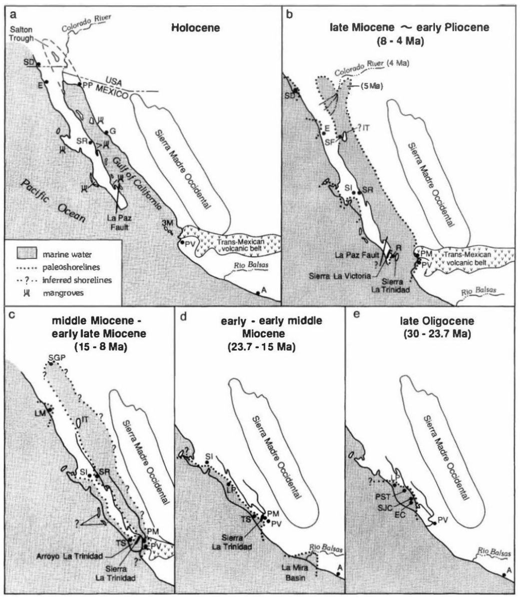
a
Holocene
Salton Trough
Colorado River
SD
E
PP
USA
MEXICO
G
SR
Gulf of California
Sierra Madre Occidental
Pacific Ocean
La Paz Fault
3M
PV
Trans-Mexican volcanic belt
Rio Balsas
A
marine water
paleoshorelines
inferred shorelines
mangroves
b
late Miocene ~ early Pliocene (8 - 4 Ma)
Colorado River (4 Ma)
(5 Ma)
SD
E
SF
?IT
SI
SR
Sierra Madre Occidental
La Paz Fault
R
Sierra La Victoria
Sierra La Trinidad
PM
PV
Trans-Mexican volcanic belt
Rio Balsas
c
middle Miocene - early late Miocene (15 - 8 Ma)
SGP
LM
IT
SI
SR
Sierra Madre Occidental
TS
PM
PV
Arroyo La Trinidad
Sierra La Trinidad
d
early - early middle Miocene (23.7 - 15 Ma)
SI
LP
Sierra Madre Occidental
TS
PM
PV
Sierra La Trinidad
Rio Balsas
La Mira Basin
A
e
late Oligocene (30 - 23.7 Ma)
LP
PST
SJC
EC
PV
Sierra Madre Occidental
Rio Balsas
A

Paleogeography of the Gulf of California. Figures are based on distributions of marine mollusks and associated microfauna! and radiometric data [Smith]

Microfossils - Miocene, Pliocene, Pleistocene

Foraminifera: benthic (bottom-dwelling) and planktic (free-floating)
Can be used to interpret the paleoenvironmental conditions during deposition of the Imperial Formation in southern California.

Benthic foraminifera assemblages indicate the Imperial Formation was deposited at neritic depths (0-152 m) and possibly upper bathyal depths (152-244 m) (depth estimates are based on upper depth limits of key benthic foraminiferal species)

Planktic foraminifera assemblages indicate a transition from warm water species to cooler water species up section, suggesting an increase in surface water temperatures over time.

Biostratigraphic and paleoecologic summary.[McDougall]]

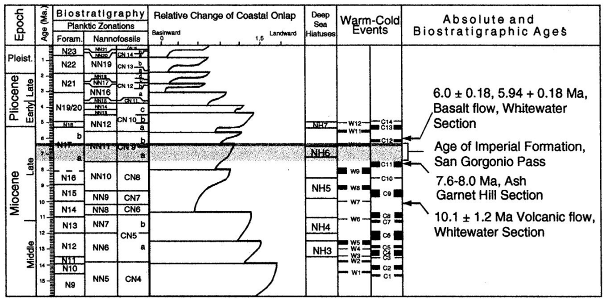

Lithology summaries:

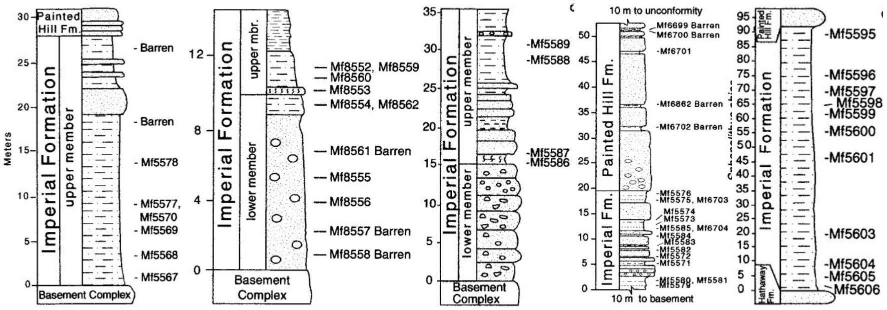
Meters
Painted Hill Fm.
Imperial Formation
upper member
lower member
upper mbr.
Basement Complex
Painted Hill Fm.
Imperial Fm.
10 m to unconformity
10 m to basement
Barren
Mf5578
Mf5577, Mf5570
Mf5569
Mf5568
Mf5567
Mf8552, Mf8559
Mf8560
Mf8553
Mf8554, Mf8562
Mf8561 Barren
Mf8555
Mf8556
Mf8557 Barren
Mf8558 Barren
Mf5589
Mf5588
Mf5587
Mf5586
Mf6699 Barren
Mf6700 Barren
Mf6701
Mf6862 Barren
Mf6702 Barren
Mf5595
Mf5596
Mf5597
Mf5598
Mf5599
Mf5600
Mf5601
Mf5603
Mf5604
Mf5605
Mf5606
Hathaway Fm.

WWII WWIV WWA/X WWP Cabazon

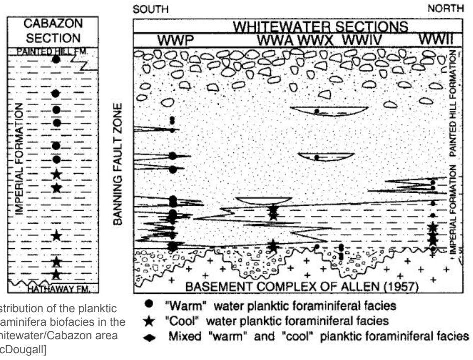
CABAZON SECTION
PAINTED HILL FM.
IMPERIAL FORMATION
HATHAWAY FM.
BANNING FAULT ZONE
SOUTH
NORTH
WHITEWATER SECTIONS
WWP
WWA WWX WWIV
WWII
PAINTED HILL FORMATION
IMPERIAL FORMATION
BASEMENT COMPLEX OF ALLEN (1957)
● "Warm" water planktic foraminiferal facies
★ "Cool" water planktic foraminiferal facies
◆ Mixed "warm" and "cool" planktic foraminiferal facies

Distribution of the planktic foraminifera biofacies in the Whitewater/Cabazon area [McDougall]

Trace Fossils

Gastrochaenolites(a bivalve) left the most common trace fossil in the “Gastrochaenolites Assemblage”. These borings are densely concentrated in marble outcrops. While the boring organism isn't observed here, the same ichnospecies of Gastrochaenolites is found in corals and oysters in the Imperial Formation, and some rare borings contain shells of the mytilid bivalve *Lithophaga*.

Other trace fossils are present in the study area, including Entobia (clionid sponges), Typanites (worms or barnacles), Maeandropolydora (polychaetes), and echinoid pits. These fossils represent a diverse environment on carbonate substrate-controlled, rocky shore, consisting of communities of bivalves, sponges, worms, and echinoids

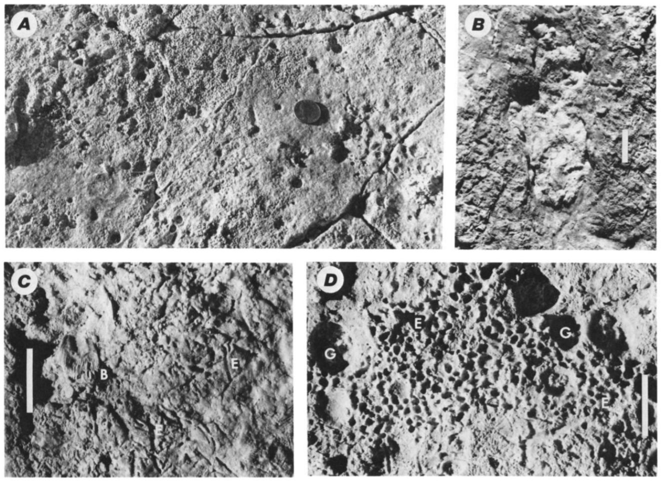
A
B
C
B
E
D
E
G
G
E

Diverse boring assemblage, locality 90062; scale bars are 1 cm. A) Bored marble surface showing Entobia (perforate pattern) and Gastrochaenolites (circular holes); coin is 24 mm in diameter. B) Coalescing echinoid pits, filled with light-colored skeletal packstone; MPM 28231. C) Canals of Entobia (E) and barnacle plate (B) resting on bored surface; MPM 28232. D) Boxwork of Entobia chambers (E) and distal parts of truncated Gastrochaenolites chambers (G); MPM 28 [Watkins]

References:

Smith, J. T. (1991). Cenozoic Marine Mollusks and Paleogeography of the Gulf of California: Chapter 31: Part V. Physical Oceanography, Primary Productivity, Sedimentology.
URL:https://pubs.geoscienceworld.org/aapg/books/edited-volume/1339/chapter/107171542/Cenozoic-Marine-Mollusks-and-Paleogeography-of-the

Watkins, R. (1990). Paleoecology of a Pliocene rocky shoreline, Salton Trough region, California. Palaios, 167-175.
URL:https://www.jstor.org/stable/3514813?seq=1

McDougall, K. A., Poore, R. Z., & Matti, J. C. (1999). Age and paleoenvironment of the imperial formation near San Gorgonio Pass, southern California. The Journal of Foraminiferal Research, 29(1), 4-25.
URL:https://pubs.geoscienceworld.org/cushmanfoundation/jfr/article/29/1/4/76779/Age-and-paleoenvironment-of-the-Imperial-Formation

Fry, K. (2011, November 27). Cochella Valley Ancient Fish Traps and Petroglyphs. Youtube
URL:https://www.youtube.com/watch?v=dIMbEo5aICM&feature=youtu.be

Burks, M. B. / E. (2016, March 16). Fossils unearthed along State Route 15 in San Diego. KPBS Public Media.
URL: https://www.kpbs.org/news/science-technology/2016/03/16/fossils-unearthed-along-state-route-15-san-diego

Arnold, R. (1903). The paleontology and stratigraphy of the marine Pliocene and Pleistocene of San Pedro, California (Vol. 31). The Academy.
URL:https://books.google.com/books?hl=en&lr=&id=VMkyAQAAMAAJ&oi=fnd&pg=PA9&ots=Qzj3eWaiY-&sig=jpRTc4anSV6K9z_HcJaz6ZEG-i8#v=onepage&q&f=false

McDougall, K., Beard, L. S., Karlstrom, K. E., Young, R. A., & Billingsley, G. H. (2011). Update on microfossil studies in the northern Gulf of California, Salton Trough, and lower Colorado River. In CRevolution 2—Origin and Evolution of the Colorado River System, Workshop Abstracts (p. 218).
URL: https://pubs.usgs.gov/of/2011/1210/of2011-1210.pdf#page=224

Tarbet, L. A., & Holman, W. H. (1944). Stratigraphy and micropaleontology of the west side of Imperial Valley, California. AAPG Bulletin, 28(12), 1781-1782.
URL:https://pubs.geoscienceworld.org/aapg/aapgbull/article/28/12/1781/544946/Stratigraphy-and-Micropaleontology-of-the-West

Resources of California’s largest lake

Amanda Bednarick

Mecca
Oasis
111
CALEB
Desert Camp
North Shore
86
111
DESERT BEACH

The Salton Sea conjures images of toxic runoff, dust storms, and health problems in surrounding communities. But one person’s ecological disaster is another’s motherlode. In addition to lithium and geothermal power, the Salton Sea is a source of manganese and zinc, solar power, bird habitat, and date shakes.

Manganese and zinc

The metal-rich brines of the Salton Sea have attracted much attention recently, mainly because there is great potential to extract valuable quantities of lithium. Hydrothermal alteration of igneous and sedimentary units related to the extensional tectonic regime and chemical weathering of mountains and buttes around the basin leach metals from the rock and deliver them to the basin, where they concentrate over time. Manganese and zinc are likely to be mined out of the brines here alongside lithium. Reports estimate the total mass of zinc and manganese in the brines are 15 million metric tons and five million metric tons, respectively. These are significant quantities given the current annual global production of these metals are 13 million metric tons for zinc and 19 million metric tons for manganese. Their economic value is tied to their uses in batteries, alloys, rubber, ceramics, and various electronics and medicines.

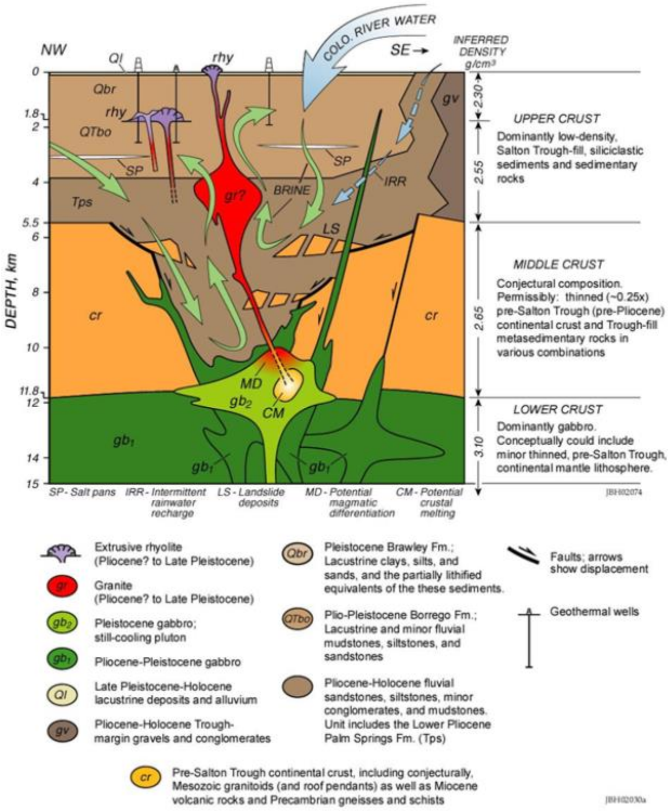
COLO. RIVER WATER
NW
SE →
INFERRED DENSITY g/cm³
Ql
rhy
Qbr
rhy
QTbo
SP
gr?
BRINE
SP
IRR
gv
Tps
LS
cr
cr
MD
gb_2
CM
gb_1
gb_1
gb_1
DEPTH, km
0
1.8
2
4
5.5
6
8
10
11.8
12
14
15
2.30
2.55
2.65
3.10
UPPER CRUST
Dominantly low-density, Salton Trough-fill, siliciclastic sediments and sedimentary rocks
MIDDLE CRUST
Conjectural composition. Permissibly: thinned (~0.25x) pre-Salton Trough (pre-Pliocene) continental crust and Trough-fill metasedimentary rocks in various combinations
LOWER CRUST
Dominantly gabbro. Conceptually could include minor thinned, pre-Salton Trough, continental mantle lithosphere.
SP - Salt pans
IRR - Intermittent rainwater recharge
LS - Landslide deposits
MD - Potential magmatic differentiation
CM - Potential crustal melting
JBH02074
Extrusive rhyolite (Pliocene? to Late Pleistocene)
gr
Granite (Pliocene? to Late Pleistocene)
gb_2
Pleistocene gabbro; still-cooling pluton
gb_1
Pliocene-Pleistocene gabbro
Ql
Late Pleistocene-Holocene lacustrine deposits and alluvium
gv
Pliocene-Holocene Trough-margin gravels and conglomerates
Qbr
Pleistocene Brawley Fm.; Lacustrine clays, silts, and sands, and the partially lithified equivalents of the these sediments.
QTbo
Plio-Pleistocene Borrego Fm.; Lacustrine and minor fluvial mudstones, siltstones, and sandstones
Pliocene-Holocene fluvial sandstones, siltstones, minor conglomerates, and mudstones. Unit includes the Lower Pliocene Palm Springs Fm. (Tps)
Faults; arrows show displacement
Geothermal wells
cr
Pre-Salton Trough continental crust, including conjecturally, Mesozoic granitoids (and roof pendants) as well as Miocene volcanic rocks and Precambrian gneisses and schists
JBH02030a

From Hulen et al., 2002

Solar power

Several solar power companies have installed fields of solar panels in the area surrounding the Salton Sea, amounting to what one source called the fourth largest solar complex in the world. It is sunny here almost every single day of the year, and it is >100 degrees Fahrenheit >100 days per year. Unsurprisingly, the energy produced through solar here is enough to power tens of thousands of homes each year.

The potential for solar power means more renewable energy and the generation of some jobs, at least temporarily. And some farmers are realizing they can improve their economic situations by using their land to farm solar energy instead of crops. But on the flip side, converting land that would otherwise be used for agriculture into solar panel land decreases flow into the Salton Sea, because agricultural runoff is its main source of water. Some also complain that solar farm construction depletes the water supply, exacerbating the problem. (There are, of course, additional reasons flow is decreasing). Decreased water flow contributes to the dust problem and decreases the viability of the fish and bird habitat. Nearby communities are arguably experiencing more harm than good on the whole as a result of this move toward solar.

SOLAR
DESTROY
LIFE

LETTERS UNANSWERED. PLAYA MORE EXPOSED.
THE TIME IS NOW!
SALTON SEA
AIR QUALITY WORSENING. HABITAT DEGRADED.

Bird habitat

The Salton Sea is an oasis of water and food to birds migrating along the Pacific Flyway who find themselves flying through hundreds of miles of desert. Hundreds of species use it as a pit stop, many of which are sensitive or endangered.

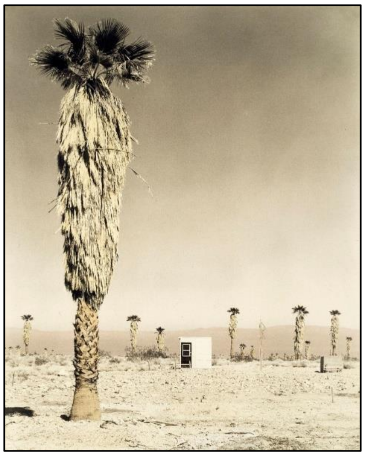

Date shakes

Imperial and Coachella Valleys are among the USA's top producers of dates. The long season, irrigation from the Colorado River, and alluvial soils are prime date-growing conditions.

References

- Hulen, J. B., Kaspereit, D., Norton, D. L., Osborn, W., Pulka, F. S., & Bloomquist, R. (2002). Refined conceptual modeling and a new resource estimate for the Salton Sea geothermal field, Imperial Valley, California. *Transactions-geothermal resources council*, 29-36.
- McKibben, M. A., Elders, W. A., & Raju, A. S. (2021). Lithium and other geothermal mineral and energy resources beneath the Salton Sea. *Crisis at the Salton Sea: Research Gaps and Opportunities*, *16*.
- Dobson, P., Araya, N., Brounce, M., Busse, M., Camarillo, M. K., English, L., ... & White, M. (2023). *Characterizing the Geothermal Lithium Resource at the Salton Sea*. Lawrence Berkeley National Laboratory (LBNL), Berkeley, CA (United States).
- https://undark.org/2023/07/03/scientists-warned-of-a-salton-sea-disaster-no-one-listened/
- https://www.theguardian.com/us-news/2023/may/21/solar-farms-energy-power-california-mojave-desert

The Resources of the Salton Sea: A Catalyst for a Green Energy Transition?

Jonathan Bennett | Ge 136b | Winter 2024

Geologic History of the Salton Sea

The SS-GR is located 60 km north of the United States-Mexico border, on the southeastern shore of the Salton Sea, within the tectonically active Salton Trough, an active continental rift zone. The region has been shaped by a complex tectonic history involving subduction, extension, and strike-slip faulting.

The tectonic evolution of the region began with the subduction of the Farallon slab beneath the North American plate, which persisted until approximately 12 million years ago (Ma). As subduction ceased, the tectonic regime transitioned into a strike-slip system associated with the San Andreas Fault. Simultaneously, extensional forces created the Salton Trough (Fig. 1), a basin that continues to subside due to ongoing crustal thinning and fault activity. The Salton Trough is characterized by step-over faults linking the East Pacific Rise to the San Andreas Fault system, which facilitates significant geothermal activity and the generation of lithium-rich brines[1].

Since the late Miocene (approximately 8.5-7 Ma), continuous sediment deposition from marine, deltaic, alluvial, and lacustrine environments have filled the Trough. The periodic rerouting of the Colorado River led to the formation of ancient evaporative lakes, known as Lake Cahuilla, which played a significant role in the concentration of evaporites, including lithium and potassium-bearing deposits. Over the past 40,000 years, cycles of flooding and evaporation further enhanced mineral concentration in residual brines. A one-dimensional evaporation model suggests that evaporation alone can increase lithium concentrations up to 120 ppm with a 40X brine concentration factor.

In addition to surface processes, the geothermal system plays a crucial role in lithium enrichment. The region is influenced by high heat flux due to crustal thinning, deep magmatic intrusions, and Quaternary volcanism, which drive the geothermal heating of sedimentary units and the formation of hypersaline lithium-rich brines. These conditions facilitate hydrothermal circulation, where deep-seated fluids leach lithium from volcanic and sedimentary rocks, transporting it into the brine. Modeling of fluid-rock interactions in the SS-GR indicates that lithium-bearing minerals, such as hectorite (Li-clay), cookeite (Li-chlorite), and Li-rich feldspars, continuously dissolve and reprecipitate (Fig. 2), maintaining lithium concentrations in the range of 200 to 400 ppm.

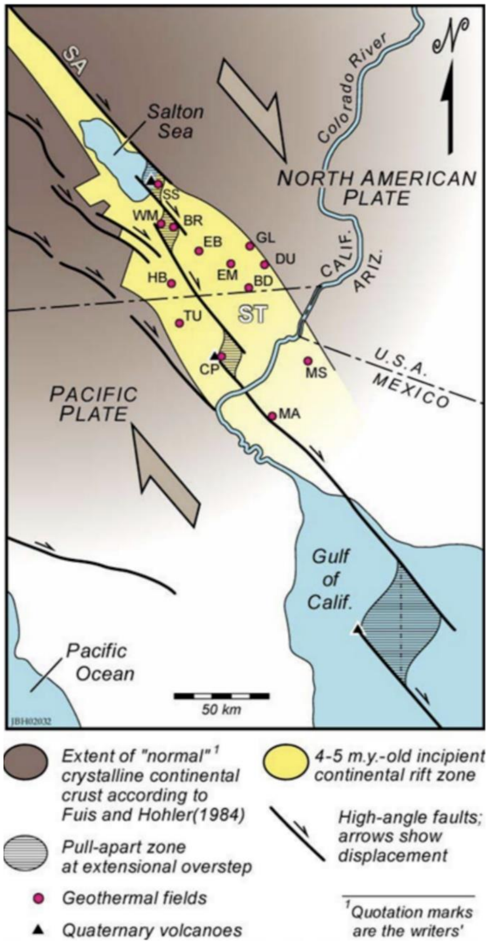
SA
Salton Sea
NORTH AMERICAN PLATE
Colorado River
N
SS
WM
BR
EB
GL
DU
HB
EM
BD
TU
ST
CP
MS
MA
CALIF.
ARIZ.
U.S.A.
MEXICO
PACIFIC PLATE
Gulf of Calif.
Pacific Ocean
50 km
JBH02032
Extent of "normal"1 crystalline continental crust according to Fuis and Hohler(1984)
4-5 m.y.-old incipient continental rift zone
Pull-apart zone at extensional overstep
High-angle faults; arrows show displacement
Geothermal fields
Quaternary volcanoes
1Quotation marks are the writers'

Figure 1: Location and tectonic background for the Salton Trough, from Hulen et al., 2002.

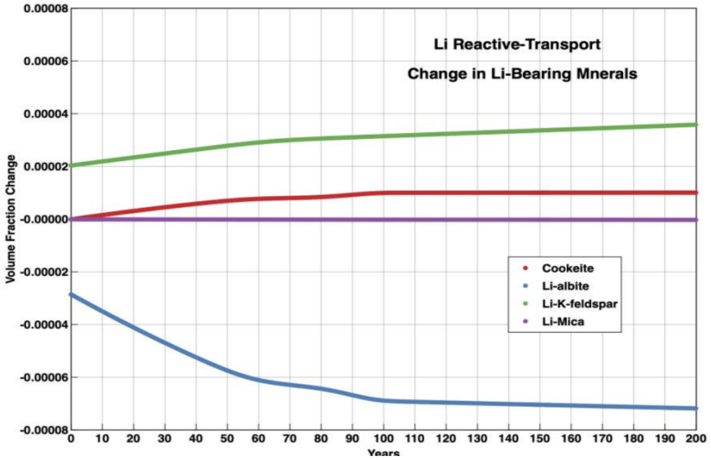

Figure 2: Modelled change in Li-bearing mineral abundances over time, showing Li-albite dissolving, but cookeite and Li-K-feldspar precipitating in its place, from Dobson, Araya, Brounce, et al., 2023.

Another key factor is the presence of a brine interface within the geothermal field, where a denser, lithium-rich hypersaline brine underlies a less saline geothermal fluid. This interface follows the depth of the 250°C isotherm, linking its formation directly to the region's heat source. This interface serves as a zone of active mineralization, where lithium accumulates due to fluid mixing and precipitation-dissolution reactions. Geochemical analysis of brine compositions suggests that these brines have been lithium-enriched over time through a combination of upward convective transport, evaporative concentration, and continuous mineral dissolution[2].

Overall, the tectonic setting, hydrothermal activity, and evaporative concentration cycles have made the Salton Sea one of the most lithium-rich geothermal systems in the world.

Resources of the Salton Sea and Their Uses

The Salton Sea Geothermal Resource Area (SS-GR) is one of the most lithium-rich geothermal brine deposits in North America, holding significant economic and strategic potential. The lithium concentrations in the SS-GR brines range from 200 to 400 parts per million (ppm), with an estimated 4.1 million metric tons of lithium carbonate equivalent (LCE) identified in the well-characterized portions of the reservoir. Should the full extent of the resource be realized, this amount could balloon to as much as 18 million metric tons of LCE, making it a globally significant lithium source. Companies such as Berkshire Hathaway Energy Renewables (BHER), EnergySource Minerals, and Controlled Thermal Resources (CTR) are actively investing in the development of direct lithium extraction (DLE) technologies (Fig. 3), which, if fully implemented, could produce over 600,000 metric tons of LCE annually[3].

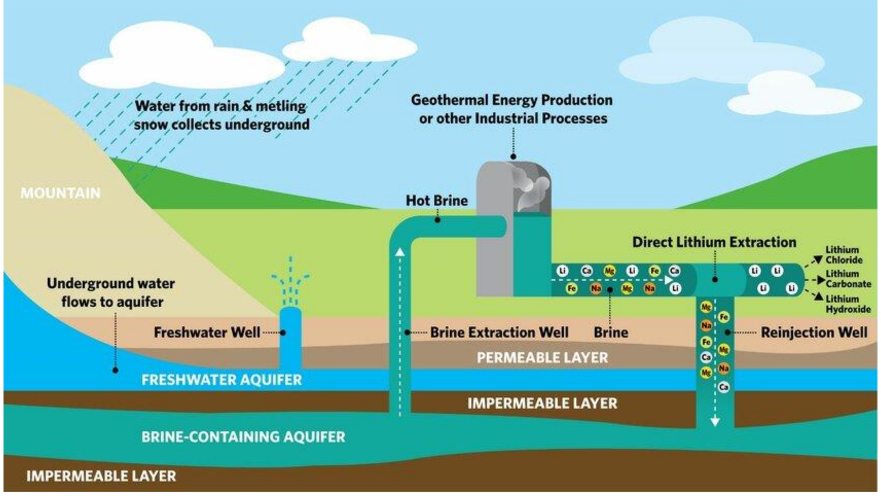

Figure 3: A basic schematic displaying how direct lithium extraction works in conjunction with geothermal energy production, from Parker et al., 2022.

In addition to lithium, the brines contain high concentrations of other valuable elements, including potassium (14,467 mg/kg), sodium (49,249 mg/kg), calcium (25,684 mg/kg), and zinc (463 mg/kg). Potassium is a key component in agricultural fertilizers, as it is crucial for maintaining soil fertility and enhancing crop yields. Sodium is widely used in chemical manufacturing, water treatment, and glass production. Calcium plays an essential role in cement and concrete production, making it required for the well-being of the construction industry while also being utilized in steelmaking, pharmaceuticals, and food processing. Zinc is critical for galvanization as it provides corrosion resistance for steel and iron. It is also a key ingredient in batteries, alloys, and human nutrition supplements.

Further geochemical analyses indicate that the SS-GR brines also contain trace amounts of other critical and rare metals, such as manganese, boron, and rubidium. Manganese is used in steel production to improve hardness and strength, as well as in lithium-ion battery cathodes, making it a crucial component in electric vehicle (EV) batteries. Boron is a key element in fiberglass, ceramics, and high-strength glass used in electronics and space technologies, while rubidium is utilized in specialty glasses, atomic clocks, and biomedical research[4].

The high total dissolved solids content of these brines suggests that additional valuable resources, including rare earth elements and other trace minerals, could be extracted with advanced separation and refining techniques, further enhancing the economic feasibility of the region.

As American mining firms continue to advance DLE technologies and geometallurgical techniques, it would not be surprising to see the broader Salton Sea area become a key example for sustainable resource development, as these methods are far less pollutive and invasive than traditional hardrock extraction. With these facts in mind, this area could play a substantial role in the United States' desire for mineral independence and a transition towards green energy.

References:

[1] Hulen et al., 2002. *Refined Conceptual Modeling and a New Resource Estimate for the Salton Sea Geothermal Field, Imperial Valley, California.* ResearchGate. [2] Dobson, P., Araya, N., Brounce, M., et al., 2023. *Characterizing the Geothermal Lithium Resource at the Salton Sea.* Lawrence Berkeley National Laboratory. [3] Parker et al., 2022. *Potential Lithium Extraction in the United States: Environmental, Economic, and Policy Implications.* ResearchGate. [4] U.S. Geological Survey, 2024. *Mineral Commodity Summaries 2024.* U.S. Geological Survey, Reston, VA.

Smelling the Salton Sea:
Sulfur Dynamics in a Polluted Saline Lake

Jordan Chastain, Ge136B

The Salton Sea is California's largest lake, but it may not be for long. Water levels are steadily declining due to drought conditions and policy decisions to reroute freshwater inflow. It also smells gross, which is majorly due to biological activity. Today, the main water sources for this basin are agricultural runoff and wastewater, which has caused extreme increases in salinity for the last few decades, affecting the active microbial metabolisms. A major component of this salinity is sulfate, as shown in Figure 1.

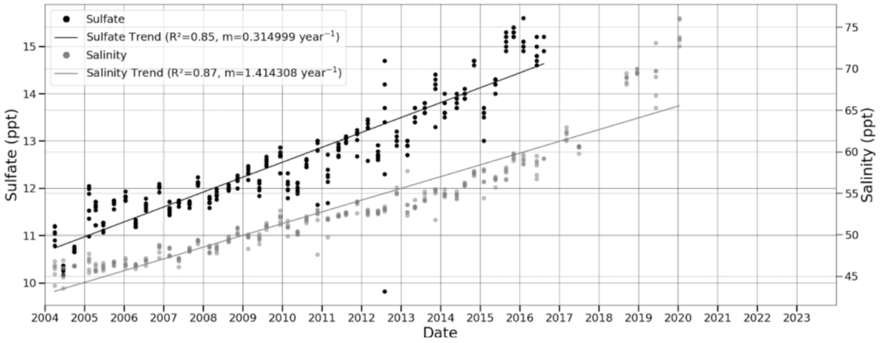

Figure 1. Sulfate and salinity measurements in the Salton Sea over the last twenty years[1].

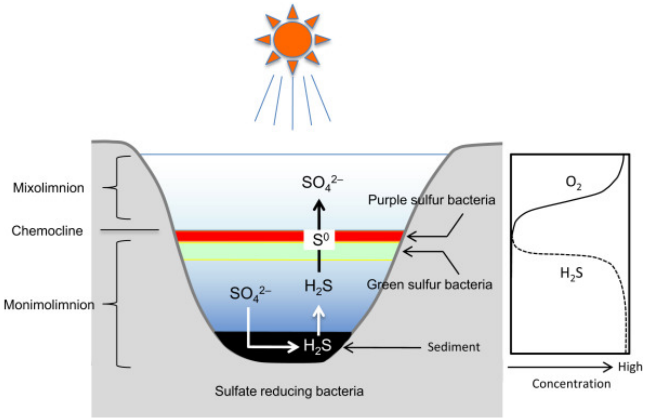

Mixolimnion
Chemocline
Monimolimnion
SO₄²⁻
S⁰
H₂S
SO₄²⁻
H₂S
Purple sulfur bacteria
Green sulfur bacteria
Sediment
Sulfate reducing bacteria
O₂
H₂S
High
Concentration

Figure 2. Stratification in lake water chemical concentrations can occur in high-salinity lakes, where oxygen concentrations are lower and sulfate reducing bacteria can thrive in sediments[3].

When lakes have high salinity and sulfate, interesting biological dynamics can develop. Oxygen does not dissolve as readily in hypersaline waters, which can allow for oxygen-depleted areas to easily form and persist if there is any way to spatially remove oxygen[2]. Sulfate reducing bacteria use sulfate in their metabolism and form hydrogen sulfide (H_2S), which can then react with oxygen near them in deep waters and create anoxic conditions, as shown in Figure 2. Oxygen diffusion from the atmosphere into water is relatively slow, as is the reaction of oxygen with H_2S. So, if conditions persist that allow for sulfate reducing bacterial growth, then they can outpace oxygen addition to the water with their H_2S production, increasing the range of oxygen depletion. Frequent mixing events can prevent H_2S from building up at depth by exposing deep waters directly to the atmosphere, oxidizing that reduced sulfide back to sulfate and homogenizing oxygen concentrations. As shown in Figure 3, seasonal variations can lead to water column mixing or stratification as air temperatures change. This means that in spring and fall, mixing is common enough that stratification and H_2S accumulation does not occur. Biological activity in cold winter weather is minimal, preventing accumulation then as well. In summer however, temperature gradients allow for

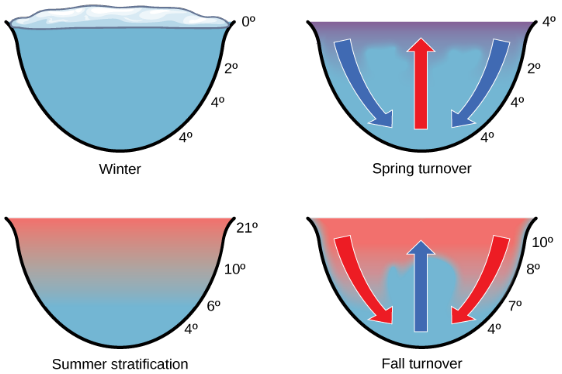

0º
2º
4º
4º
Winter
4º
2º
4º
4º
Spring turnover
21º
10º
6º
4º
Summer stratification
10º
8º
7º
4º
Fall turnover

Figure 3. Seasons change the temperature distributions in shallow lakes, leading to seasonal differences in water column mixing[4].

The Salton Sea: Hazards and Resources

Abby Keebler

The Shrinking Salton Sea

The southwestern U.S. currently faces a water shortage, rapidly depleting major reservoirs like Lake Mead and Lake Powell even as demand for water remains high. The Salton Sea, filled by a breach of the Colorado River, is impacted by droughts and the water ration policies enacted to mitigate water shortages. California was using more than its allocated amount of water from the Colorado River, so in 2003, the Quantification Settlement Agreement was signed to divert some of the Imperial Valley's water to San Diego each year. Imperial Valley farmers adopted more water-efficient farming practices and successfully reduced water consumption, leading to a significant decrease in the Salton Sea's agricultural runoff water supply [1]. Without its typical water supply, the Salton Sea is receding rapidly, exposing its lakebed to the air.

Environmental Hazards of the Salty Sea

Exposed lake sediments are extremely fine-grained and easily entrained as atmospheric dust by the strong winds of the Imperial Valley. The Salton sea is an endorheic basin; its waters are extremely saline (44 g/L, as compared to 35 for the Pacific Ocean), producing evaporites [2]. Additionally, runoff from surrounding farmlands has led to highly concentrated agricultural pollutants in the lake sediments. Residents of the Imperial Valley are subjected to health hazards from breathing in various harmful substances:

A Salton Sea dust storm sweeps over Imperial Valley communities.

- Heavy metals like lead, arsenic, selenium, and cadmium can lead to inflammation, oxidative stress, asthma, and other respiratory diseases [3]
- Lead and mercury are neurotoxins which are linked to cognitive/memory decline and developmental problems in children [4]
- Heavy metals are also known carcinogens and cadmium exposure is linked to renal failure [5]

Hell's Kitchen Lithium Project

The Salton Sea brines contain large amounts of lithium, a critical energy resource. The U.S. currently has one operating lithium mine (Silver Peak, NV). Lithium is found in brine aquifers. The lithium brine is pumped up into shallow pools, then allowed to evaporate, concentrating the lithium until it can be pumped into a nearby facility to be extracted and refined. The removal of such large quantities of water from aquifers has negatively impacted freshwater supply in nearby wells [6]. Other hazards include the potential for mine runoff to contaminate nearby waterways and the development of sinkholes due to dewatering.

At the Salton Sea, a different method of lithium extraction is being pioneered by operators of existing geothermal power plants. Here, they propose to extract lithium from hot brines which are already being pumped for the power plant, then reinject the water into the aquifer [7]. Overall, the environmental impact of this extraction method is much lower than traditional methods for extracting lithium from brines, since land does not need to be converted to evaporation pools, the plant can run off of green geothermal energy, and water is returned to the aquifer after extraction. Imperial County has extremely high rates of poverty and respiratory disease due to poor air quality. Community organizers like Luis Olmedo are advocating to ensure the project does not increase environmental hazards and brings economic benefits directly to residents:

"When the economic system is out of balance and the poor pay the price for the negligence of the rich and those who waste our natural resources, we end up with communities like this one. We are constantly breathing polluted air, which has repercussions on our respiratory system. These are our minerals. The minerals are on public lands," said Olmedo. He emphasizes that the need is for stable jobs and long-term investments. "What are we going to get out of this? Are they just going to come and exploit the whole resource and then leave? Or will they help us and stay here for the long run?" [7]

All About Birds !!!

For migrating birds on the Pacific Flyway, the Salton Sea is a critical rest stop. 90-95% of California's original wetlands are gone, making the Salton Sea one of the last (and largest) places to stop during birds' journeys through Southern California. Over 400 species of birds have been spotted here, and many populations are well-represented—USFWS reports that 95% of the North American population of eared grebes and 90% of white pelicans migrate through the sea.

The southern part of the Salton Sea is designated as the Sonny Bono Salton Sea National Wildlife Refuge, operated by the U.S. Fish and Wildlife Service. The Refuge is intended to preserve the habitat necessary to support migrating birds with a focus on ponds, marshes, and open-water wetlands. In addition to protecting habitat from development, the Refuge works with farmers to grow crops like ryegrass and wheat for geese and sandhill cranes to eat during the fall/winter migration [8]. Farmers also grow swamp timothy, watergrass, and sprangletop in duck ponds for waterfowl like ducks, sandpipers, herons, and ibis [8]. USFWS often performs prescribed burns to ensure the habitats are primarily populated with native plants. Biologists conduct wildlife surveys to understand bird population dynamics.

Birds visiting the Salton Sea face unique challenges. Microbes can easily grow due to year-round warm temperatures and high nutrient density, and diseases like avian botulism can easily spread among populations since the Salton Sea is a high-traffic area [8].

Some Cool Birds !!!

Burrowing Owl

Yuma Ridgeway's rail | Sandhill Crane

Western Snowy Plover

Eared Grebe | American Bittern

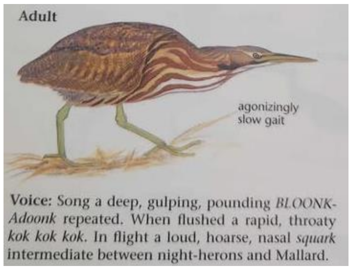

Voice: Song a deep, gulping, pounding *BLOONK-Adoonk* repeated. When flushed a rapid, throaty *kok kok kok*. In flight a loud, hoarse, nasal *squark* intermediate between night-herons and Mallard.

References:

[1] Water Education Foundation. (2022). Quantification Settlement Agreement. [2] Montazar (2013). Salton Sea and Salinity. [3] Farzan et al. (2019). Assessment of Respiratory Health Symptoms and Asthma in Children near a Drying Saline Lake. [4] World Health Organization. (2024). Lead poisoning fact sheet [5] Doccioli et al. (2023). Association of cadmium environmental exposure with chronic kidney disease: A systematic review and meta-analysis, *Science of the Total Environment* [6] Tucson Sentinel. (2024). The untold threat to water in rush to mine American lithium. [7] Belanger (2024). The green treasure below a toxic lake. [8] U.S. Fish and Wildlife Service. (2025). Sonny Bono Salton Sea National Wildlife Refuge.

Efforts towards restoration of the Salton Sea

Adam Artymowicz

The tap is turned off

The Salton Sea is an endorheic artificial lake fed by runoff from farms in the Imperial Valley. A shallow body of water almost size of Lake Tahoe, it experiences enormous evaporative loss, so its size is sensitively dependent on the amount of inflow from the surrounding farms, and recently that inflow has been shrinking.

For more than a century, the Imperial Valley's access to Colorado River water has been assured by the valley's senior water rights — the Imperial Irrigation District (IID), which supplies the valley's farms, gets first dibs on roughly 80% of California's share of water from the river [8]. This means that in the event of a drought, cities like Los Angeles and San Diego (which get roughly half their water from the Colorado River), face reductions in their water use before Imperial Valley farms do.

In the early 2000s, in the midst of an extended drought, Southern California cities looked to protect themselves from this possibility. In 2003, the IID agreed to sell nearly 20% of its water to Southern California cities, and use the profits to increase efficiency, for instance by reducing leakage from the All-American and Coachella canals [11]. The net effect for the Salton Sea was a decrease in water inflow, causing it to shrink.

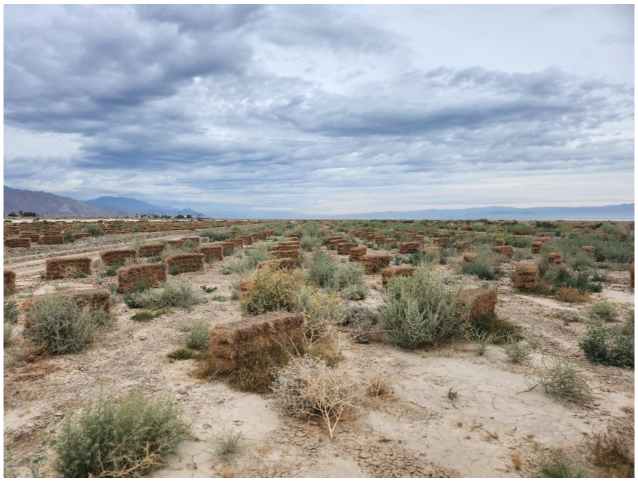

Figure 1: The SSMP's Vegetation Enhancement project on the west side of the Sea. Hay bales are placed between plantings to prevent damage from blowing dust [9]

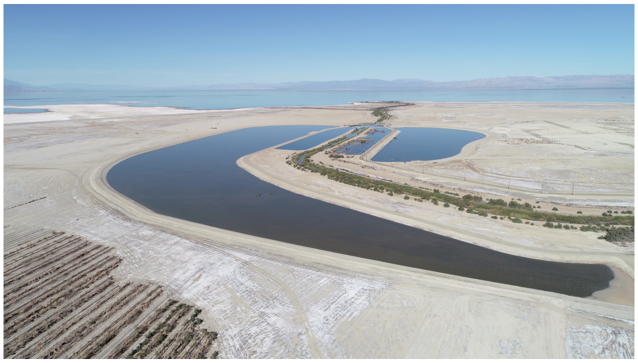

Figure 2: Located at the southern end of the Sea, the SSMP's Species Conservation Habitat will "provide feeding, resting, and breeding habitat for birds and fish, particularly fish-eating birds" [10]

Averting disaster

By causing the Salton Sea to shrink, the 2003 agreement could mean an environmental and public health disaster (see Abigail Keebler's report). This danger was recognized by the California State Legislature, who dutifully passed a pair of bills shielding all signatories agreement from liability for environmental effects [2, 3].

The state of California, having made itself solely responsible for mitigating the effects of a shrinking Salton Sea [7], went about preparing a restoration plan. It commissioned the California Natural Resources Agency to prepare one, who returned in 2007 with a proposal for a full restoration of the Sea, costing $8.9 billion [1]. Impeccably timed for the beginning of the 2008 recession, this plan was rejected by the state legislature, who deemed it too expensive [7].

Progress on Salton Sea restoration stalled for a decade until, in 2017, California finally approved a restoration plan (perhaps motivated by the IID's threats to withhold its promised water to San Diego if the state of California didn't meet its environmental obligations)[5]. With a relatively modest $383 million budget compared to the original $8.9 billion, the 10-year Salton Sea Management Plan (SSMP) does not share the 2007 proposal's ambitious goal of full restoration. Instead, it focuses on limiting damage using dust suppression and habitat reconstruction, by treating the land area exposed by the receding sea, the SSMP plans to treat 30,000 acres, roughly 40% of the newly exposed lakebed between 2018 and 2028 [4].

Dust suppression projects within the SSMP include so-called "vegetation enhancement" in which native, salt-resistant plants are grown to prevent soil erosion and reduce dust emissions; and "surface roughening" projects which involve digging furrows perpendicular to the prevailing wind direction in order to slow wind speeds across the surface of the exposed lakebed. Habitat reconstruction projects involve creating ponds, basins, and "water conveyance features" to establish habitats for fish that historically inhabited the Salton Sea, as well as migratory birds that eat these fish [10].

Pipe dreams

Beyond 2028, the future of the Salton Sea remains uncertain, but some ambitious proposals exist for long-term restoration plans. In 2018 and again 2021, California Natural Resources Agency showed interest in an ambitious proposal to replenish the Salton Sea using water from a source other than the Colorado River [6]. Since the Salton Sea lies some 200 feet below sea level, the most common proposal in this vein is to build a pipeline to desalinate and transport the water by gravity from the Sea of Cortez. Unfortunately, after reviewing 18 proposals for such concepts, the state of California ultimately did not recommend the approach, citing "high cost, environmental damage, minimal benefits to Mexico beyond construction and operations jobs, and potential that benefits would not be realized" [12].

References

[1] California Department of Water Resources. Salton sea species conservation habitat project: Final eis/eir. `https://water.ca.gov/-/media/DWR-Website/Web-Pages/Programs/Integrated-Regional-Water-Management/Salton-Sea-Unit/Salton-Sea-Species-Conservation-Habita SaltonSea-Species-ConservationHabitat-Project-Final-EIS-EIR-2013_ay_19.pdf`, 2013. Accessed: 2025-02-08.

[2] California Legislature. Bill text: Senate bill no. 317 (chaptered 2003). `http://www.leginfo.ca.gov/pub/03-04/bill/sen/sb_0301-0350/sb_317_bill_20030929_chaptered.html`. Accessed: 2025-02-08.

[3] California Legislature. Bill text: Senate bill no. 654 (enrolled 2003). `http://www.leginfo.ca.gov/pub/03-04/bill/sen/sb_0651-0700/sb_654_bill_20030911_enrolled.html`. Accessed: 2025-02-08.

[4] California Natural Resources Agency. Ssmp phase 1: 10-year plan. `https://resources.ca.gov/CNRALegacyFiles/wp-content/uploads/2018/10/SSMP-Phase-1-10-Year-Plan.pdf`, 2018. Accessed: 2025-02-08.

[5] Desert Sun. California has new $383 million plan for shrinking salton sea. Accessed: 2025-02-08.

[6] Desert Sun. Salton sea panel advises against importing water from sea of cortez. Accessed: 2025-02-08.

[7] Brendan Hughes. Turning off the tap: Will california let the salton sea go down the drain? *California Western Law Review*, 56(1):Article 8, 2020. Accessed: 2025-02-08.

[8] Marc Reisner. *Cadillac Desert: The American West and Its Disappearing Water.* Penguin Books, New York, 1986.

[9] Salton Sea. Ssmp vegetation flyer. `https://saltonsea.ca.gov/wp-content/uploads/2022/09/SSMP_Vegetation-flyer_Aug-26-Final.pdf`, August 2022. Accessed: 2025-02-08.

[10] Salton Sea Restoration Projects. Species conservation habitat project. `https://projects.saltonsea.ca.gov`. Accessed: 2025-02-08.

[11] San Diego County Water Authority. Quantification settlement agreement final. `https://www.sdcwa.org/sites/default/files/files/QSA_final.pdf`. Accessed: 2025-02-08.

[12] Transform, UC Santa Cruz. Summary report on pipeline alternatives. `https://transform.ucsc.edu/wp-content/uploads/2022/09/Summary_Report_9-29-22_Final.pdf`, September 2022. Accessed: 2025-02-08.

Obsidian and Volcanism in the Salton Sea (Salton Buttes)

Jose Rodolfo Chreim, GE 136B, Winter 2024

February, 2025

Introduction

The Salton Buttes, figure 1a, are a group of five volcanoes in Southern California, on the Salton Sea, and consist of a 7-kilometer-long chain of five glassy looking (obsidian) lava domes - Mullet Island, North Red Hill, Obsidian Butte, Rock Hill, and South Red Hill - formed by effusive eruptions between 1,800 and 2,300 years ago. It is fueled by the heat emanating from zones of partially molten rock (magma) deep below the Earth's surface They lie within the Salton Trough, a tectonic depression - formed by the San Andreas and the San Jacinto Faults - that forms the northward extension of the Gulf of California, and are associated with a fumarole field and a geothermal field, with evidence of buried volcanoes underground. Initially believed to date back to the late Pleistocene epoch, recent studies have determined that the Salton Buttes formed much more recently, during the Holocene epoch [1]. Their eruptions were predominantly effusive, producing silica-rich rhyolitic lava, which cooled to form features such as Obsidian Buttes.

Geological background

The Salton Buttes lie on the southeastern shores of the Salton Sea Geothermal field, 1b, which has persistent small to moderate earthquakes monitored by both USGS and Caltech. Their peaks have an elevation of -40 m. The five lava domes, formed from viscous lava rising in a volcanic vent 250 m wide, rise 30–40 m above the surrounding terrain, and are no wider than 1 km each, with both Red Hills and Obsidian Butte being the largest. Obsidian is surrounded by lava flow and is notable for its abundance of obsidian; Mullet has an 'onion-skin' like foliation and has hot springs and mofettes. The presence of the lava domes, along with the ongoing geothermal activity, suggests that the magmatic system beneath the Salton Buttes remains active.

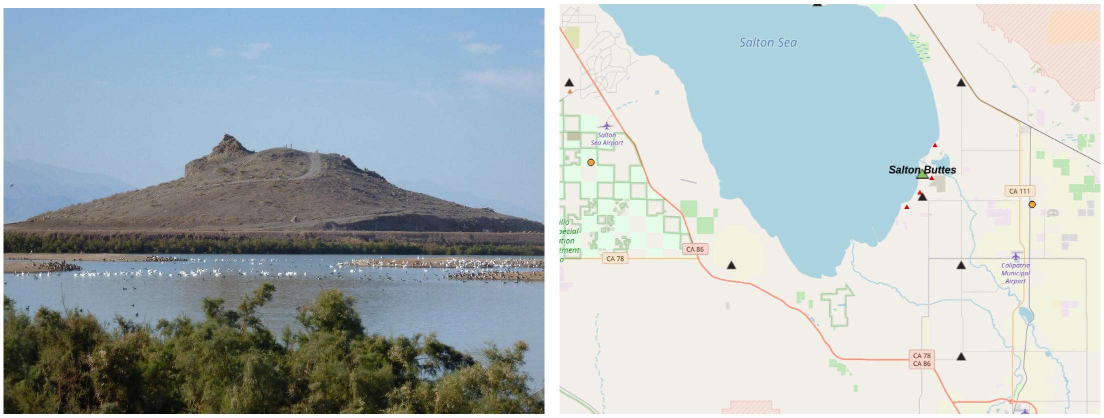

(a) View of the Salton Buttes [2]

(b) Salton Sea Geothermal field evidencing Salton Buttes area [2]

Figure 1: Salton Sea Geothermal field and Salton Buttes

The fumarole field is characterized by gryphons and salses, which exhale CO_2, steam, as ammonia and hydrogen sulfide. Some of the vents are as high as 2 m. As for the geothermal field, one of the largest and warmest on Earth - with temperatures of $360°C$ at 1.5–2.5 km depth - volcanic rocks have been found, such as andesite, basalt, dacite, diabase, gabbro, and rhyolite, the latter mostly forming the domes. This composition led to the formation of obsidian, a natural volcanic glass that forms when lava cools rapidly without significant crystal growth.

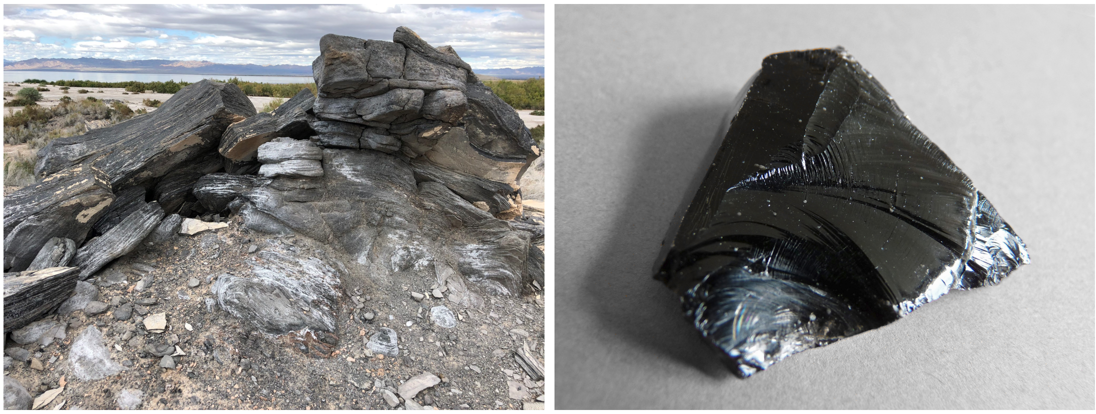

(a) Obsidian *In Natura* in the Salton Sea Area [5]

(b) Sample of obsidian rock [6]

Figure 2: Obsidian *in natura* and a sample

Obsidian

Obsidian, figure 2a, is a naturally occurring volcanic glass formed when lava from a volcano cools rapidly with minimal crystal growth [3]. It is produced from felsic lava, rich in the lighter elements such as silicon, oxygen, aluminium, sodium, and potassium, and is commonly found within the margins of rhyolitic lava flows known as *obsidian flows*; such flows have a high content of silica, giving them a high viscosity, which inhibits atomic diffusion through the lava and, consequently, nucleation in the formation of mineral crystals. Together with rapid cooling, this results in a natural glass forming from the lava. Obsidian, figure 2b, is hard, brittle, igneous, and amorphous; it therefore fractures with sharp edges. In the past, it was used to manufacture cutting and piercing tools, and it has been used experimentally as surgical scalpel blades [4]. Today, this stone is mostly used as a gem or ornament. The obsidian from Obsidian Buttes has been identified in distant archeological sites, like in the Colorado Desert, San Diego County, Northern Mexico, and the Southwestern US. In pre-modern times, the Obsidian Butte was an important regional source of such mineral; consequently, the region has been extensively quarried to the point that it has lost most of its original appearance.

References

[1] Heather M. Wright, Jorge A. Vazquez, Duane E. Champion, Andrew T. Calvert, Margaret T. Mangan, Mark Stelten, Kari M. Cooper, Charles Herzig, and Alexander Schriener Jr. Episodic holocene eruption of the salton buttes rhyolites, california, from paleomagnetic, u-th, and ar/ar dating. *Geochemistry, Geophysics, Geosystems*, 16(4):1198–1210, 2015.

[2] United States Geological Survey. Salton buttes. Available at https://www.usgs.gov/media/images/salton-buttes.

[3] Richard E Hughes. Trace element composition of obsidian butte, imperial county, california. *Bulletin, Southern California Academy of Sciences*, 85(1):35–45, 1986.

[4] M. Steven Shackley. Natural and cultural history of the obsidian butte source, imperial county, california. *California Archaeology*, 11(1):21–43, 2019.

[5] Out of the Office 4 Good. Travel & Hiking Adventures. Walking on volcanic domes in the salton sea area: Mar 2020. Available at https://www.outoftheoffice4good.com/post/walk-around-obsidian-butte-and-surrounding-area-salton-sea.

[6] Ji-Elle. Obsidian rock. Available at https://www.mindat.org/show.php?id=8519.

Algodones Dunes

Maria Schmeer

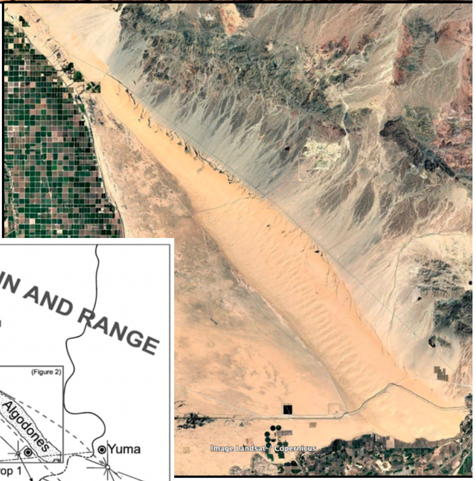
Image Landsat / Copernicus

Algodones Dunes is an erg, or a dune sea that is broad and flat with hardly any vegetation. The area is 45 miles long and 6 miles wide and includes the BLM-managed Imperial Sand Hills, one of the largest active dune patches in the U.S. at over 23,000 acres (~36 sq mi). It is bordered by the Chocolate Mountains to the east and cut by the All-American Canal and I-8 at the south. Its long axis runs parallel to the Salton Sea, which is to the northwest.

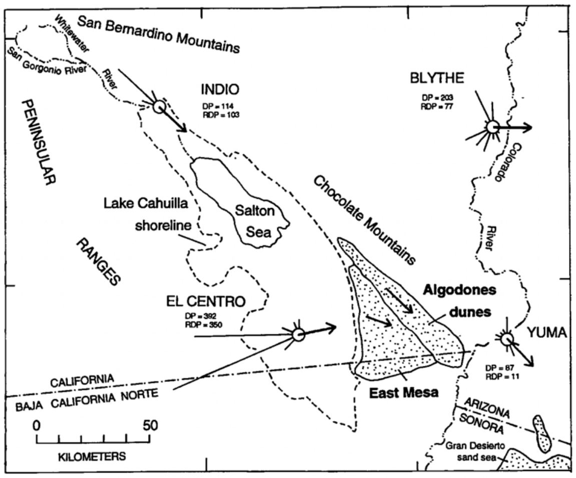
San Bernardino Mountains
Whitewater River
San Gorgonio River
PENINSULAR RANGES
INDIO
DP = 114
RDP = 103
BLYTHE
DP = 203
RDP = 77
Colorado River
Lake Cahuilla shoreline
Salton Sea
Chocolate Mountains
Algodones dunes
EL CENTRO
DP = 392
RDP = 350
YUMA
DP = 87
RDP = 11
East Mesa
CALIFORNIA
BAJA CALIFORNIA NORTE
ARIZONA
SONORA
Gran Desierto sand sea
0
50
KILOMETERS

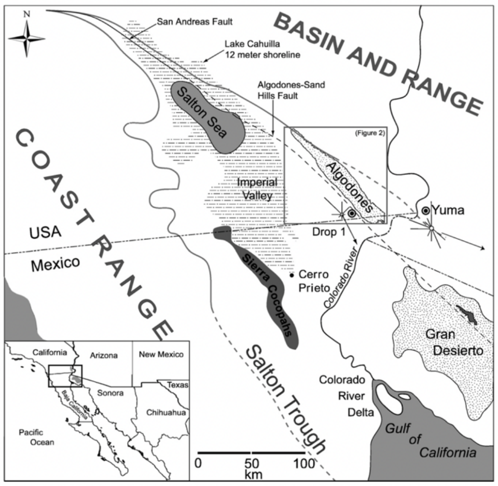
N
San Andreas Fault
Lake Cahuilla 12 meter shoreline
Algodones-Sand Hills Fault
BASIN AND RANGE
(Figure 2)
Salton Sea
COAST RANGE
Imperial Valley
Algodones
Yuma
USA
Mexico
Drop 1
Sierra Cocopahs
Cerro Prieto
Colorado River
Gran Desierto
Colorado River Delta
Gulf of California
Salton Trough
California
Arizona
New Mexico
Texas
Sonora
Chihuahua
Baja California
Pacific Ocean
0
50
100
km

Timmy C. and Zendaya enjoying some dunes.

The Algodones dunes are located in the Cahuilla Basin, a structural trough that includes the Gulf of California. This dune sea was once a floodplain of the Colorado River as the river would flow into the Gulf of California. Lake Cahuilla, a large freshwater lake, would form in the basin after high flows when the river would shift course and drain into the Salton Trough. The sands of this lake and those from a prominent ~12m tall shoreline were then transported by strong seasonal westerly and northerly winds, forming the dunes and transporting the sand eastward. These winds continue to force the migration of the dunes in similar easterly directions today. In addition to relict shoreline features found to the west, the large volume of sand in this basin and the dunes' primary orientations imply that the waves and currents of Lake Cahuilla were active and strong and were caused by winds would have been in the same northwesterly direction back then as they are now, indicating that any changes in climate did not significantly affect the geomorphology of this area.

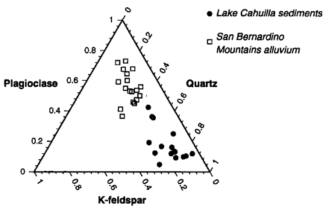

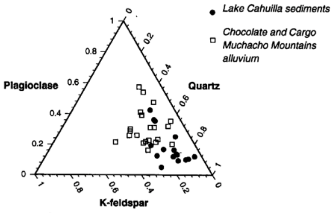

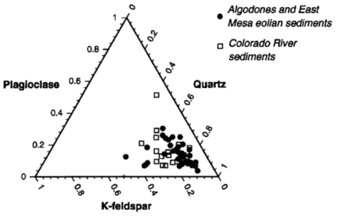

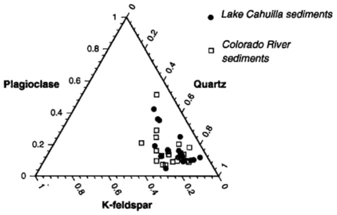

Geochemical analyses of the sand support their source interpretation. The minerology (high in quartz, low in plagioclase) and low trace element concentrations are consistent with Colorado River sediments (which undergo constant weathering/erosion/deposition cycles) and are distinctly different from sediments from the San Bernadino and Chocolate Mountains, which have undergone less transport. In the modern day, small streams carrying igneous and metamorphic sourced sediments from the nearby mountains are the current primary supplier of sand and gravel into the basin but not to the dunes themselves. Many sand grains towards the south are coated with ferric oxide (light reddish-brown color), which is a weathering product and could indicate that these are older sand masses, and that the dune field used to be more active in the past but has since slowed and is not gaining sediments. The sand dunes in the East Mesa region are most stable, likely because of a higher water table that supports more vegetation.

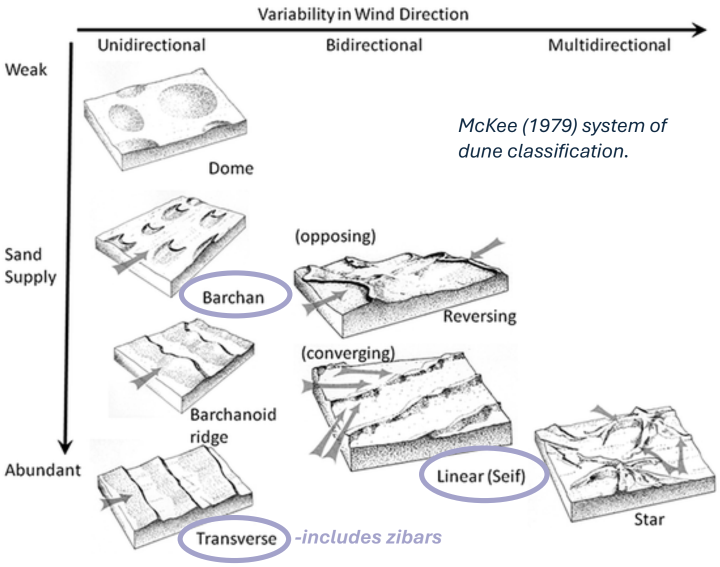
Variability in Wind Direction
Unidirectional
Bidirectional
Multidirectional
Weak
Sand Supply
Abundant
Dome
Barchan
(opposing)
Reversing
Barchanoid ridge
(converging)
Linear (Seif)
Star
Transverse
-includes zibars

McKee (1979) system of dune classification.

The complexity and spatial diversity of the dune patterns present are quite remarkable for such a narrow area. The complexity comes from the spatial superpositions of various simple dune types, and from all the dune patterns occurring on top of additional topographic lineations (which are possibly relict waves of shoreline dunes from Lake Cahuilla).

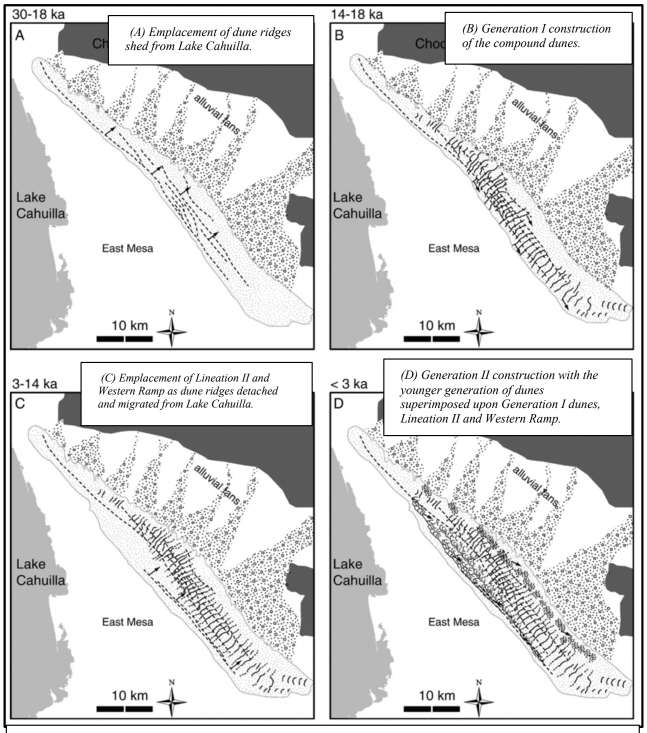
30-18 ka
A
(A) Emplacement of dune ridges shed from Lake Cahuilla.
14-18 ka
B
(B) Generation I construction of the compound dunes.
3-14 ka
C
(C) Emplacement of Lineation II and Western Ramp as dune ridges detached and migrated from Lake Cahuilla.
< 3 ka
D
(D) Generation II construction with the younger generation of dunes superimposed upon Generation I dunes, Lineation II and Western Ramp.
alluvial fans
Lake Cahuilla
East Mesa
10 km
N

Schematic depiction of origin of the complex and spatially diverse dune pattern of the Algodones.

The types of dunes present include: 1) linear dunes, 2) zibars (coarse grained, low relief type of transverse dunes), 3) simple crescentic dunes (barchan dunes), 4) compound crescentic dunes (small barchan dunes on top of large barchan dunes), and 5) parabolic dunes (like opposite-facing barchans, that form behind an obstacle such as vegetation).

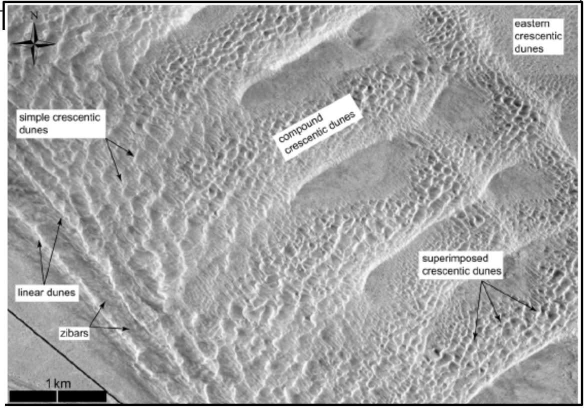
N
eastern crescentic dunes
simple crescentic dunes
compound crescentic dunes
linear dunes
zibars
superimposed crescentic dunes
1 km

Some large crescentic dunes in the center of the dune field can be over 80m (~260ft) tall and half a mile wide, with the smaller superimposed dunes up to 20m (~65ft). There are some places where the dune slip faces (the steep slope on the downwind side of the dune, where sand 'slips' down; also 'leeward slope') overlook the bare sandless ground. These bare areas and the parallel and overlapping stacks of dunes are characteristic of barchan dunes destabilizing at the end of the dune field.

Origin of the linear dunes by extension of the western terminations of the simple crescentic dunes.

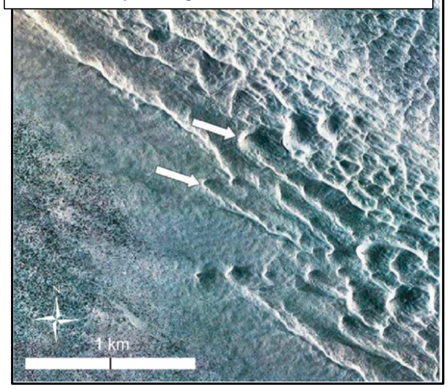

Pattern-analysis (a type of statistics used to analyze these dunes) suggests that the compound crescentic dunes at the east, with their unique sizes and orientations, are from an older generation of the construction of the dune field. The younger generation of dunes on the western side includes the simple crescentic dunes (finer grained), linear dunes (which originate as elongated arms of barchan dunes, as the fine-grained sand is depleted), and zibars (with the leftover coarser grains).

Imperial Sand Dunes Recreation Area

While much of the area is protected, a portion is also open for off-road vehicle recreation. The dunes were settings for several movies, including Tatooine in Return of the Jedi.

[1] Derickson, D., Kocurek, G., Ewing, R. C., & Bristow, C. (2008). Origin of a complex and spatially diverse dune-field pattern, Algodones, southeastern California. *Geomorphology*, *99*(1–4), 186–204**.**
[2] Muhs, Daniel R.; Bush, Charles A.; Cowherd, Scott D.; and Mahan, Shannon, "Geomorphic and Geochemical Evidence for the Source of Sand in the Algodones Dunes, Colorado Desert, Southeastern California" (1995). *USGS Staff -- Published Research.* 1292. **[3]** Norris, R. M., & Norris, K. S. (1961). Algodones Dunes of Southeastern California. *Geological Society of America Bulletin*, *72*(4), 605.

Richard Horak - Bugs in the Algodones Dunes! What tomfoolery are they up to?

The ecosystem

76 mm annual rainfall, high winds, and temperatures ranging from 39.2 to 120.2 Fahrenheit. Western edge is open dune habitat with sparse Psammophytic and creosote shrub **Fig 2B**. Eastern edge benefits from water run off from the Chocolate and Cargo Muchacho Mountains supporting denser vegetation and microphyll woodland **Fig 2C**.

Overall results of insect surveys within the dunes

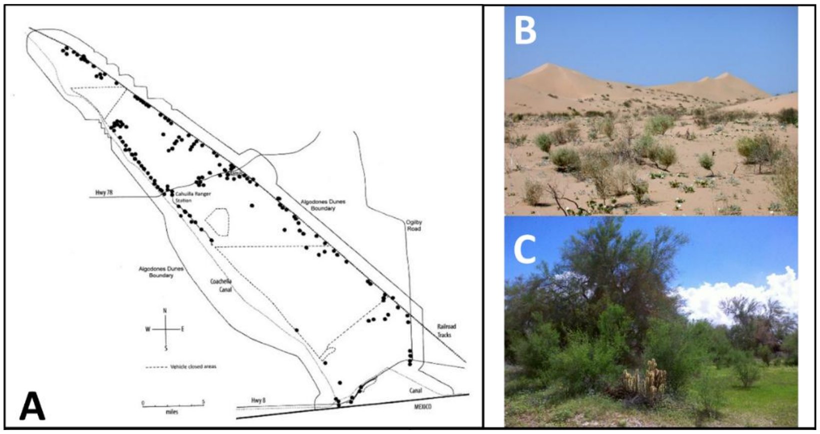

A 9 year survey by the U.S. Bureau of Land Management found 1847 species including 79 endemic species. Of these, 42.1% belong to the order Hymenoptera (bees, ants, wasps), 17.3% to Coleoptera (beetles), 12.3% to Diptera (flies, mosquitoes), 10.1% to Lepidoptera (butterflies and moths), and 6.3% to Hemiptera (aphids, cicadas). With the distribution of larval life habits being: 29.6% herbivores, 28.7% parasitoids, 18.1% predators, 10.9% pollinators, 6.2% detritivores, and 2.4% scavengers. The rest falling into parasitic, aquatic, or coprophages.

Insect sources and surprises in the endemic population

The vast majority of the species were not endemic. All Hemiptera species found were agricultural pests likely sourced from the Imperial valley such as aphids. Aquatic insects originated from canals and irrigation channels such as dragonflies or mosquitoes. The majority of Lepidoptera were migratory.

Of the endemic species, all species of Hymenoptera were parasitoids **Fig 2A/E**. Endemic pollinators or herbivores survive on Wiggins' Croton, or other flowering plants **Fig 2B/E/F**. Surprisingly, a large proportion of the endemic species were scavengers and fungivores **Fig 2B/D/G**, suggesting fungi is a cryptic by major energy source within this desert ecosystem.

Fungivores and the fungi they feed on

Fungivorous beetles typically fall within two life strategies. Some, such as **Fig 2G** lay eggs within the sand near woody shrubs, the larvae then hatch and feed on mycorrhizal fungi that is associated with the vegetation. The other strategy, employed by beetles such as **Fig 2B** is to become a farmer, digging holes into a woody plant and spreading fungus found on their skin. Once the fungus has grown and degraded the wood and converted it into more easily digestible sugars, the beetle returns to feast. Regardless of strategy, this utilizes the fungus as an "external stomach" allowing insects which cannot digest the cellulose and lignin found in woody plants to still gain carbon and energy from the plant.

Sand food (Pholisma sonorae)

This is a very cool endemic plant species that isn't very related to this talk. It is a parasite of fungus or other plants and does not photosynthesize. Its roots can reach 2+ meters in length to find water. It was used by indigenous people as a food source.

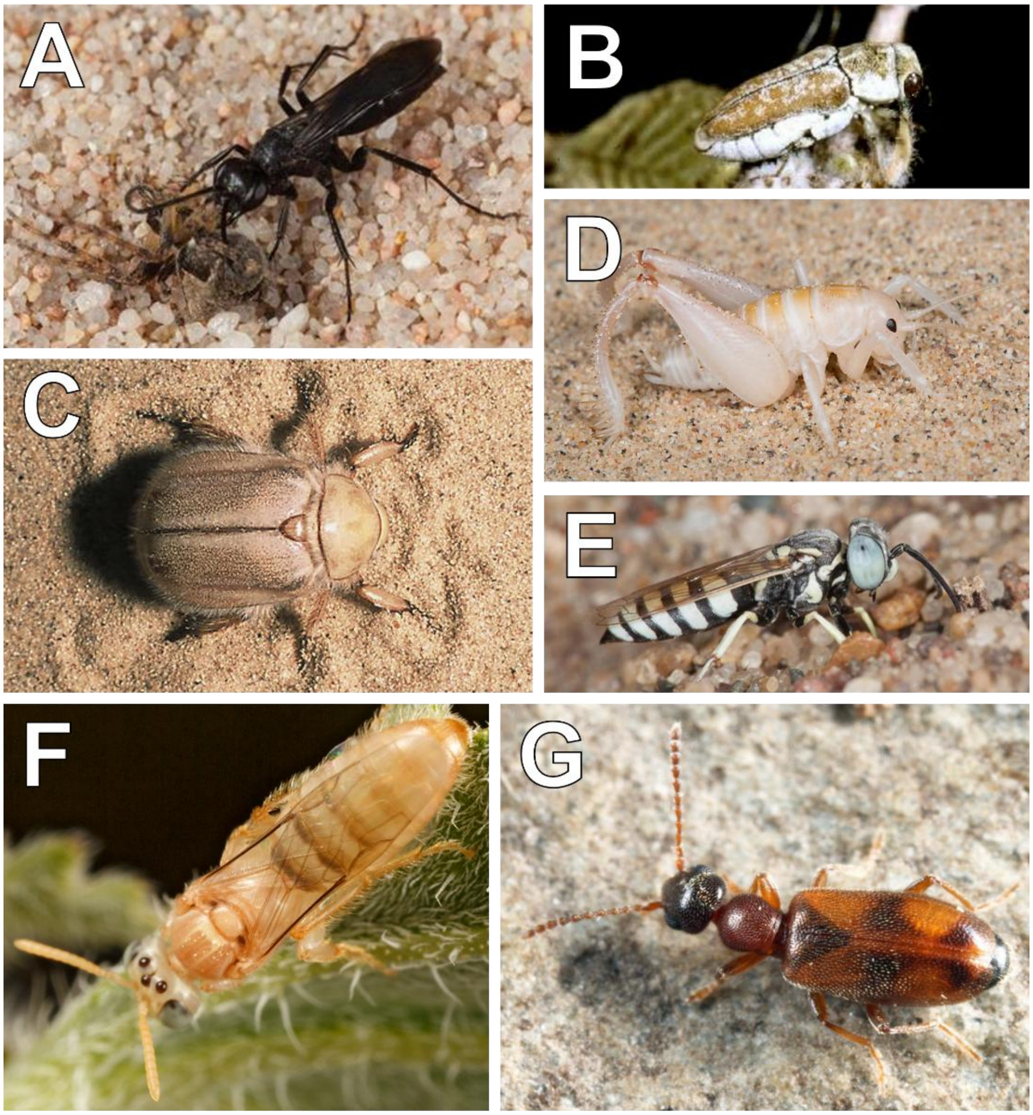

Fig 2: Selection of endemic insects

A) *Ageniella pernia* – spider wasp - parasitoid
B) *Lepismadora algodones* – jewel beetle - herbivore
C) *Pseudocotalpa sonorica* – scarab beetle - herbivore
D) *Macrobaenetes algodonensis* – sand treader cricket – scavenger
E) *Microbembex elegans* – sand wasp – pollinator/parasitoid
F) *Perdita algodones* – andrenid bee - pollinator
G) *Anthicus cervinus* – flower beetle – pollinator/fungivore

Citations

Kimsey LS, Zavortink TJ, Kimsey RB, Heydon SL (2017) Insect biodiversity of the Algodones Dunes of California. Biodiversity Data Journal 5: e21715. https://doi.org/10.3897/BDJ.5.e21715

Marius SW, Lynn SK (2010) The Pompilidae of the Algodones Dunes, California, with description of new species (Hymenoptera: Pompilidae). The Pan-Pacific Entomologist 86(1), 2-9. https://doi.org/10.3956/2009-30.1

Alex RVD, Matthew HVD (2008) Impact of Off-Road Vehicle Use on Dune Endemic Coleoptera. Annals of the Entomological Society of America 101(2), 411-417. https://doi.org/10.1603/0013-8746(2008)101[411:IOOVUO]2.0.CO;2

Colorado River Hydrology

Forrest McCann Ge136b 2025

Facts: The Colorado River flow from Colorado to the Gulf of California and is approximately 1,450 miles long. The Colorado River Basin is about 637,000 square kilometers and spans parts of Colorado, Wyoming, Utah, Nevada, New Mexico, California, and Mexico. Water from the Colorado River serves approximately 40 million people across each of those states and 13,000 square kilometers of agricultural lands [1].

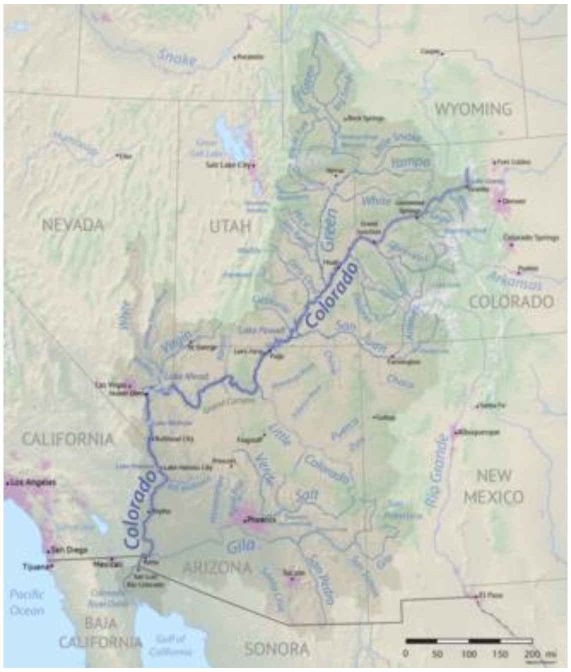
Snake
WYOMING
NEVADA
UTAH
COLORADO
Green
Yampa
White
Colorado
San Juan
Arkansas
Virgin
Lake Mead
Las Vegas
Salt Lake City
Denver
CALIFORNIA
Los Angeles
San Diego
Tijuana
Mexicali
Little Colorado
Verde
Salt
Gila
Phoenix
ARIZONA
NEW MEXICO
Rio Grande
Pacific Ocean
BAJA CALIFORNIA
Gulf of California
SONORA
0 50 100 150 200 mi

.

Figure 1. Map labeling the Colorado River and some major tributaries. The highlighted region marks the watershed of the Colorado River.

Hydrology: Much of the water flowing into the Colorado River comes from snowpack in the Upper Colorado Basin. About 70% of the river's annual flow comes from the Rocky Mountains specifically. Atmospheric rivers contribute about 30.8% of total snow accumulation across 11 to 12 atmospheric river events per year [2]. Since 2000, warming has worsened streamflow into the Colorado River and is accompanied by highly variable precipitation [3]. Work using a Variable Infiltration Capacity model (ie how does precipitation, soil moisture, lithology, and topography affect rivers) under eight climate model projections for the region predict mean declines in annual streamflow in the whole Colorado River Basin due to overall less precipitation, decreased snowpack, and increased soil evaporation [2]. The percent contribution at the subbasin level did not appreciably change under modelled scenarios, which indicates that streamflow declines are happening everywhere in the Colorado River basin.

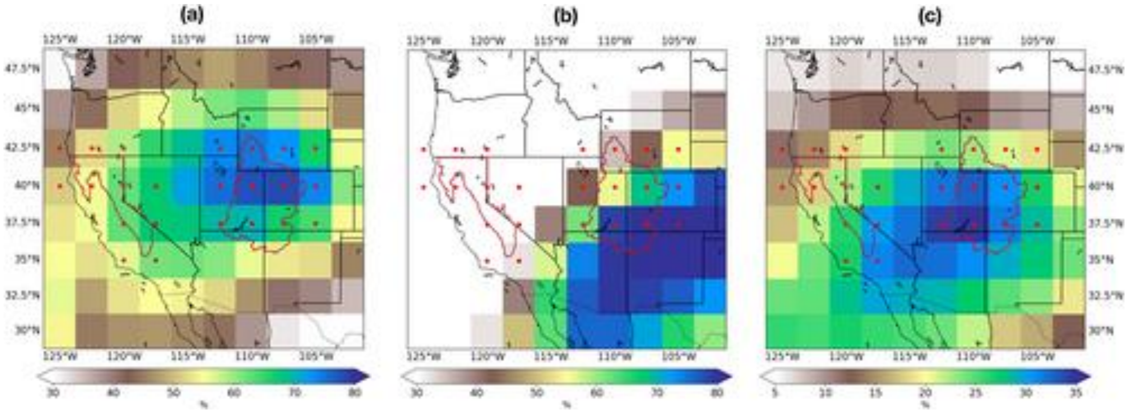

Figure 2. Adapted from Xiao and Lettenmaier (2021). The red dots indicate which cells impact the Sierra Mountains and Upper Colorado River Basin snowpacks (in red lines). Panel (a) depicts the frequency of atmospheric rivers affecting both the Sierra Nevada and the Upper Colorado River Basin. Panel (b) depicts the frequency of non-Sierra Nevada atmospheric rivers. Panel (c) depicts the fraction of snow accumulation due to atmospheric rivers.

Future research on Colorado River basin hydrology aims to understand how precipitation might change in a warming climate. Efforts to understand how likely different combinations of wet/dry and warm/cold winters are to occurs is of particular importance for understanding changes in average precipitation and average temperature. Further, trying to accurately partition precipitation between subbasins and between phases remains an active area of study.

The Colorado River Compact (1922): The Colorado River Compact was an agreement between states in the Colorado River Basin that allots water to the states and Mexico. The compact allocated 7.5 million acre feet (maf) to the Upper Basin (Colorado, Utah, Wyoming, New Mexico, Arizona) and 7.5 maf to the Lower Basin (California, Arizona, Nevada). The compact did not specify tribal allotments of water and failed to specify allotments in years with shortages. The cooperation between hydrologists, policy makers, and stakeholders in the Colorado River basin is of the utmost importance to inform water usage in the present and future [4].

References:

[1] "Colorado River," *Wikipedia*. Feb. 06, 2025. Accessed: Feb. 10, 2025. [Online]. Available: https://en.wikipedia.org/w/index.php?title=Colorado_River&oldid=1274326138#Course

[2] M. Xiao and D. P. Lettenmaier, "Atmospheric Rivers and Snow Accumulation in the Upper Colorado River Basin," *Geophys. Res. Lett.*, vol. 48, no. 16, p. e2021GL094265, 2021, doi: 10.1029/2021GL094265.

[3] Z. Wang, E. R. Vivoni, K. M. Whitney, M. Xiao, and G. Mascaro, "On the Sensitivity of Future Hydrology in the Colorado River to the Selection of the Precipitation Partitioning Method," *Water Resour. Res.*, vol. 60, no. 6, p. e2023WR035801, 2024, doi: 10.1029/2023WR035801.

[4] "Sharing Colorado River Water: History, Public Policy and the Colorado River Compact | Water Resources Research Center | The University of Arizona." Accessed: Feb. 10, 2025. [Online]. Available: https://wrrc.arizona.edu/publication/sharing-colorado-river-water-history-public-policy-and-colorado-river-compact

Geodes: More than Just a Pretty Face(ies)

Sophia Westerkamp

Introduction

Geodes are a wildly popular rock structure that can be found displayed across museums, homes and private rock collections. Despite their widespread popularity, the exact formation mechanism for geodes has remained elusive. While geodes may seem to be a fairly common type of rock structure, they do not occur randomly in nature. Instead, most geodes are found in localities such as stratified volcanic deposits (eg, basalts and tufts) or stratified sedimentary carbonate deposits (eg, limestones and dolomites) [1]. One such locality is the Hauser Geode Beds of Southern California. Figure 1 displays a variety of different types of geodes that we may find at Hauser, including agate, chalcedony, amethyst and calcite [2].

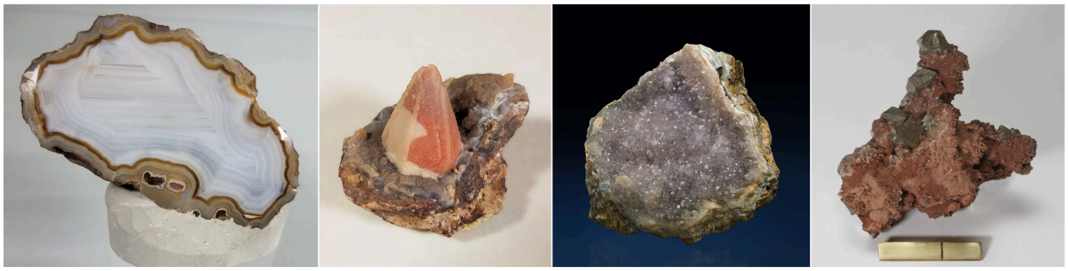

Figure 1: Different types of geodes that can be found at Hauser Geode Bets. From left to right: agate, chalcedony, amethyst and calcite. Figure taken from [2].

Igneous Geodes

Igneous geodes are formed when gasses in basaltic lava flows form vesicles in the hardening rock [1, 3]. As water seeps into these open spaces, quartz minerals deposit on the sides of the vesicle. Initially, chalcedony - a form of cryptocrystalline quartz is deposited on the walls of the vesicle. After initial nucleation of the chalcedony, inwardly-projecting microcrystalline quartz or other minerals can form inside the structure in a drusy texture [2]. Changes in the chemical composition of the groundwater precipitating the geode can lead to material and color changes in the layers of the geode [1]. An example of this textured layering can be seen in Figure 2C.

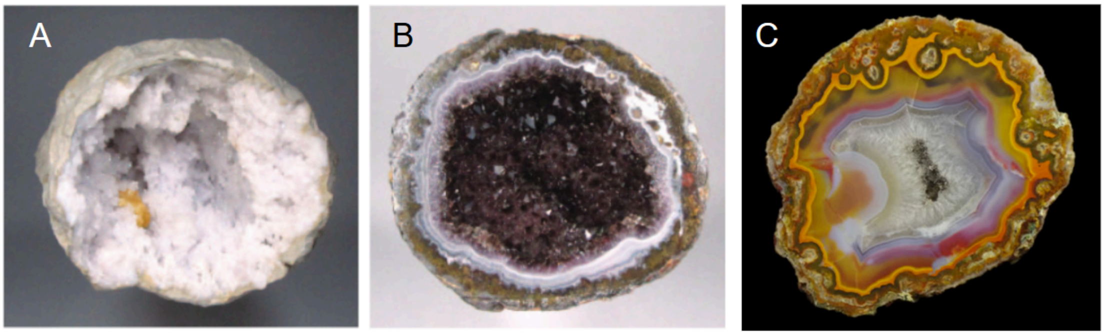

Figure 2: A) A 9-cm sedimentary geode. A thin chalcedony rind is filled in by a druse of small quartz crystals and dolomite crystals. Figure taken from [3]. B) A 9cm igneous geode with a thick chalcedony rind of agate filled in with smoky quartz crystals. Figure taken from [3]. C) A geode specimen with outer layers of agate slowly giving way to macrocrystalline drusy interior crystals. Each colored band represents a compositional change in the groundwater that the geode precipitated from. Figure taken from [1].

Sedimentary Geodes

Sedimentary geodes are usually found in dolomites, limestones and shale [1]. While there are many proposed mechanisms for geode formation in sedimentary structures, only one will be presented in depth here. First, a hollow region is formed in a sedimentary rock through some sort of fluid weathering. In this pocket, geodes form through an interplay between the driving force of geode growth against the strength of the lithified rock [4]. Geodes tend to grow from sources that are high in free energy compared to crystalline quartz. As the quartz inclusion grows, a region depleted in high-free energy source material will be formed around the growing quartz crystals. Eventually, the quartz growth will bump against its host rock. This increase in the free energy of the quarts dampens the quartz growth rate, but places stress on the host rock, promoting dissolution and allowing for further quartz growth [4].

Geode Structure and Kinetics

Geodes exhibit self-organization due to their formation in conditions strongly displaced from thermodynamic equilibrium [4]. This self-organization is readily observable in the three commonly-occurring types of agate patterns in geodes (Figure 3).

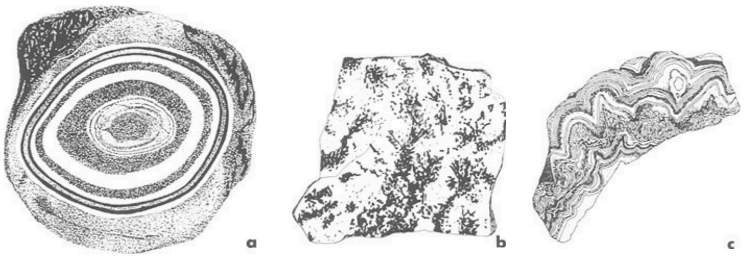

Figure 3: The three common types of agate self-organization: a) orbicular, b) mossy, c) scalloped. Figure from [4]

Focusing on the concentric orbicular patterning, these circular growths may occur due to a mechanochemical instability such as Liesegang (cross co-precipitate gradient) phenomena. In Liesegang banding, concentric rings (or other repetitive precipitation patterns) occur through a supersaturation-nucleation-depletion cycle [4].

Quartz - from Agate to Amethyst

While the wide variety of coloration found in geodes may appear to be entirely different minerals, the most common mineral found in geodes is quartz. Commonly, quartz makes up microscopic crystals of agate (Figure 1). Within agate, the microcrystalline SiO_2 inclusions are distributed into various zoned patterns that may appear to be separate minerals. However, the zonation is actually related to oscillations in the OH^- contained in the quartz fiber's structural sites. In the case of orbicular agate (Figure 3a), the color contrast may be due to periodic alternations of the crystallographic *c*-axis of the SiO_2 crystals [4].

The chemistry and mineralogy of quartz is heavily dependent on its defect structure [5]. Therefore, the presence or absence of very minor quartz defects can result in prominent changes in the quartz structure and coloration. The color of quartz found in geodes is heavily dependent on the chemistry of the supersaturating fluid, and small changes in fluid chemistry may result in varying colors and textures within a single geode.

Most geodes display an increase in grain size as you move towards the center of the structure [4]. One of the most common forms of large-grain-size quartz in geodes is amethyst, as seen through their iconic purple coloration. The purple coloration of amethyst arises from iron entering lattice sites within SiO_2, altering the crystallographic structure of the mineral and how its atoms interact with light.

Geode Hunting

Geodes are often discovered as individual spherical structures, disconnected from the surrounding rock. Because the outer chalcedony rind of geodes is more resistant to weathering than the surrounding (often sedimentary) rock, geodes tend to outlast their host rock [3], making them easily discoverable by wandering geologists.

References

1. King, Hobart. “Geodes.” *Geology.com.*
2. “Hauser beds (Hauser Geode beds; Hauser Beds Mine), Thumb Peak, Palo Verde Mining District, Palo Verde Mountains, Imperial County, California, USA.” *Mindat.org.*
3. Rakovan, John. "Word to the wise: Geode (and friends)." *Rocks & Minerals* 92.1 (2017): 85-91.
4. Ortoleva, Peter, Yueting Chen, and Wei Chen. "Agates, geodes, concretions and orbicules: Self-organized zoning and morphology." *Fractals and dynamic systems in geoscience* (1994): 283-305.
5. Götze, Jens, Yuanming Pan, and Axel Müller. "Mineralogy and mineral chemistry of quartz: A review." *mineralogical magazine* 85.5 (2021): 639-664.

Shallow-Creeping Faults in Imperial Valley, California

Victor Vescu · G3 · MCE/GPS · Ge136b · WT25

What is fault creep?

Faults release shear stress by slipping at various rates and can be divided into locked/stick-slip (slipping very fast over short seismic intervals and barely otherwise) and creeping (slipping at slow, measurable rates over periods of time that can vary wildly).

One key factor understood to determine whether a fault slips seismically or by creeping are the friction properties governing its movement. One popular friction theory is rate-and-state friction (Figure 1). Under rate-and-state, locked faults can be modelled as velocity weakening (increased slip rate leads to a decrease of the friction coefficient) or velocity strengthening (increased slip rate leads to an increase of the friction coefficient). Velocity weakening fault sections tend to slip seismically and velocity strengthening fault sections are more likely to creep. Some faults can undergo a process called dynamic weakening which changes their friction properties such that they can go from velocity-strengthening to velocity-weakening and back. This is important because it enables creeping faults to accommodate large earthquakes. This is a popular theory for the 2011 Tohoku Earthquake.

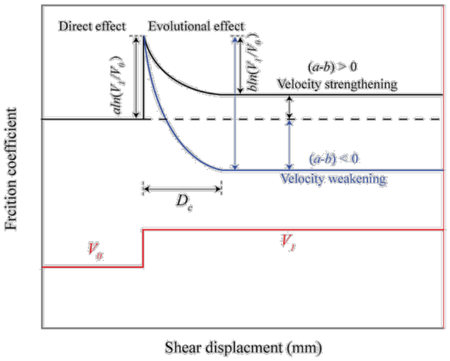
Direct effect
Evolutional effect
$a\ln(V_s/V_0)$
$b\ln(V_s/V_0)$
$(a\text{-}b) > 0$
Velocity strengthening
$(a\text{-}b) < 0$
Velocity weakening
D_c
V_0
V_s
Friction coefficient
Slip rate (μm/s)
Shear displacment (mm)

Figure 1: Diagram of idealized rate-and-state friction law.

Fault creep on the San Andreas

The San Andreas exabits both stick-slip and creeping behavior. The central San Andreas, between the towns of Parkfield and San Juan Bautista is known for its creeping behavior and is believed to disallow large earthquakes that start in the North/South from reaching all the way to the South/North. This is because, in the absence of dynamic weakening mechanisms, creeping, velocity-strengthening fault sections tend to lock the fault with the arrival of a rupture front (Figure 2). The other section of the San Andreas known for its creep events is the Brawley Seismic Zone, which includes faults near the Salton Trough and Imperial Valley.

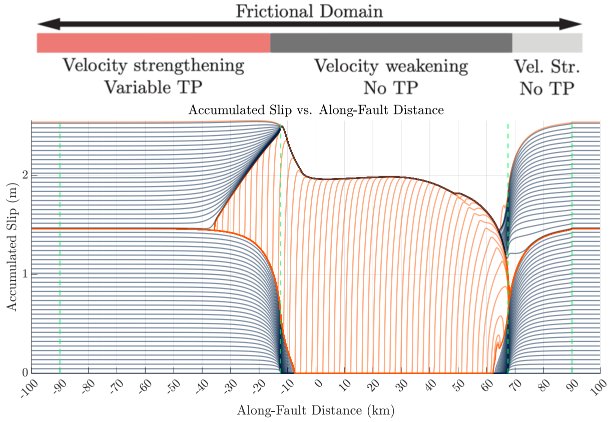

Figure 2: Simulation result showing a creeping fault section stopping an incoming earthquake rupture.

Creeping Fault Behavior in Imperial Valley

In the Spring of 2023, two fault systems in Imperial Valley (Figure 3) experienced large slip events that were recorded in high resolution by ground-based and space-based measurements. These were:

(1) Imperial Fault

Fault Type: Right-lateral strike-slip

Length: 69 km

Last major ruptures: (1) October 15, 1979, M_w 6.4; (2) May 18, 1940, M_w 6.9; several other small ruptures and instances of triggered slip

Slip-rate: Between 15 and 20 mm/yr

Aseismic slip event: Began in March 2023, lasting nearly a month

Propagation speed: 0.4 km/day

Peak slip: 8 mm (measured at creepmeters)

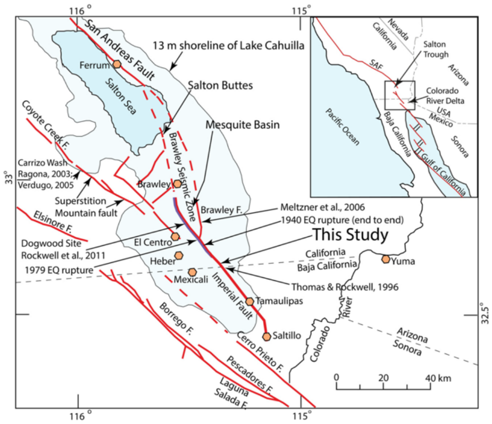
116°
115°
San Andreas Fault
13 m shoreline of Lake Cahuilla
Ferrum
Salton Sea
Salton Buttes
Mesquite Basin
Coyote Creek F.
Brawley Seismic Zone
Carrizo Wash
Ragona, 2003;
Verdugo, 2005
33°
Brawley
Superstition
Mountain fault
Brawley F.
Elsinore F.
Meltzner et al., 2006
1940 EQ rupture (end to end)
This Study
Dogwood Site
Rockwell et al., 2011
El Centro
Heber
1979 EQ rupture
California
Baja California
Yuma
Mexicali
Thomas & Rockwell, 1996
Imperial Fault
Tamaulipas
River
32.5°
Borrego F.
Saltillo
Colorado
Arizona
Sonora
Cerro Prieto F.
Pescadores F.
Laguna
Salada F.
0
20
40 km
Nevada
California
Salton
Trough
SAF
Arizona
Colorado
River Delta
USA
Mexico
Pacific Ocean
Baja California
Sonora
Gulf of California

Figure 3: Map showing the location of the Imperial Fault and Superstition Hills/Mountain Fault in relation to regional landmarks.

(2) Superstition Hills Fault

Fault Type: right-lateral strike-slip
Length: 30 km
Last major ruptures: November 24, 1987, M_w6.6; other minor historic ruptures and slip events
Slip-rate: between 1.7 and 5.5 mm/yr
Aseismic slip event: Began in May 2023, lasting several weeks
Propagation speed: 6–9 km/day
Peak slip: 40 mm (at creepmeters) and 47.6 mm (InSAR)

Satellite radar (InSAR – Figure 4), Global Navigation Satellite Systems (GNSS – Figure 5), and creepmeters (Figure 6) can be used to study the mechanics of slow slip along creeping faults and how faults might behave during large earthquakes. The 2023 slow slip events in the Imperial Valley were some of the most detailed ever recorded for shallow faults with surface displacement. Slow slip propagation varies significantly between faults, highlighting complex mechanical behaviors. Fluid pressure, fault heterogeneity, and stress conditions all play a role in shaping fault creep.

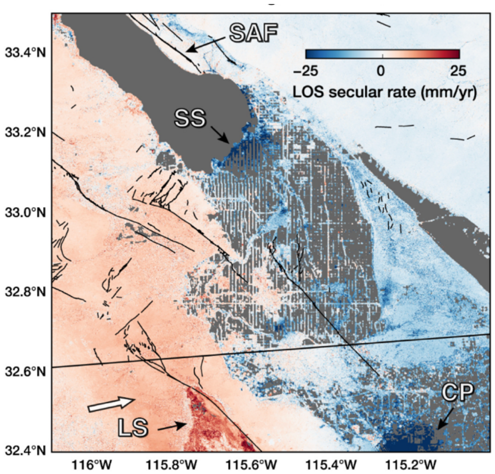

Figure 4: InSAR velocity map of Imperial Valley and Brawley Seismic Zone.

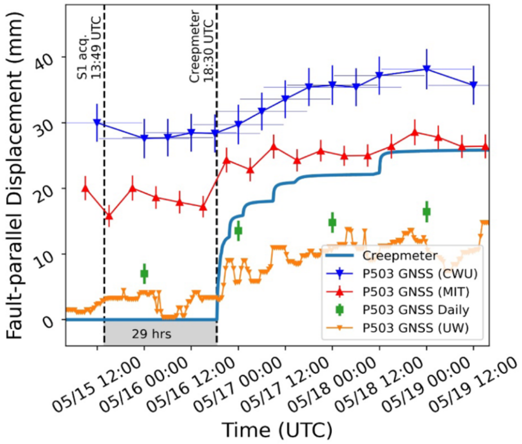

Figure 5: Displacement Data for Imperial Fault from GNSS and creepmeters during the May 2023 slow slip event.

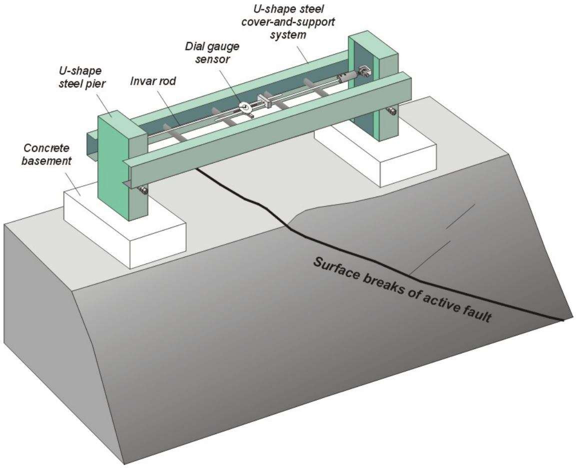
U-shape steel cover-and-support system
Dial gauge sensor
U-shape steel pier
Invar rod
Concrete basement
Surface breaks of active fault

Figure 6: Diagram of a ground-based creepmeter.

What can we say about the frictional behavior in Imperial Valley?

During the 2023 slow slip events, the Superstition Hills Fault moved in a pulse-like manner, similar to slow slip events observed in subduction zone. The Imperial Fault slipped much slower, suggesting different fault friction properties. Fault heterogeneity and dilatant strengthening (fluid-related processes) may explain the differences in creep behavior. The fact that the faults slipped within a couple months of one another suggests that stress redistribution plays a role in ongoing aseismic deformation. All these observations lead us to conclude that the Imperial Valley faults do not follow simple friction laws (velocity-strengthening or velocity-weakening).

References

[1] Materna, K., Bürgmann, R., Lindsay, D., Bilham, R., Herring, T., Crowell, B., & Szeliga, W. (2024). Shallow slow slip events in the Imperial Valley with along-strike propagation. *Geophysical Research Letters*, *51*(12), e2023GL108089.
[2] Lyons, S. N., Bock, Y., & Sandwell, D. T. (2002). Creep along the Imperial Fault, southern California, from GPS measurements. *Journal of Geophysical Research: Solid Earth*, *107*(B10), ETG-12.
[3] Rockwell, T. K., & Klinger, Y. (2023). 2000 yrs of earthquakes inferred from subsidence events on the Imperial fault, California: Effect of lake-level changes and implication for variable slip rates. *Earth and Planetary Science Letters*, *618*, 118271.

Ting-Juan Liao

El Niño–Southern Oscillation & Santa Ana Winds

1. What is El Niño–Southern Oscillation?

El Niño, meaning "The Boy" in Spanish, refers to the warm sea temperature anomaly that occurs around Christmas in the Pacific Ocean, particularly near Peru. Conversely, La Niña, meaning "The Girl" in Spanish, is characterized by significantly lower sea temperatures compared to normal days. Scientists have discovered that El Niño/La Niña oscillations have a cycle of approximately 2 to 7 years.

El Niño/La Niña is not solely a surface temperature anomaly but also involves the atmosphere, leading to its name, the El Niño Southern Oscillation (ENSO). In normal years, the Pacific South Equator current transports ocean water from the East Coast to the South. In response, the compensating upwelling current brings cool, deep ocean water and nutrients to the surface, making the East Pacific an ideal fishing spot. However, during El Niño, the weaker eastward winds fail to support the Pacific South Equator current. This results in weakened upwelling and a lack of cool water, which is the primary cause of El Niño.

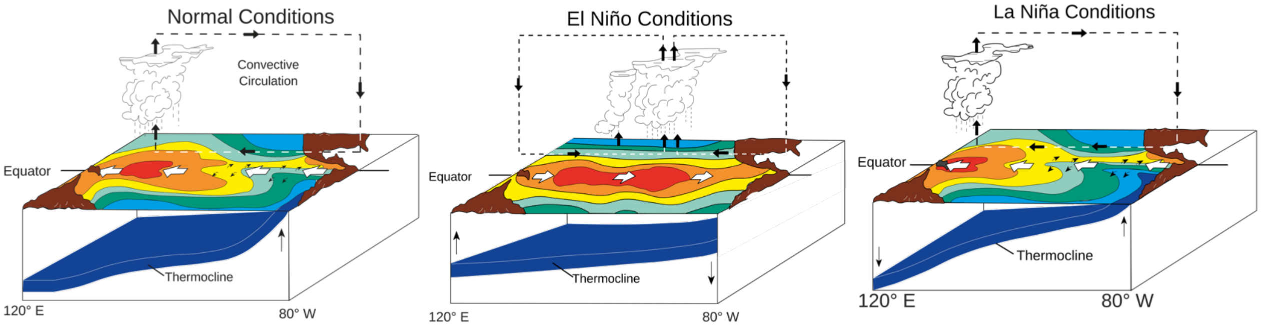
Normal Conditions
Convective Circulation
Equator
Thermocline
120° E
80° W
El Niño Conditions
Equator
Thermocline
120° E
80° W
La Niña Conditions
Equator
Thermocline
120° E
80° W

Figure 1. Schematic diagram of Normal conditions (left) and El Nino Conditions. Credit: NOAA / PMEL / TAO Project Office, Dr. Michael J. McPhaden, Director.

2. Walker Circulation

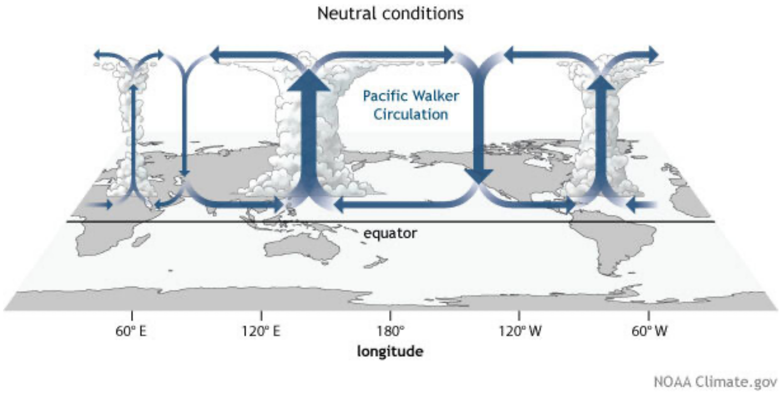
Neutral conditions
Pacific Walker Circulation
equator
60° E
120° E
180°
120° W
60° W
longitude
NOAA Climate.gov

Figure 2. Walker Circulation. Credit: NOAA

Walker circulation, caused by heat distribution differences between the ocean and land, involves motions in the zonal and vertical directions. Additionally, the tropical atmosphere exhibits significant meridional motion, exemplified by the Hadley Circulation. During neutral ENSO conditions, the Walker Circulation’s upward branches rise strongly across the Maritime Continent and weakly over eastern Africa and northern South America. These rising branches coincide with bull’s-eyes of precipitation during December through February. Conversely, the downward branches of dry, stable air sink strongly over the eastern Pacific Ocean and more weakly over the Arabian Sea.

3. Santa Ana Winds

Santa Ana Winds are katabatic winds originating from the Great Basin and descending to sea level. A katabatic wind, derived from the Ancient Greek word “katábasis,” meaning “to descend,” is a downslope wind generated by a high-density air mass descending under the influence of gravity into a less dense air mass below. When two air masses with different densities are located above a slope, the one with lower density will descend and move downhill.

Higher pressure at lower altitudes causes the downhill wind to adiabatically increase in temperature. Relatively, humans are affected by this temperature increase. The high-pressure airmass from the Great Basin and Mojave Desert becomes a strong, warm, and dry wind around the coast.

During El Niño years, the East Pacific tends to have lower pressure compared to normal years. This could potentially lead to stronger Santa Ana Winds since it is associated with a larger pressure gradient.

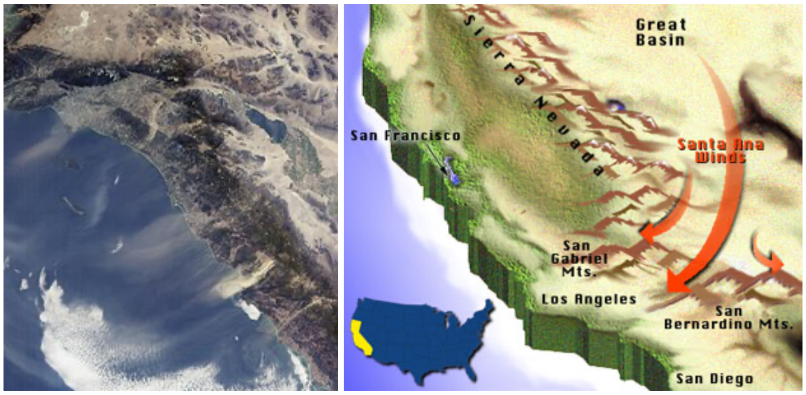

Figure 2. Santa Ana Winds. Credit: NASA/GSFC/LaRC/JPL, MISR Team

Reference:

- Trenberth, K. E. (1997). The Definition of El Niño. Bulletin of the American Meteorological Society, 78(12), 2771-2778. https://doi.org/10.1175/1520-0477(1997)078<2771:TDOENO>2.0.CO;2
- Poulos, Greg; Zhong, Shiyuan (Sharon) (November 2008). "An Observational History of Small-Scale Katabatic Winds in Mid-Latitudes". Geography Compass. 2 (6): 1798–1821.
- Guzman-Morales, J., Gershunov, A., Theiss, J., Li, H., & Cayan, D. (2016). Santa Ana Winds of Southern California: Their climatology, extremes, and behavior spanning six and a half decades. Geophysical Research Letters, 43(6), 2827-2834.

Rattlesnakes by Isaac N. Aguilar Rivera

If the United States was run by snakes, San Diego would be the capital. Welcome to one of the most biodiverse regions in North America for reptiles. San Diego County has the highest diversity of reptiles and amphibians in the country, including more than 70 species of lizards, snakes, frogs and salamanders. The herpetological diversity of San Diego is one facet of the climatic transition zone between coastal, montane, and desert ecosystems that has facilitated the diversification of rattlesnakes (*Crotalus spp.*); 5 species inhabit this region. Rattlesnakes are venomous and should not be disturbed. No, juvenile venom is not "more potent", but they cannot rattle until their first shed when an added segment to their rattle can click against the first "button".

Southern Pacific (*C. oreganus*)

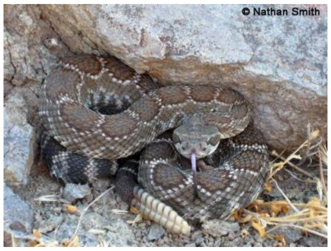

Red Diamond (*C. ruber*)

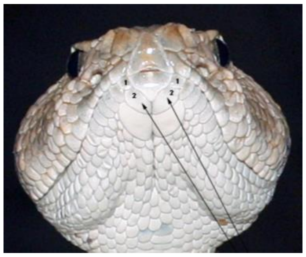

Sidewinder (*C. cerastes*)

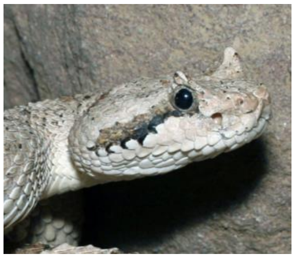

Western Diamondback (*C. atrox*)

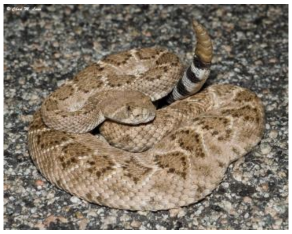

SW Speckled (*C. mitchellii*)

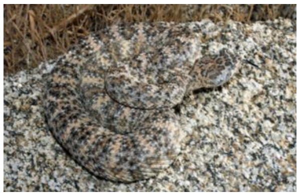

According to Hutchinson (1978), a species' ecological niche is defined as a hypervolume in n-dimensional environmental space that allows a population to persist indefinitely; in reality, a fundamental and realized niche is distinguished by the emergent effects of species interactions. The environmental heterogeneity of the eastern San Diego landscape induces variations in temperature, humidity, and prey availability across the region that has resulted in morphological and behavioral adaptations among local reptile populations. Often, subtle features differentiate species identification.

Snakes' contributions to the co-evolution of the geosphere and biosphere in San Diego is evident by the dynamics of soil composition, erosion, sedimentation, biogeochemical and nutrient cycling. Their ecological interactions with the physical environment perpetuate feedback loops between biological activity and geospheric processes, which shape landscapes over evolutionary timescales. Fossorial species like the Western Shovel-nose (*Chionactis occipitalis*) and the Long-nosed (*Rhinocheilus lecontei*) snakes actively disturb soil through their movement and nesting behavior. This bioturbation process enhances soil aeration and alters sediment distribution, playing a role in geomorphological processes in these arid environments. Rattlesnakes and other pit-dwelling species use existing burrows created by small mammals and contribute to both sediment accumulation and transport. Predator-prey dynamics redistributes organic matter across the landscape. In nutrient poor environments like deserts, nitrogen and phosphorus in the excrements or decomposition of snakes enriches soil chemistry and develops valuable microhabitat real estate for other organisms. Rodent population control by these terrestrial apex predators is a significant service that indirectly mitigates excessive soil erosion from burrowing and overgrazing of vegetation and root systems that stabilize sediment layers.

Over evolutionary timescales, snakes also contribute to the paleontological record by embedding their remains in sedimentary deposits. Fossilized skeletal remains of snakes provide direct evidence of historical climate and habitat conditions, although occurrences are rare due to their fragile skeletal structure. Their distribution in fossil beds can offer insight into the past including fluctuations in aridity, tectonic activity, and sediment deposition. The San Diego and Los Angeles Natural History Museums do archive snake fossil collections from Southern California. The La Brea Tar Pits in Los Angeles have yielded fossils from 12 different snake species that likely also inhabited San Diego deserts.

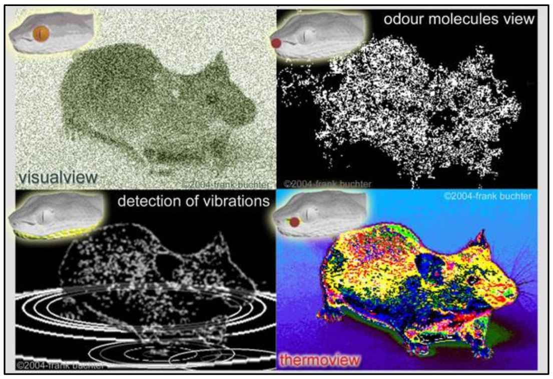

Figure 1: Illustrative interpretation of pit-snake perception

Scales: Microstructural features of scales are highly specialized for minimizing water loss, mechanoreception, and defense. Keeled scales with ridges and grooves may function to enhance structural rigidity and channel moisture across the surface of the skin. Imbricative arrangement contributes to scale flexibility for efficient locomotion. Cutaneous receptors between scales are sensitive to pressure and vibration, enhancing predation in the absence of visual cues.

Sensory Organs: Rattlesnakes possess specialized heat-sensing pits located between their eyes and nostrils, enabling them to detect infrared radiation emitted by endothermic prey. These pits function through specialized TRPA1 calcium ion channel proteins that are sensitive to temperature changes as small as 0.003°C. Genetic evidence suggests that the TRPA1 gene is under strong positive selection in pit-bearing snakes, and that adaptive evolution related to infrared detection enhances their ability to hunt nocturnally and detect camouflaged prey in low-visibility environments (Geng *et al.*, 2011). The geological formation of desert landscapes determines the microclimates where rattlesnakes hunt and influences the evolutionary selection for enhanced sensory abilities. Desert sediments have distinct geothermal properties including high heat retention that further enhances the utility of these sensory pit organs for detecting prey.

Venom: Rattlesnake venom is a sophisticated biochemical cocktail designed for both subduing prey and initiating digestion. The qualities vary among individuals, species, and populations in response to evolutionary selection and ecological factors such as prey availability, predator interactions, and habitat structure. Venom typically contains a synergistic blend of neurotoxins, proteolytic enzymes, and metalloproteins that contribute to prey immobilize and physiochemical degradation. Interestingly, rattlesnakes in regions with a high density of prey may exhibit a greater proportion of neurotoxins whereas populations preying on tougher, more resistant species may develop venoms rich in proteolytic enzymes. Some prey, such as ground squirrels and woodrats, have evolved venom resistance that contribute to selective pressures which increase venom potency or alter toxin composition – enabling a classical co-evolutionary arms race. Geological barriers can isolate different rattlesnake populations and influence the evolution of distinct venom profiles through allopatric speciation.

Body Shape & Locomotion: Diverse locomotive strategies emerge from the elongated, limbless body plan of snakes. Sidewinders (*C. cerastes*) are named for their unique locomotion (Fig. 2) that minimizes surface contact for transversing loose sands and limiting heat absorption. Sidewinding mechanics involve propagating both vertical and horizontal waves, where body sections alternate between static ground contact and thrusting forward. Research on the kinematics has revealed that Sidewinders primarily increase speed by increasing the frequency of sidewinding rather than stride length (Tingle *et al.*, 2022).

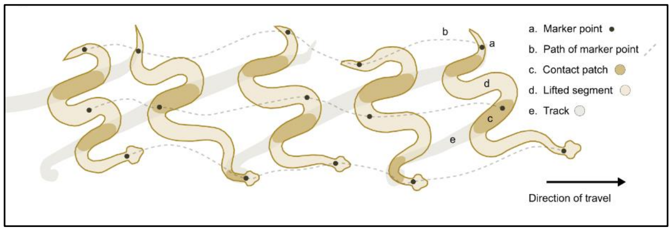

Figure 2: Sidewinding kinematics (Tingle et al., 2022)

References

Geng J, *et al*. 2011. *Adaptive evolution of the TRPA1 gene in pit-bearing snakes: implications for infrared sensation*. PLoS One. 6(12):e28689. doi: 10.1371/journal.pone.0028689.

Hutchinson GE. 1978. *An introduction to population ecology*. New Haven (CT): Yale University Press.

Tingle JL, *et al*. 2022. *Kinematic strategies of sidewinding locomotion in rattlesnakes*. Journal of Experimental Biology. 225(24): jeb244634. doi:10.1242/jeb.244634.

Biological Soil Crust (Biocrusts)

Zahra Shivji

Despite the heat and dryness of desert topsoils, microbial consortia thrive in the spaces between plants and rocks. These communities form structures called biocrusts which range from millimeters to centimeters thick and are aggregations of microbes and minerals [1]. Within these crusts, diverse microorganisms cooperate to cycle nutrients and create protective structures to evade wind and drought conditions. In dryland ecosystems, biocrusts are the dominant life form and cover up to an estimated 70% of surface soil [2]. Biocrusts are especially important to carbon and nitrogen cycling and erosion prevention in California's Mojave Desert.

Community Members

In general, biocrusts can be composed of bryophytes, lichens, eukaryotic algae, cyanobacteria, bacteria, and fungi [2]. In hot arid climates like the Mojave, light algal crusts (LAC) are the most common in the landscape. LAC's are composed of photosynthetic cyanobacteria and other algae that transform from almost undetectable when dormant (in the absence of water) to bright green after rainfall (Fig 1). Another type, lichen crusts, are composed of co-occurring groups of fungi and their algal partners (Fig 2). These crusts are typically more distinguishable than LAC but are less common in Southern California. Moss biocrusts also can also be found in the Mojave but only where water is found for extended periods of time such as under rocks or along riparian corridors [3].

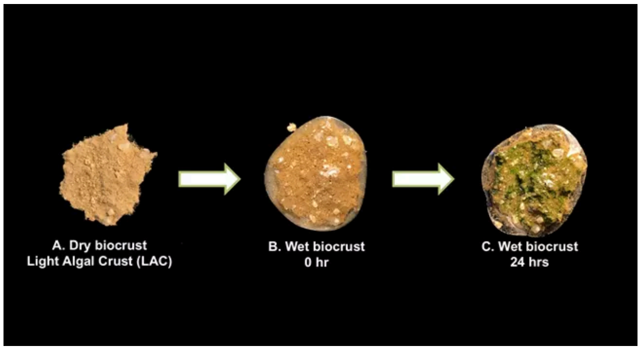

Figure 1. Light algal crust (LAC) from Joshua Tree National Park shows how dramatically the appearance of the microbial community changes after rehydration [1].

Nutrient Cycling

Biocrust organisms primarily fall into two categories: (1) photosynthetic primary producers like cyanobacteria that produce organic compounds and fix nitrogen, and (2) heterotrophic consumers like fungi that often provide protective structures for the cyanobacteria/algae. In LAC, where there are no fungal partners, cyanobacteria excrete "sticky" extracellular polymeric substances (EPS) to link themselves together and to hold themselves to the soil surface. EPS also helps the communities retain water and capture mineral-rich dust. The nitrogen fixation capability (converting atmospheric N_2 into bioavailable forms like ammonia and amino acids) of biocrusts is essential to support life in nutrient-limited desert soil.

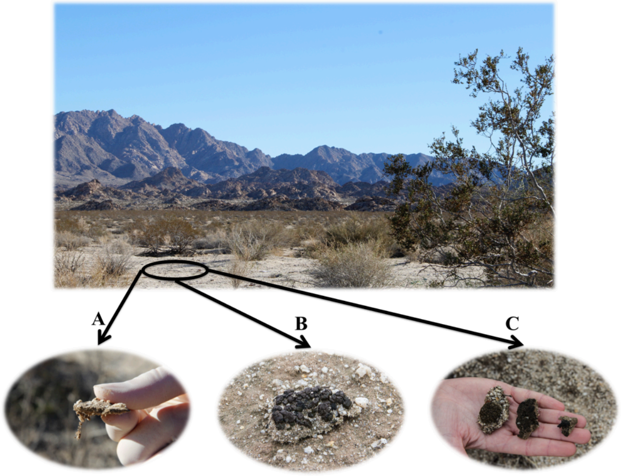

Figure 2. Biocrusts in the Mojave (A) LAC and (B, C) lichen biocrusts. Lichen biocrusts have much more voluminous structures and are more easily spotted than LAC [1].

Hypolithic Biocrusts

One interesting adaptation of biocrusts is their ability to grow beneath translucent and opaque stones embedded in the soil surface like quartz [4]. The stones act as a barrier to the harsh desert conditions by reducing UV radiation, buffer against extreme diurnal temperature fluctuations, and trap moisture in the soil by reducing evaporation and nucleating fog condensation [4]. Hypolithic biocrusts are found both in hot and cold desert environments and range as far as Death Valley to Antarctica and the Tibetan Plateau (consortia composed of different cyanobacteria and algal species in different environments).

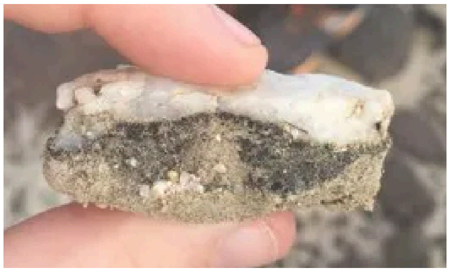

Figure 3. Hypolithic biocrusts grow on the bottom surface of quartz in the Mojave [3].

Climate Change Impacts and Restoration Efforts

Increases in global temperature and decreased precipitation in drylands and adjacent areas has been shown to slow growth and recovery (following mechanical and drought/heat perturbations) of biocrusts which is concerning considering their outsized ecosystem functions [5]. In many cases, biocrusts repress desertification by preventing topsoil erosion, increasing soil moisture, and sequestering nutrients into soils. If these vital resources are lost, it could exacerbate climate change impacts across desert ecosystems. Across the Western U.S., biocrust restoration efforts have been attempted in sites damaged by off-roading. There are three main stages to biocrust restoration: (1) soil stabilization to enable microorganism colonization, (2) resource manipulations to increase nutrient and water content to favor microbial growth, and (3) soil inoculation via dried biocrust powders and slurries [6]. This process has a high success rate, with one study having restoration success in all plots tested.

References

[1] Nuttapon Pombubpa, Tania Kurbessoian, Jason E. Stajich, Nicole Pietrasiak, Tasha La Doux. Exploring the Microbial Diversity in Biological Soil Crusts at Joshua Tree National Park. US National Park Service.
[2] Belnap, J., Eldridge, D.J., Kaltenecker, J.H., Rosentreter, R., Williams, J. and Leonard, S., 2001. Biological soil crusts: ecology and management. US Department of the Interior, Bureau of Land Management. US Geological Survey, Technical Reference, 2, pp.1-110.
[3] *Brianne Palmer. 2020.* It's alive! The hidden microbial communities below our feet. https://mojavedesertlandtrust.medium.com.
[4] Fisher, K., Jefferson, J.S., Vaishampayan, P. 2020. Bacterial Communities of Mojave Desert Biological Soil Crusts Are Shaped by Dominant Photoautotrophs and the Presence of Hypolithic Niches. *Frontiers in Ecology and Evolution*, *7.*
[5] Phillips, M.L., McNellis, B.E., Howell, A. *et al.* Biocrusts mediate a new mechanism for land degradation under a changing climate. *Nat. Clim. Chang.* 12, 71–76 (2022). https://doi.org/10.1038/s41558-021-01249-6.
[6] Scott R. Abella, Kristin H. Berry, Stefanie Ferrazzano. 2023. Techniques for Restoring Damaged Mojave and Western Sonoran Habitats, Including Those for Threatened Desert Tortoises and Joshua Trees. Desert Plants.